SINGLE-CHANNEL AND WHOLE-CELL ELECTROPHYSIOLOGICAL CHARACTERIZATIONS OF L-TYPE $Ca_V1.2$ CALCIUM CHANNEL SPLICE VARIANTS: RELEVANCE TO CARDIAC AND NERVOUS SYSTEM FUNCTIONS

PETER BARTELS

NATIONAL UNIVERSITY OF SINGAPORE

2013

SINGLE-CHANNEL AND WHOLE-CELL ELECTROPHYSIOLOGICAL CHARACTERIZATIONS OF L-TYPE $Ca_V1.2$ CALCIUM CHANNEL SPLICE VARIANTS: RELEVANCE TO CARDIAC AND NERVOUS SYSTEM FUNCTIONS

PETER BARTELS

-Diploma Biologist-

University of Cologne, Germany

A THESIS SUBMITTED FOR THE DEGREE OF DOCTOR OF PHILOSOPHY

DEPARTMENT OF PHYSIOLOGY

YONG LOO LIN SCHOOL OF MEDICINE

NATIONAL UNIVERSITY OF SINGAPORE

2013

Declaration

"I hereby declare that this thesis is my original work and it has been written by me in its entirety. I have duly acknowledged all the sources of information which have been used in the thesis.

This thesis has also not been submitted for any degree in any university previously."

Peter Bartels

4th of January, 2013

"Ja, Kalzium, das ist alles"

Otto Loewi (1873-1961), German Pharmacologist

Acknowledgements

Facing the PhD was a thrilling challenge with many ups and downs. It would not have been possible without the help and support of so many people in so many ways…I am deeply thankful…

First and foremost, I would like to thank my supervisor Tuck Wah Soong for his patience, guidance, and never ending support he gave me. It sparked my passion and hunger for future endeavors in the exciting field of calcium channel research.

I thank my TAC members Sanjay Khanna and Chian Ming Low who were always supportive and ready to answer my questions. Thank you for all the suggestions throughout the project.

I am also very thankful to the many current and former members of the Soong lab.

Especially, I would like to thank Mui Cheng, Yuk Peng, Tan Fong and Chye Yun who gave me useful insights into the field of molecular biology and Dejie Yu for her great support of fresh cells and electrophysiology. Dr Liao Ping for his construct, Dr Li Guang and Dr Juejin Wang for insights into their research area and help in biochemistry. Alex, Zhai Jing, Qingshu and Huang Hua for general support. Markus Rouis Quek Weng Sung, whom I supervised throughout his bachelor project and who delivered valuable data. Finally Dr. Nupur Nag and Hendry Cahaya for much laughter beside the bench.

I express gratitude to my collaborators in Austria, Nicolas Singewald and Simone Sartori (University of Innsbruck) for offering precious animal samples and Stefan Herzig and Uta Hoppe from Germany (University of Cologne) for the support of human samples.

Finally, I am most grateful to my beloved mother in Germany. Without your support I would not have reached my goal. Rosi my beloved wife. She gave me support and strength throughout the hard days.

Table of Content

List of Publications

Diploma thesis:

Peter Bartels, Kerstin Behnke, Guido Michels, Ferdi Gröner, Toni Schneider, Margit Henry, Paula Q. Barrett,Ho-Won Kang, Jung-Ha Lee, Martin H.J. Wiesen, Jan Matthes, Stefan Herzig."Structural and biophysical determinants of single $Ca_V3.1$ and $Ca_V3.2$ T-type calcium channel inhibition by N_2O", **Cell calcium** 46(2009) 293-302.

PhD thesis:

Guang Li, Ping Liao, Juejin Wang, **Peter Bartels**, Hengyu Zhang, Dejie Yu, Mui Cheng Liang, Kian Keong Poh, Chye Yun Yu, Fengli Jiang, Tan Fong Yong, Guangqin Zhang, Mary Joyce Galupo, Jin Song Bian, Sathivel Ponniah, Scott Lee Trasti, Uta C. Hoppe, Stefan Herzig and Tuck Wah Soong. "Cardiac Electrical Remodeling via Alternative Splicing of $Ca_V1.2$ Channels produces Ventricular Arrhythmia". **(Manuscript in preparation)**

Bartels Peter, Liao Ping, Soong Tuck Wah." N-terminal regulation and surface expression of alternatively spliced human $Ca_V1.2$". **(Manuscript in preparation)**

Abstract:

The L-type $Ca_V1.2$ calcium channel forms a hetero-oligomeric complex which is comprised of a transmembrane pore-forming α_1-subunit, associated and modulated by auxiliary β- and $\alpha_2\delta$-subunits. $Ca_V1.2$ channels are abundantly expressed in the cardiovascular and nervous systems where their activation initiates a rapid influx of Ca^{2+} ions through their membrane spanning pores, triggering various cell responses such as excitation-contraction coupling in the heart muscle, gene expression and synaptic plasticity in the CNS. Alternative splicing of $Ca_V1.2$ has been associated with changes in the electrophysiological and pharmacological properties of the channel (Liao et al., 2007; Liao et al., 2004; Tang et al., 2004) and is furthermore implicated in severe cardiovascular and neuronal dysfunctions (Splawski et al., 2004; Tiwari et al., 2006). This PhD thesis focuses on how the significance of alternative splicing in generating channel functional diversity could be evaluated by using an *in vitro* expression system as well as a more complex *ex vivo* system. We show that the exclusion of the single cassette exon 33 of $Ca_V1.2$ in a mouse genetic mutant, deleted specifically of alternative exon 33, results in *Torsade de pointes*, a severe form of arrhythmia well documented in cardiovascular disease of humans. Specific exon exclusion, which results in altered channel gating property, triggers arrhythmia in our animals and is due to a 4 times higher single-channel open probability of $Ca_V1.2_{\Delta 33}$ compared to the wild type channel. This emphasizes that

single alternative exon exclusion in $Ca_V1.2$ can result in severe electrophysiological changes coupled to cardiac electrical remodeling leading to ventricular arrhythmia of the heart.

In a related question, the electrophysiological and expression characteristics of the mutually exclusive N-terminal exons 1a/b of $Ca_V1.2$ was evaluated. This pair of mutually exclusive exons in combinations with another pair of mutually exclusive exons 8/8a define the smooth muscle SM isoform of exon 1b/8 and the cardiac muscle CM isoform of 1a/8a (Abernethy and Soldatov, 2002; Biel et al., 1990; Liao et al., 2004; Tang et al., 2004; Zuhlke et al., 1998). Preliminary data support the hypothesis that the SM 1b isoform compared with the cardiac muscle CM isoform 1a showed higher level of membrane surface expression. Data obtained from whole-cell recordings clearly indicated for a 2-fold increase in current density for the SM channels, which could be determined by a tail current analysis. A gating current analysis obtained from tail currents did support the notion that the higher current density was due to higher channel surface expression. Furthermore, we could demonstrate that exon 1b in combination with exon 8a changes the channel kinetic by shifting the steady-state inactivation to a more hyperpolarized potential. Similar findings indicating for the possible role of exon 1b in channel inactivation could be obtained from single-channel recordings. However, the basic single-channel properties did not reveal any differences in channel gating supporting our findings that an elevated current density is more likely due to a higher SM $Ca_V1.2$ channel surface expression than to a higher channel gating probability.

In a collaborating work with the group of Nicolas Singewald, Austria, we wanted to address the question of whether alternative splicing of $Ca_V1.2$ is a major contributor in fear response in HAB, LAB, NAB animals. In this context dissected brain areas associated with the fear circuitry were analyzed with the transcript-scanning method (Soong et al., 2002) to determine the transcript levels for various mutually exclusive exons of $Ca_V1.2$ in the amygdala, hippocampus and prefrontal cortex. We detected no overt changes in splicing patterns that would predict any electrophysiological changes in $Ca_V1.2$ brain regions associated with fundamental emotional and social traits. Interestingly, from its physiological function the brain channel isoform $Ca_V1.2$ seems to be more of a cardiac version in regards to the high expression of exons 8a/22/32.

Taken together, this PhD thesis provided additional conceptual support in regards to the physiological and pathophysiological implications and consequences that underlie alternative splicing in $Ca_V1.2$ calcium channel isoforms. The work further demonstrates that electrophysiological characterization at the single-channel level is a powerful tool to help further dissect the mechanisms to account for alterations in whole-cell channel properties in alternative splice variants of the $Ca_V1.2$ channels in both *ex-vivo* and *in-vitro* systems.

List of tables

List of figures

Abbreviations

AD/DA	Analog to digital converter
ATP^+	Adenosine triphosphate
fA	Femto Ampere
nA	Nano Ampere
pA	Pico Ampere
ANOVA	Analysis of Varianz
AV	Atrioventricular
$BaCl_2$	Barium chloride
bp	Base pair
BLAST	Basic Local Alignment Search Tool
BNC	banana network cable
°C	Degree Celsius
$CaCl_2$	Calcium chloride
CACNA1	Genes of the calcium channel α-subunitsα1A-H and α1S
CD1	Cluster of differentiation 1
CICR	Calcium Induced Calcium Release
CO_2	Carbone dioxide
CPU	Central processing unit
CREB	cAMP-responsive element binding
CsOH	Caesium hydroxide
CVDs	Cardiovascular Diseases
DHP	Dihydropyridines
DMEM	Dulbecco's Modified Eagle Medium
DNA	Deoxyribonucleic acid
DTT	Dithiotreitol
e.g.	Exempli gratia; for example
EGTA	Ethylene glycol tetraacetic acid
EPM	Elevated plus maze
ERK	Extracellular signal-regulated kinase
fig.	Figure
GFP	Green fluorescent protein
h	Hour
HAB	High- anxiety behavior
HEK	Human Embryonic Kidney
HEPES	(4-(2-hydroxyethyl)-1-piperazineethanesolfonic acid
HBS	Hepes buffered saline
HIV	Human immunodeficiency virus
HP	Holding potential
HVA	High-voltage activated
Hz	Hertz
KHz	Kilo Hertz

KCl	Potassium chloride
KOH	Potassium hydroxide
KO	Knock out
L	Liter
LAB	Low-anxiety behavior
LB	Luria-broth medium
LVA	Low-voltage activated
k	Kilo
kb	Kilo base pairs; 10^3 base pairs
MAP	Mitogen activated protein
M	Molar
mM	Milimolar
ms	Millisecond
$MeSO_3$	Methylsulfate
$MgCl_2$	Magnesium chloride
min.	Minute
mRNA	Messenger Ribonucleic acid
mV	Millivolt
µl	Micro liter; 10^{-3} liter
ng	Nano gram; 10^{-9} gram
OA	Open arm
P_{CMV}	Promoter (cytomegalovirus)
PD	Parkinson's disease
PTM	Posttranscriptional modification
MAPK	Mitogen-activated protein kinase
MCS	Multiple cloning site
N	Number or amount
NAB	Normal-anxiety behavior
NCBI	National Center for Biotechnology Information
NCX	Na/Ca exchanger
NIH	National Institute of Health
PBS	Phosphate Buffered Saline
PCR	Polymerase chain reaction
pH	Potentia hydrogenii
PKC	Protein kinase C
PP2B	Phosphatase 2 B
PTSD	Post-traumatic stress disorders
RMS	Root mean square
RNA	Ribonucleic acid
rpm	Revolutions per minute
RYRs	Ryanodine Receptors

RT	Room temperature
SA	Sinoatrial Node
SERCA	Sarco-Endoplasmatic Reticulum Calcium ATPase pump
shRNA	Short hairpin Ribunucleic acid
SNP	Single Nucleotide Polymorphism
SR	Sarcoplasmic Reticulum
SSRI	Serotonin selective reuptake inhibitor
TEA	Tetraethyl ammonium
TP	Testing Potential
U	Uracil or Voltage
UTR	Untranslated Region
UV	Ultra Violet
V	Volt
VGCCs	Voltage-gated calcium channels
VSMC	Vascular smooth muscle cells
WT	Wild type
w/v	Weight per Volume

Chapter I

1. INTRODUCTION

1.1 Role of voltage-gated calcium channels VGCCs in human physiology

The examination of the physiological role of voltage-gated Ca^{2+} channels VGCCs has been the research focus of scientists for a long time. The families of Ca^{2+} channels are expressed in various cell types where they open upon sensing membrane depolarization to allow an influx of divalent Ca^{2+} ions into the cell. The influx of Ca^{2+}ions is carefully controlled by fine-tuned mechanisms as these divalent ions cannot be metabolized and therefore need to be sequestered within intracellular organelles or shunted out of the cell into the external matrix. However, the cytoplasmic increase in Ca^{2+} ions triggers a number of physiological responses including: (1) muscle contraction via activation of Ca^{2+} dependent/sensitive Ryanodine receptors RyRs by releasing Ca^{2+} ions out of the Sarcoplasmic Reticulum (SR) into the cytoplasm (Bers, 2002; Reuter, 1979); (2) transduction of Ca^{2+} signals via complex signaling pathways (CREB/MAPK), regulating gene expression in the cell (Dolmetsch et al., 2001; Greenberg et al., 2008);(3) releasing of neurotransmitters from the pre-synaptic terminals and modulation of neuronal plasticity in the brain(Catterall and Few, 2008; Moosmang et al., 2005). Furthermore, various clinically relevant drugs against VGCCs or against their auxilliary subunits have been reported to reduce neuropathic pain (Fossat et al., 2010; Olivera et al., 1994)or even having an influence on severe major depression and bipolar disorder (Mallinger et al., 2008; Pazzaglia et al., 1998).

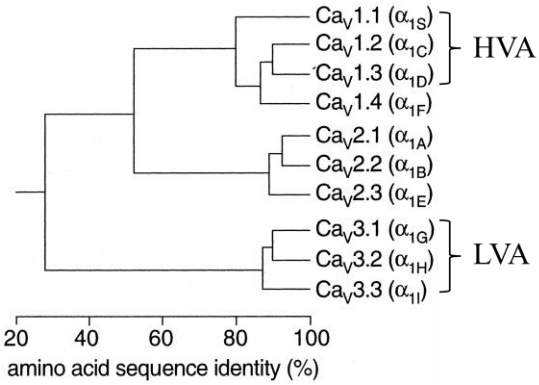

Figure 1: Overview of the Ca_V calcium channel family. The pedigree showing the sequence identity of the 10 genes encoding for HVA high- and LVA low voltage-activated calcium channels. Adopted and modified from Catterall et al., 2003.

The physiological and pharmacological properties of recorded nativeCa^{2+} currents had led to the assumption of the presence of various types of VGCCs (Reuter, 1979).

Bean and Nilius could demonstrate in1985for the presence of two different Ca^{2+} currents in cardiomyocytes with high and low threshold activation characteristics, and with fast and slow channel inactivation components. The Ca^{2+} current activation profiles in smooth, cardiac and skeletal muscle were very similar and predominantly detectable at higher voltage steps whereas inactivation was long lasting when $Ba^{2+}$was used as a charge carrier (Tsien et al., 1988). Additionally, these currents could be blocked by Ca^{2+} channel antagonists such as dihydropyridines, phenylalkylamines and benzothiazepines (Reuter 1979; Tsien et al., 1988). This led to the categorization of the high-voltage activated (HVA), long-lasting (L-type) calcium channels and their low-voltage activated counterparts showing a faster and transient (T-type) inactivation kinetic (Nowycky et al., 1985) and being insensitive to conventional Ca^{2+} channel antagonists. The L-type channels were further known to be regulated by second messenger proteins, auxiliary subunits and Ca^{2+} binding proteins. In 1975 Hagiwara could show the different types of

L-type calcium channels in starfish eggs which was then further characterized by Carbone and Lux in voltage-clamped dorsal root ganglion cells (Carbone and Lux, 1984). Nowycky and colleagues could later demonstrate from dissociated DRG and single-channel experiments about the presence of the N-type calcium currents which were activated at voltage ranges in between the potentials that activate L-and T-type currents. Additionally, this channels could be blocked selectively by the peptide ω-conotoxin GVIA from the marine cone snail *Conus geographus* (Tsien et al., 1988; Olivera et al., 1994). Characterizations of other Ca^{2+} channel subtypes followed like the P/Q- and R-types being identified by pharmacological blockade using various other spider toxins (Llinás and Yarom, 1981; Llinás et al., 1989). Whereas, L- and T-types can be found in nearly all cell types, the latter subtypes can be found predominantly in the central nervous system CNS.

1.2 The L-type family of voltage-gated calcium channels

The gene family of voltage-gated calcium channels (VGCC) consists of 10 membrane spanning proteins (Ca_V) (Figure1) that all differ in their unique electrophysiological and pharmacological properties. The voltage-gated calcium channels are hetero-multimeric protein structures that are composed of a pore-forming α_1-subunit that opens in response to membrane depolarization, whereas the accessory proteins such as the $\alpha_2\delta$, β and γ subunits modulate channel kinetics, surface expression and serve as molecular chaperones (Hullin et al., 2003; Bannister et al., 2011)

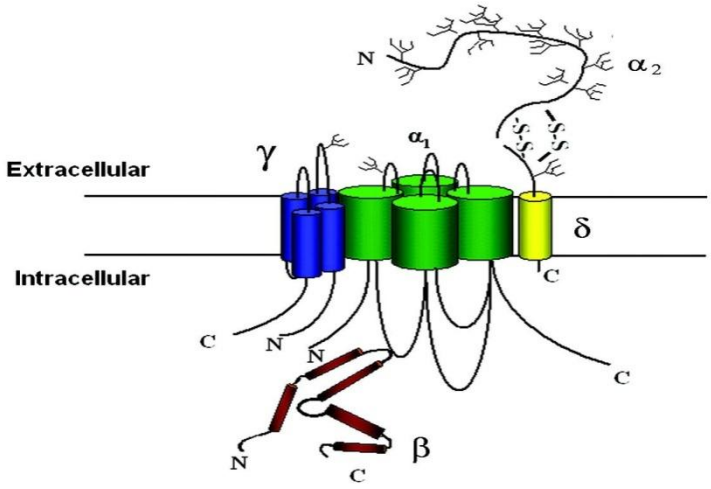

Figure 2 Schematic overview of the α_{1C} channel pore with auxiliary $\alpha_2\delta$, β and γ subunit. α_{1C} is incorporated into the plasma membrane by its various transmembrane segments. Adopted from (Arikkath and Campbell, 2003).

Owing to the pharmacologically distinct character of $Ca_V1.2$ in human physiology, these channels are important targets for already well established therapeutics (Catterall et al.,

2003). Furthermore, $Ca_V1.2$ channels may demonstrate promising new targets in the treatment of mental disorders due to their previously described physiological role in mood and mental conditions (Bauer et al., 2002; Sinnegger-Brauns et al., 2004; Casamassima et al., 2010).

The physiological/pathophysiological implications of alternative splicing in $Ca_V1.2$ channels have been suggested by our group and others in an extensive manner. In this context it could be demonstrated that several diseases maybe linked directly to aberrant or altered splicing of α_{1C}. There is extensive and growing evidence for altered splicing patterns contributing to cardiovascular diseases (Gidh-Jain et al., 1995; Tiwari et al., 2006) as well as exon-dependent phenotypes in complex neurological disorders such as the Timothy Syndrome (Splawski and Keating, 2004) or spinocerebellar ataxia-6 (Watase et al., 2008). These reports described altered splicing patterns of mutually exclusive exons as 21/22 or 8/8a from $Ca_V1.2$ which change their transcript levels during development or are simply affected by a single nucleotide polymorphism (SNP), resulting in severe pathophysiological consequences.

A central aspect of this PhD thesis is to better understand the structural and functional diversity of $Ca_V1.2$ generated by alternative splicing and to further understand the physiological relevance of these altered protein structures. For that, we analysed alternative splicing loci within the *CACNA1C*gene which we believe do have a prominent relevance on the overall electrophysiology of the channel structure resulting in altered channel gating, with a possible consequence on physiology/pathophysiology.

Throughout the last decade, growing evidences strongly suggest the possible role of L-type calcium channels in mental diseases such as bipolar disorder or schizophrenia (Levy and Janicak, 2000; Sklar et al., 2011). Some calcium channel blockers, e.g. verapamil, in combination with lithium were demonstrated to have a positive effect on people with depression (Mallinger et al. 2008). However, the understanding of the physiologic mechanism for this efficacy is largely unknown. An indirect effect could also be stated for complex neuronal diseases as Parkinson's disease (PD). Chan *et al.*(2010) showed in their work that the subtype unselective calcium channel blocker isradepine was capable of slowing down the onset of dying neurons in the substantia nigra by a "rejuvenation" process in neurons(Chan et al., 2010).

These reports emphasized the significant roles of calcium channels in biomedicine and form a fundamental motivation for this PhD thesis. Investigating the molecular nature of $Ca_V1.2$ can contribute to a better understanding of the patho-mechanisms of diseases associated with alternative splicing and may help to inform on new pharmacological strategies in the management of human diseases such as $Ca_V1.2$ channelopathies.

1.2.1. Physiological implication of calcium channel $Ca_V1.2$ in the cardiovascular system

The human heart is a powerful myogenic muscular organ which pumps around 2.5 billion times during an average human lifespan, supporting the circulatory system of the body with blood (Bers, 2000). The conducting system of the heart is a specific system allowing

the cells and the heart for its automaticity. From the sinoatrial (SA) node the conduction spreads over to the atrioventricular (AV)note, further to the His bundle to the very end of the ventricular tip allowing a time delayed depolarization over the whole sarcolemma of the heart within half a second. Any aberrant function of this well defined system inevitably leads to severe pathological conditions of the heart often affecting the whole body.

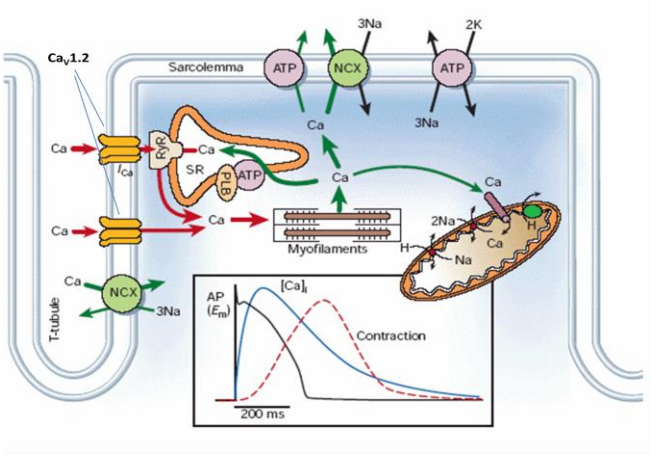

Figure 3: Excitation-contraction coupling. Activation of $Ca_V1.2$ calcium channels trigger the calcium release from the sarcoplasmatic reticulum (SR) and initiate the contraction (systolic) phase of the heart. A fine tuned assembly of various proteins aid in regulating calcium homeostasis in cardiac muscle cells. Adopted and adjusted from Bers 2000.

The molecular background behind this electrical conducting system is the presence of voltage-gated ion channels which sustain a balanced system of fine-tuned voltage-gated membrane proteins allowing ion flow across the membrane. The physiological implications of voltage-gated calcium channels of the heart are the conduction of Ca^{2+} ions into cardiomyocytes upon membrane depolarization to initiate excitation-contraction coupling. Based on their electrophysiological properties high- (HVA) and low- (LVA)

1. INTRODUCTION

Voltage activated calcium channels fulfill different physiological requirements, according to the electrical conductance in the heart. The L-type $Ca_V1.3$ and $Ca_V1.2$ and T-type $Ca_V3.2$ and $Ca_V3.1$ channels are known to be highly expressed in the heart and their expression pattern is developmentally regulated and tissue dependent. At early embryonic stages $Ca_V1.3$ is predominantly expressed in the ventricles. This is changed by a later embryonic state where the "nearly" mature heart will predominantly express $Ca_V1.2$ in the ventricles(Marsh, 1989). Similar expression and developmental rearrangements can be described for the T-type in the heart, where $Ca_V3.1$ is mainly expressed (Cribbs, 2010) and the $Ca_V3.2$ form is finally absent in the adult murine heart (Niwa et al., 2005)

The $Ca_V1.3$ channels which play a role in pace-making activity are highly expressed in the sinoatrial node and atrioventricular node (Mangoni et al., 2003; Zhang et al., 2005), while the $Ca_V1.2$ channels serve its function mainly in the ventricular cardiomyocytes where they are conduits for Ca^{2+} influx into the myocardial cells(Bers and Guo, 2005; Schröder et al., 2007). From fetal to adult development of the heart, calcium channel composition is subject to a highly dynamic remodeling process (Reuter et al., 1983; An et al., 1996). The $Ca_V1.2$ calcium channels in rats are known to be expressed to a different extent in a developmental and tissue dependent manner (Liao et al., 2005; Tang et al., 2008). This calcium current I_{Ca} triggers the calcium induced calcium release (CICR) from the sarcoplasmatic reticulum (SR) via Ryanodine receptors (RYRs) which set in motion for the muscle to contract (contraction phase). During relaxation phase, the clearance of Ca^{2+} ions from the cytosol brings the Ca^{2+}concentration back to a normal physiological level. Subsequent relaxation of the muscle cell (dilatation phase) is promoted by the

activities of the Na/Ca exchanger (NCX) and the Sarco-Endoplasmatic Reticulum Calcium ATPase pump (SERCA) (see fig. 3).Further reports described another role of the $Ca_V1.2$ channels and that involved the cleaved carboxy-portion of $Ca_V1.2$ channel that was purported to translocate into the nucleus to initiate gene transcription (Ospina et al., 2005).

1.2.2 Cardiovascular diseases (CVDs) in the global society

Cardiovascular diseases still remain as the most dominant burden to human and economic costs in the modern society and they are the number one cause of death and disability in the world. In 2008, 17 million people died of CVDs and of these 3 million deaths were of individuals who were below the average age of 60 years (WHO, Global Atlas on cardiovascular disease prevention and control, 2011). The economic costs of CVDs in the USA are estimated to be at a level of €310 billion compared to €146 billion for cancer and €22 billion for HIV infection (Thom et al., 2006). The trend in the last two decades in CVD prevalence around the world has been alarming as the number is increasing in the second- and third-world countries, whereas it is slowly declining in the first-world countries. Among CVDs, arteriosclerosis and cardiac arrhythmia represent only two out of a wide spectrum of diseases affecting the vascular and cardiac systems that should be addressed in the context of this PhD work in more detail.

For that, these facts about CVDs make it compelling to further understand the complexity of physiological and pathophysiological conditions of the human heart for better intervention and to find new therapeutic approaches in cardiovascular disease management.

1.2.3 Mental disorders in modern global society

Mental diseases are one of the most costly and challenging diseases in modern societies aside from cardiovascular diseases, cancer and metabolic disease (Bloom et al., 2011). A survey carried out by the National Institute of Health, NIH, revealed that mental disorders have an societal cost of US$193 billion per year on the American economy with an increasing trend (Kessler et al., 2003).According to the WHO, more than 30% of people face at least one severe mental episode during their lifetime (WHO International Consortium in Psychiatric Epidemiology (Anon et al., 2000). Among all mental disorders, anxiety disorders seem to be the most common in all countries, followed by mood disorders such as depression and bipolar disorders (The World Mental Health Survey Initiative). In the European society, anxiety disorders, depression, post-traumatic stress disorders (PTSD) or panic disorders occur with a prevalence of 11-20% spearheading the most frequent occurring disease among mental disorders (Sobocki and Wittchen, 2005).

Although medical intervention is broad and often useful, medication can only alleviate the symptoms and not cure the disease. The antidepressants of the SSRI class (Prozac®, Seroxat®) and benzodiazepines (Xanax®) or tricyclic antidepressants (Elavil®) are effective and commonly prescribed drugs in anxiety disorders (Ravindran and Stein, 2010)with often a good response helping to enhance quality of living. However, they often come with severe side effects for those who respond to the drug. For that, a deeper understanding of the physiological and pathophysiological conditions of mental diseases

is required to explore new drug targets and to tailor individual therapies to patients with mental problems.

1.2.4 Neurobiology of fear and anxiety

Fear and anxiety are well encoded fundamental emotional traits accompanying human beings throughout their whole live. A clear cut between both features is often hard to make and dependent on the scientific discipline. In neuroscience, fear can be defined as a response to an explicit threat whereas anxiety is understood as a response to a rather undetermined, potential hazardous situation (Sylvers et al., 2011). Although both traits are closely interrelated, fear and anxiety certainly differ in terms to their behavioral response. Latter one often results in severe pathological forms of anxiety disorders where a response is not anymore proportional to the receiving stimuli (PTSD, phobia). In that case, the aimed evolutionary beneficial character of anxiety to serve and protect and to increase the survival chances has been lost.

In humans and rodents, limbic and cortical areas as the amygdala, hippocampus, thalamus, hypothalamus and the prefrontal cortex are known to be phylogenetically related structures (Pine 2009, Canteras et al., 2010). The well known facts about molecular biological imbalance in terms of neurotransmitter release, the high comorbitity of anxiety and depression of 60% (Kessler et al., 2003) and the apparently slight crossing between physiological and pathological states are the subject to current research interest.

1.2.5 A physiological implication of voltage-gated calcium channels in mood disorders

Although the possible implication of L-type calcium channels$Ca_V1.2$ and $Ca_V1.3$ in fear memory and anxiety disorders is nothing unfamiliar (Bauer et al., 2002; McKinney and Murphy, 2006; Busquet et al., 2008; 2010), there is new and compelling evidence about the role of $Ca_V1.2$ channels in mental disorders (Bauer et al., 2002; Sinnegger-Brauns et al., 2004; McKinney and Murphy, 2006; Busquet et al., 2008; Ferreira et al., 2008; Greenberg et al., 2008; Busquet et al., 2010; Green et al., 2010; Sklar et al., 2011). The group headed by Nicolas Singewald could demonstrate in their publication from 2008 about the physiological implication of $Ca_V1.2$ in fear extinction (Busquet et al., 2008). In this study the group evaluated the contribution of $Ca_V1.2$ and $Ca_V1.3$ in fear extinction. As there is no selective calcium channel blocker available till today to distinguish between the two channel subtypes, DHP insensitive $Ca_V1.2DHP^{-/-}$ mice were used to address this question. In accordance with previous publications, WT $Ca_V1.2$ mice showed impaired fear extinction upon systemic administration of nifedipine whereas the DHP effect was completely abolished in their $Ca_V1.2DHP^{-/-}$ counterparts, indicating that fear extinction are mediated by $Ca_V1.2$ and not by $Ca_V1.3$. However, this effect seemed to be mediated by peripheral $Ca_V1.2$ channels as intracerebroventricular (i.c.v) injection of 1 mg/kg nifedipine did not trigger the fear extinction effect in WT.

Based on the findings from our and other laboratories (Tang et al., 2004, Liao et al., 2004, Tiwari et al., 2006, Splawski et al., 2004) on how alternative splicing can influence the physiological/pathophysiological equilibrium of certain disease we asked if mental

circumstances may also lead to general or maybe fundamental anomalies in the splicing profile of $Ca_V1.2$. Hence, we wanted to elaborate if various splice combinations of mutually exclusive exons in $Ca_V1.2$ influence electrophysiological (Liao et al., 2007, Li et al., manuscript in progress) properties of the channel. As a model to address our question we used mouse strains showing different levels of anxiety. The genotype of these High-, Low- and No- anxiety animals, respectively named HAB, LAB and NAB is unclear. The animals were tested upon their performance on the elevated plus maze and bred with equal performers.

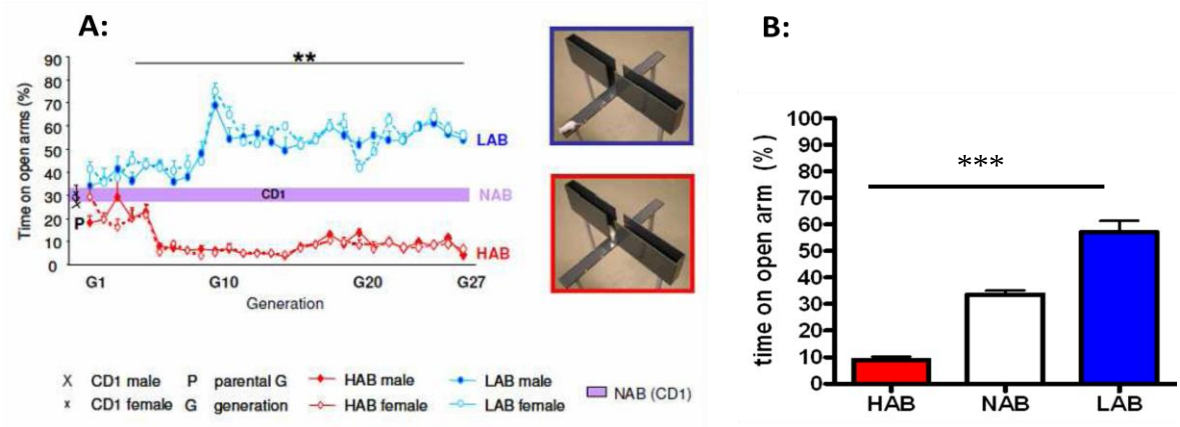

Figure 4 Diagram showing the performance on HAB, NAB and LAB animals on the elevated plus maze EPM in regards of time spent on the open arm (gender and generation specific). Kindly provided by Dr. Ludwig Czibere and Prof Landgraf. B Statistics is based on 7 animals per group, one way ANOVA, $p < 0.05$).

1.3 Trait anxiety mouse model HAB/LAB/NAB. Implications of $Ca_V1.2$ in mental disease

The animal models for trait anxiety were kindly provided by our collaborating partner Prof. Dr. Nicolas Singewald, Innsbruck, Austria. The models for the study of pathological anxiety were selectively and bi-directionally bred for extremes in anxiety-

related behavior by Prof. Rainer Landgraf and colleagues (Behavioral and Neuroendocrinology, Max Planck Institute of Psychiatry, Munich, Germany). The outbreed CD1 animals were categorized for selective and bidirectional breeding according to their performance on the elevated plus-maze (EPM) and their exposure time to the open arms (OA). The aim of a bidirectional selective breeding process is the accumulation of genes associated with a specific trait, thus shifting the phenotypes from the population mean. Rodents are characterized by a natural innate fear of unprotected and heightened areas (Pellow et al., 1985; Lister, 1987) and the EPM principle generates an avoidance conflict between the exploratory drive of the animal and its innate fear. A genetic predisposition for trait anxiety is considered to correlate with the time spent on the EPM open arms. The open arm dwell time (%) of the mice is an indicator for the breeding partner respectively and the animals were bred with the corresponding partners to generate the behavioral extreme phenotypes. Animals spending less than 10% of the test time on the open arms were categorized as the high anxiety-related behavior (HAB) line, whereas mice spending most of the test time on the open arms (~50% or more) were categorized as low anxiety related behavior (LAB) line. Normal anxiety-related behavior (NAB) mice display an intermediate phenotype (time spent on open arms ~30%). Various publications have reported the usefulness and importance of theses mouse lines in identifying genetic factors that regulate the development of anxiety (Murgatroyd, 2005; Bosch and Neumann, 2008; Busquet et al., 2008) For this PhD study, we further characterized the animals with regards to their innate trait anxiety and molecular biological characteristics as transcriptional modification of the calcium channel $Ca_V1.2$.

Recent publications have shown a possible physiological/pathophysiological implication of $Ca_V1.2$ in anxiety and depression (Busquet et al. 2008, Sinnegger-Brauns et al., 2004).

1.4 Molecular aspects of $Ca_V1.2$ L-type calcium channels in human physiology

1.4.1 Alternative splicing

Posttranscriptional modification (PTM) is a molecular remodeling process of the early pre-mRNA which allows a system to adapt in a tissue- and development-dependent manner (Black, 2003). Alternative splicing, as a main contributor to post-transcriptional modification (PTM), besides RNA editing, is a highly organized and defined shuffling process of alternative exons to assemble protein variations with diverse biological and functional options. It is estimated that more than 60% (Modrek and Lee, 2002) of human genes undergo alternative splicing; hence this puzzling process depicts a major contributor to protein isoform diversity in all vertebrates. The shuffling of exons can happen in many different ways (figure 4). Most of the exons are constitutively expressed, which means that they are always included and translated. The excision of the intronic region is guided by pre-determined nucleotide sequences, such as GU at the 5'splice donor site marking the exon/intron boundary and the AG di-nucleotide sequence at the 3'splice acceptor site and the branch point (Burge et al., 1999). These splice sites are initial sequences for the spliceosome that recognize the boundary sequences whereas an

adenine within the branch site represents a key element for the excision of the intron. Exons that are either excluded or included are called cassette exons.

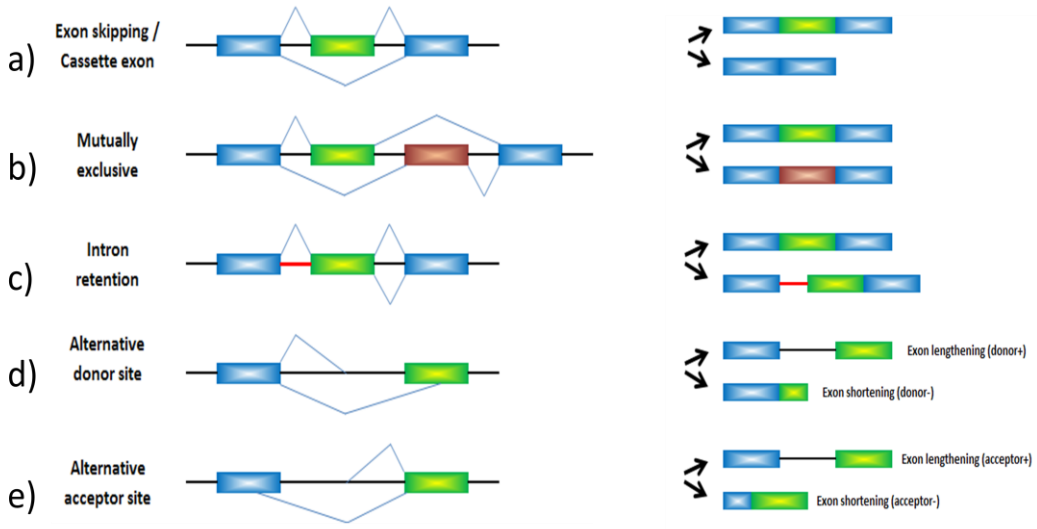

Figure 5: Shematic overview of alternative splicing as a fundamental molecular process of PTM. Exon shuffling can be arranged to many different transcripts. In each scenario) to d), a single RNA transcript is spliced into two possible mRNA fragments finally resulting in a broad spectrum of functional diversified proteins.

Inclusion or exclusion of exon pairs can be mutually exclusive, meaning only the specific exon sequence or its counterpart is added to the final transcripts. However, recent findings by our group showed that mutually exclusive exons can indeed appear in a sequence together, resulting in a dominant negative effect (Tang et al., 2007). Exon extension or truncation is also known either at the 5'splice or 3'splice site whereas the mature transcript results in a longer or shorter exon version. Finally, intron retention is the most controversial form of splicing as the intronic region is maintained in the mature transcript (Matlin et al., 2005) and often degraded due to inserted stop codons (Lareau et al., 2004). Taken together, alternative splicing results in a wide array of transcripts that once encoded can produce a large range of protein isoforms that respond differently to

ligand binding, enzymatic activity, or protein localization, resulting in various changes in cellular or developmental processes. Although alternative splicing is processed with high fidelity, errors in the splicing machinery often lead to severe errors with sometimes fatal cellular and pathophysiological consequences (Black, 1998; Grabowski and Black, 2001; Splawski et al., 2004; Tiwari et al., 2006). In the following paragraph, these consequences shall be addressed in more detail in regards to the expression of the $Ca_V1.2$ calcium channels.

1.4.2 Alternative splicing of L-type $Ca_V1.2$ calcium channel isoforms

1.4.2.1 Functional role in biology and disease

Understanding the structure-function and distribution of alternative exons can be of great help in providing plausible explanations for disease severity. This is especially obvious in the patients who suffer from Timothy syndrome. Mutations discovered in the mutually exclusive exons 8/8a that was found to be expressed at a higher level in heart were associated with more severe cardiac disorder phenotype (Splawski et al., 2004; 2005). Hence data obtained from *in-vitro* heterologous expression systems do have an important role to finally evaluate the functional changes which underlie splicing and produce different electrophysiological and pharmacological $Ca_V1.2$ channel variants (Liao et al., 2007).

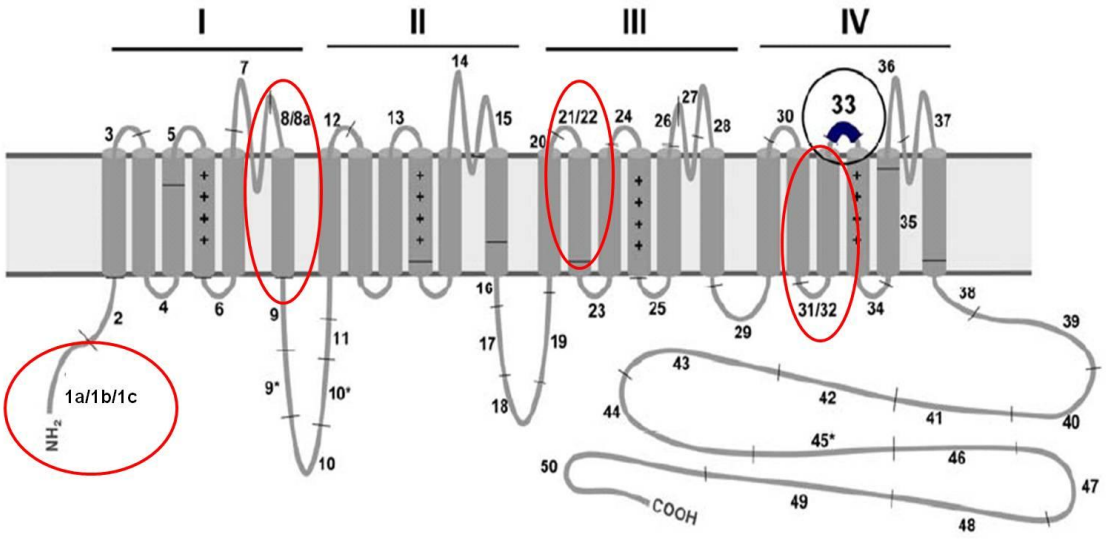

Figure 6: Hypothetical topology of the $Ca_V1.2$ splice variants. Four hexa-helical (S1-S6) transmembrane domains (I-IV) encode for the alpha1 subunit.S4 depicts the voltage sensor with 3-5 positively charged residues. The extra-cytosolic S5-S6 loop structures lines the pore and serves as a selective filter. Mutually exclusive exons are highlighted in red circles. N-terminus 1a/1b/1c, IS6 8/8a, IIIS2 and IVS3. In blue: exon 33 a cassette exon.

The human $Ca_V1.2$ channel is known to be extensively spliced where 20 out of 56 exons are subject to alternative splicing (Abernethy and Soldatov, 2002; Tang et al., 2004; Liao et al., 2005; Cheng et al., 2007; Bannister et al., 2011). The $Ca_V1.2$ splice patterns carry their own tissue signature and isoforms can be segregated into smooth-muscle and cardiac-muscle versions containing specific splice combinations (Welling et al., 1997; Liao et al., 2004; 2005; 2007). Of therapeutic importance is mutually exclusive exon 8/8a which encodes for the IS6 segment which is well known to affect the sensitivity to dihydropyridines (DHP) (Liao et al., 2007; Welling et al., 1997). Tissue-specific alternative splicing revealed that both exons affect pharmacological properties differently (Liao et al., 2007).

1.4.3.2. N-terminal human $Ca_V1.2$ isoforms and implication on structure and function relationship

The N-terminus of murine $Ca_V1.2$ can either be comprised of the mutually exclusive exons 1a/1b or the recently discovered 1c isoform by the group of Jonathan Jagger (Cheng et al., 2007). Jagger's group further demonstrated that exon 1b and 1c are both tissue dependently expressed in rat and human resistant cerebral arteries. Moreover they showed that short hairpin shRNA specific against either the 1b or 1c isoform can compensate/up regulate the opposed version by reducing the whole cell $Ca_V1.2$ currents and induce either a vasoconstriction or a vasodilatation. In the late 1990s, Nathan Dascal's group described the significant structure and functional role of a rabbit α_{1C} cardiac isoform, demonstrating that deletion of the initial 46 aa of the N-terminus resulted in an increased Ca^{2+} current density by changing the channel open probability without altering channel surface expression (Shistik et al., 1998; Kanevsky and Dascal, 2006). Further studies of exon 1a of rat heart and brain provided evidence for the interaction of PKC and the β_{2a} subunit within the first 20 aa residues, underpinning the important functional role of the N-terminus (Shistik et al., 1999)

Human long exon 1a: MLRAFVQPGTPAYQPLPSHLSANTEVKFKGTLVHEAQLNYFYISPG
Human short exon 1b: MVNENTRMYIPEENHQ

Figure 7: Amino acid sequence representing the long form (1a) 46 aa and short form (1b) 16 aa of human *CACNA1C*.

.

In this regard, it is important for this study to understand to which extent tissue-specific expression of exon 1a and 1b may change structure and functional properties of the human $Ca_V1.2$ channels. However, attempts to isolate the exon 1c isoform from human arteries was not successful and we therefore focused on the abundantly expressed cardiac and smooth muscle versions of the $Ca_V1.2$ channels (Figure6). Single-channel recordings in combination with whole-cell electrophysiological recordings should allow a closer insight into the channel gating properties and allowing for a discrimination of the mechanistic understanding of changes in channel gating. In this thesis and based on previous published data by Jagger's and Dascal's group we hypothesize that channel gating based on the two mentioned isoform 1a/1b changes the fundamental functional properties of $Ca_V1.2$.We further believe that tissue specific splicing fulfills its need

1.4.3.3. Mutually exclusive exons 21/22, 31/32 and cassette exon 33 and its contribution to physiology and disease

Since the last decade, alternative splicing has been linked to disease in several crucial publications. The Soldatov group demonstrated changes in splicing patterns of $Ca_V1.2$ in proliferation of vascular smooth muscle cells VSMC in arteriosclerosis. Remodeling of mutually exclusive 21/22 in combination with exon 41A was found to be expressed to a different extent and repertoire in arteriosclerosis tissue compared to non-arteriosclerotic tissue. The switch to exon 22 in arteriosclerotic tissue significantly changed the electrophysiological properties of $Ca_V1.2$ indicating a Pathophysiological relevance of

exon 22 in arteriosclerosis. In a related work, mutually exclusive exon 31/32 distribution was changed in an induced myocardial infarction rat model (Gidh-Jain et al., 1995). El-Sherif's group showed that the expression levels of the ratio of fetal: adult isoform in the myocardium reemerged, whereas the fetal phenotype was predominantly expressed in the rat model of post myocardial infarction. A subsequent study showed that this critical fetal isoform also reemerged in human heart failure tissue (Yang et al., 2000). An attempt to screen for human $Ca_V1.2$ splice variation was carried out by our group with the transcript scanning method to screen for full length $Ca_V1.2$ splice variants in fetal/adult brain and heart. A large variation of functional active transcripts was discovered to be expressed in a development-dependent manner bringing our focus to the IVS3-S4 segment representing a large combinatorial profile of exons 31-33. These variations revealed an unmistakable shift in steady-state activation whereas the IVS3-S4 linker length correlated with channel activation at higher depolarized potentials (Tang et al., 2004). Similar finding from *in-vitro* studies from our group demonstrated the important functional role of exon 9* and Δ33 of smooth muscle and cardiac muscle isoforms of $Ca_V1.2$ channels (Tang et al., 2007). In agreement with our *in vitro* findings from 2004, inclusion or exclusion of cassette exon 33 clearly changed basic electrophysiological properties in regards of its steady-state activation and inactivation kinetics. Furthermore, our group also demonstrated that exon 33 expression can be regulated in pathology where 20% of exon 33 was excluded in $Ca_V1.2$ within the surviving rat myocardial infracted left ventricles (Liao et al., 2008). However, these *in vitro* experiments uncovering functional changes of the $Ca_V1.2$channel properties at best only provide limited predictions for the

in vivo consequences. That is why we focused on the exclusion of cassette exon 33 in a mouse genetically targeted to remove exon 33 from the mouse genome.

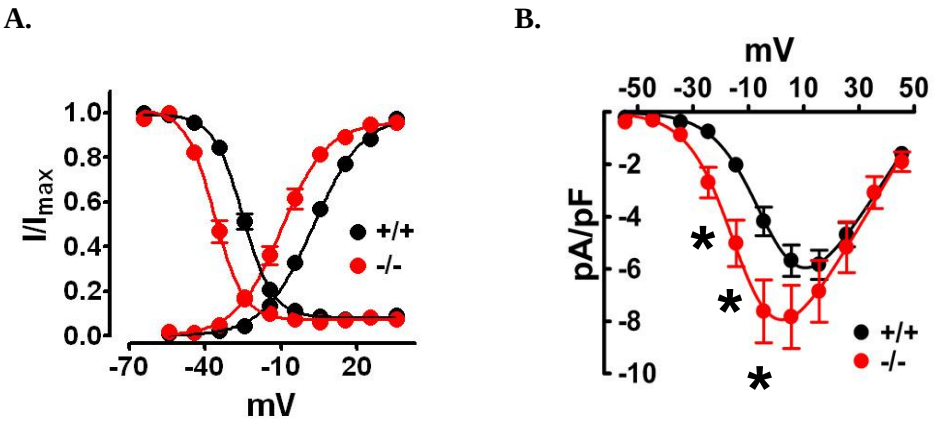

Figure 8: Whole cell steady-state kinetics of Δ33 of $Ca_V1.2$ in cardiomyocytes. A. Activation/inactivation profile in -/- is significantly left shifted towards +/+. B. Current density of -/- is enlarged by 30%. Adopted from Li et al., (manuscript in preparation).

The cardiac phenotypes of the exon $33^{-/-}$ KO were more prone to developing cardiac arrhythmia and the echocardiographic profile showed increased contractility resulting in ventricular arrhythmia of a *Torsade de pointes* form (Li et al., manuscript in preparation) The underpinning mechanism could be explained by altered steady-state activation/inactivation profile and a robust increase in calcium current density (fig. 8). However, since the larger current influx could not be explained by a higher $Ca_V1.2$ channel surface expression, we predicted that only individual channel gating can be altered due to the exclusion of exon 33. That is why single-channel recording was performed to test the hypothesis of an altered channel function of $Ca_V1.2_{\Delta33}$. The usefulness of single-channel recordings as a tool to highlight biophysical and

pharmacological changes has been reported in the past by various groups (Yue et al., 1990; Schröder and Herzig, 1999; Gröner et al., 2004) in the context of cardiovascular studies. For example, Schroeder *et al*. demonstrated in their work in 1998, that $Ca_V1.2$ from human failing heart samples show a significant increase of single-channel open probability accompanied by significantly higher channel availability. The latter result provided further explanation to a general mechanism implying Phosphatase 2B (PP2B) is compromised in the failing cardiac system increasing channel availability. However, this technique is gaining more and more popularity in the field of electrophysiology although the idea to detect and record single ion channels is not new. This thesis provides strong evidence about the usefulness of single-channel patch-clamp recordings towards the commonly used whole cell patch-clamp techniques especially in terms of structure-function changes of $Ca_V1.2$ channels that result from alternative splicing. The next paragraph will highlight the advantages of the cell attached mode of single-channel recordings in relation to the whole cell technique.

1.5. Single-channel vs. whole cell recordings in cardiovascular studies

Studying the gating of unitary single-channel events in recombinant systems or in cardiomyocytes is *per se* nothing new. Neher and Sakmann were awarded the Nobel Prize in Medicine and Physiology for this seminal technique in 1991. However, cell attached recording was exciting and new at the beginning of the 1990s but seemed to lose its popularity within the last two decades, most likely because of often unpredictable

technical problems due to noise or amplification limitations. Furthermore, an increasing amount of required data due to large scale sampling and software limitations made this technique redundant. Since whole-cell recording was also available, more approachable and often sufficient for most of the required needs, single-channel recordings became an uncommonly used technique and the expertise is still difficult to find nowadays. In any case, whole-cell recordings only allow for a limited insight into channel gating as an entire channel population expressed on the cell is recorded at the same time. Detecting single ion channel allows making predictions about open and close events on a micro scale. Furthermore, drug interaction can be studied in real-time (Michels et al., 2005) and biophysical approaches can help to understand fundamental gating principles (Bartels et al., 2009). Since the completion of the human genome project and an increasing new knowledge and interest in molecular compounds and interaction sites, electrophysiology is getting more and more popular especially in the fields of fundamental science like physiology and pharmacology. This argument inevitably leads to new interests in electrophysiological approaches and hence to a significant interest in single-channel detection. (For a broader introduction of single-channel recording please refer to the Material and Methods section of this thesis.)

1.6 Aims and goals of the study

The understanding of the structure and function of L-type calcium channels in human physiology lays the basis for decisions on what novel directions to take in expanding on the management of various pathological conditions such as cardiovascular or neurological diseases (Tiwari et al. 2006, Splawski et al., 2004). Since the last 10 years and after the completion of the first draft of the human genome project, there are more evidences to indicate that L-type calcium channels may play a direct or indirect role in mental disorders, such as in depression, bipolar disorder, schizophrenia and posttraumatic stress disorder (PTSD) (Sinnegger-Brauns et al., 2004, Busquet et al., 2008, Bauer et al., 2002). Mental disorders are, beside cardiovascular disease and diabetes; undoubtedly a huge burden for modern societies and a financial burden for the global economy. For that, a better physiological understanding and new pharmacological agents for therapeutic treatments are highly desirable in cardiovascular and neurological diseases.

The ultimate goal and aim of this PhD thesis is to further understand the functional consequences that are linked to aberrant alternative splicing of L-type $Ca_V1.2$.calcium channels in vitro and ex vivo. Our group has already demonstrated in previous work about the significant role of exon 33 inclusion/exclusion in a recombinant system and in a exon 33 knock-out mouse, they showed that a severe form of cardiac arrhythmia was expressed (Torsade des pointes) (Li et al., manuscript in preparation). Hence this work shall contribute to a better physiological understanding of how posttranscriptional modifications can correlate with complex disease like cardiovascular disease and anxiety disorders. For the latter we used our anxiety mouse models hypothesising that different

phenotypes of anxiety, respectively HAB, LAB and NAB can be correlated with aberrant splicing of $Ca_V1.2$. For that, single-channel recording technique helped to better understand the biophysical properties that go along with aberrant calcium channel gating. Furthermore, pharmacological approaches can be evaluated in more detail with this technique, allowing the investigation of interaction of the channel with potentially new therapeutics. Understanding the physiological and pathophysiological nature of L-type calcium channel splice isoforms can certainly help to understand how disease states develop in patients.

Chapter II

2. MATERIAL AND METHODS

2.1 Cell culture and plasmids

2.1.1 Culture of native HEK293 cells

Cryo shock-frosted tubes with cells were immediately transferred to a 37 °C water bath and thawed. Cells were then transferred to a 50 ml falcon tube containing 9 ml of fresh selective Dulbecco's Modified Eagle Medium (DMEM) and centrifuged for 5 min. at 500 rpm. The supernatant was discarded and the process repeated 2 times; subsequently the cell pellet resuspended in fresh medium and transferred to a T25 flask for growing overnight at 37 °C, 5% CO_2. Cells usually reach a confluency of 70-80% after 48 hours and are ready then for splitting.

After 48 hours, cell medium was evacuated and cells washed 2x with 4 ml phosphate buffer (10% PBS). To detach the adherent cells from the flask, 1 ml of a 0.05% trypsin was pipetted into the flask and removed immediately after. The HEK 293 cells were trypsinised for 2 min. at 37 °C, 5% CO_2 and the reaction stopped with 5 ml of fresh medium. Approximately 1 ml of resuspended cells was grown again in a T25 flask containing 4 ml of fresh DMEM containing antibiotics. Further splitting needed to be carried out 48-72 hours after.

2.1.2 Plasmids and generation of constructs

HEK 293 cells were transiently transfected with pcDNA3.1 vector carrying a coding sequence for either the human smooth muscle $Ca_V1.2$ *77WT 1b/8/*Δ*9/32/33(*Liao et al., 2007) or the cardiac *1a/8a/*Δ*9/32/33* (provided by Dr. Roger Zuhlke). Exon 1a/1b was

sub-cloned either into the cardiac or smooth muscle backbone resulting in *778a*and *1a77*respectively. (s. figure 9). Beside neomycin or ampicillin resistance, the vector carries a multiple cloning site (MCS), 5' downstream of a promoter region (P_{CMV}).The $Ca_V1.2$ isoforms *1a77*,*77WT*and*1a77*were kindly provided by Dr Liao Ping (NNI, Singapore).

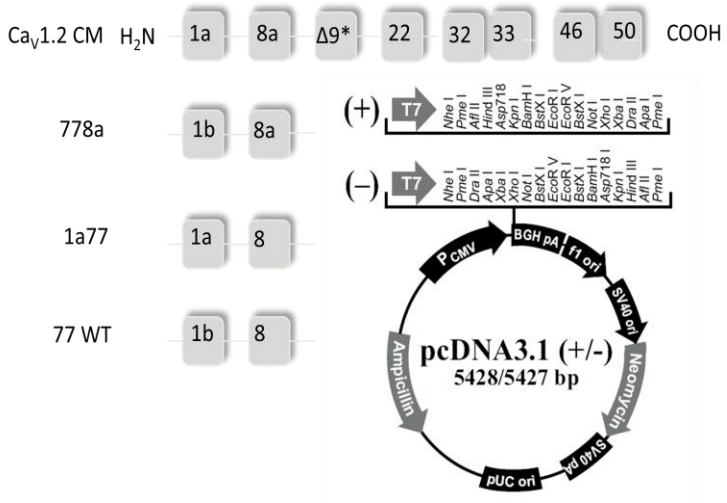

Figure 9: N-terminal splice variants with backbone structure cloned into the MCS of a pcDNA3.1 vector. Isoform 778a was created by simply swapping exon 1b from the 77WT isoform into the cardiac CM isoform. 778a was then positively identified by sequencing.

2.1.3 Sub-cloning of humCa_V1.2 variant 778a into a cardiac backbone structure

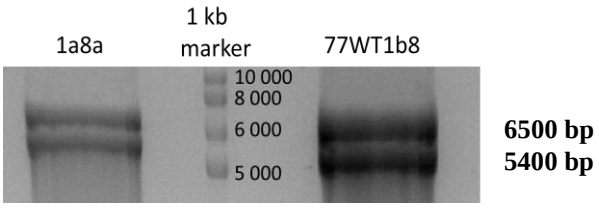

Figure 10: Identification of representative *CaCNA1C* bands on a 1% gel after digestion of pcDNA3.1 with Afe1 and Xba1. Bands showed the correct expected size of around 6500bp and 5400 bp were dissected and ligated for 4 hours at RT, respectively.

For electrophysiological studies, *778a* clone was constructed from the already existing 77WT and cardiac Ca_V1.2 CM clones. Both plasmids were digested with Afe1 and Xba1 for 2 hours and the resulting bands were identified on a 1% agarose gel (figure 10). Afe1 digested the channel coding sequence once leaving blunt ends within exon 2 whereas Xba1 digested once within the pcDNA 3.1 vector leaving sticky ends. After 4 hours of ligation at RT with T4-Ligase (Invitrogen*), E.coli* was transformed by heat shock and plated on an ampicillin containing agar plate overnight at 37 °C. On the next day 12 clones were picked and DNA was amplified with a Minikit (Quiagen). The chimera 1b/8a was digested with HindIII and the resulting band later identified against a positive control on a 1% agarose gel. A sequencing analysis and gating analysis was later carried out to check for functional integrity of the channel.

2.1.4 Transient transfection of HEK 293 cells

2.1.4.1 Calcium phosphate method

For whole-cell recordings cells at a confluence of > 70% were transiently transfected with the calcium phosphate method using HBS (ph = 6.8) and 1M $CaCl_2$. Ratio of transfected subunits was kept at 1:1:1. In a freshly autoclaved 1.5 ml tube A1C, β_2a, $\alpha_2\sigma$ and TAG were pipetted to 150 µl of $CaCl_2$ and subsequently 150µl of HBS was added drop wise. The whole reaction mix was incubated at RT for 20 min. and then given to a T25 flask containing cells and 4 ml of DMEM without antibiotics. The incubation was carried out at 37 °C, 5 % CO_2 for not longer than 6 hours. Medium was changed after 6 hours with 4 ml of DMEM containing antibiotics. On the following day, cells were trypsinised, resuspended and plated onto 60 mm Petri dishes containing 2 ml of DMEM (Ampicillin) before electrophysiolocal recordings.

2.1.4.2 The Effectene®method

Transfection was carried out usually 24 hours after subcultivation at a confluence of 20-30%, as the transfection efficiency was about 40-50% at this stage. Effectene® is a mild transfection reagents that is best used for cells recorded in the cell attached configuration. The non liposomal lipid reagent Effectene® spontaneously forms micelles and compresses the DNA. In a ratio of 1:1:1:1 of α_1c, β_2a, $\alpha_2\sigma$ and TAG were given to an enhancer solution, whereas 1 µg of DNA was added to 8 ml of enhancer, vortexed for 5 sec and incubated at RT for 5 min. The DNA concentrations were adjusted to a minimal

to ensure a low level of expression to detect single-channel events. To the reaction mix was then added 25 ml per 1µg of DNA, vortexed for 10 sec and additionally incubated again at RT for 10 min. The mix was dissolved in 1ml of fresh DMEM (antibiotics) and given to a T25 flask containing 4ml DMEM and cells. Incubation time was 6-24 hours at 37 °C, 5% CO_2. Cells were only recorded 72 hours after transfection.

2.3. Molecular biology

2.3.1 mRNA extractions from HAB, LAB and NAB mouse brains for colony screening

For mRNA extraction, brain samples (kindly dissected and provided by Dr. Simone Sartori, Innsbruck, Austria) were prepared by using either RNeasy® Kits (QIAGEN Science, Maryland, USA) for colony screening purposes or by using a guanidinium isothiocyanate solution (Trizol® method) for real-time PCR. For the Trizol®method, -80 °C frozen samples (amygdala, hippocampus and prefrontal cortex) were soaked in 0.8 – 1ml of Trizol® and homogenized with a common homogenizer (Heidolph, DIAX 900, Germany). Samples were then incubated at RT for 5 min. and centrifuged at 12 000 rpm for 15 min. Upon centrifugation, the upper phase containing the mRNA was carefully sucked up with a pipette and treated with an equal amount of isopropanol. Samples were centrifuged at 12 000 rpm for further 10 min. After centrifugation the pellet was resuspended in 70% of ethanol. Further centrifugation at 7500 rpm for 5 min extracted a

clear pellet that was dried on air and finally dissolved in RNAse free water. The RNA quantity was measured by spectrometry and used for further experiments. Samples measured at a wavelength of 260/280 had usually a ratio of > 1.6 and were immediately used for reverse transcription or stored at -80 °C.

2.3.2 Reverse Transcription and transcript-scanning by Polymerase Chain Reaction

The mRNA was reverse transcribed using oligo(dT) primers and Superscript™ III Reverse Transcriptase (Invitrogen). For obtaining first strand DNA an initial heating step of 65°C was used for five min. before a quick chill on ice. The reaction mix containing 5x first strand buffer, 0.1 M DTT and 200 Units enzyme were then incubated at 50 °C for 60 min. and additionally inactivated by heating at 70°C for 15 min. First strand DNA was then either stored at -80 °C or directly used for further experiments.

Table 1: Primer pairs used for PCR with used cycle length and expected amplicon size. **In Bold**: Specific primers used for colony screening. ***Italic***: Primers for mutually exclusive amplicon scanning.

Exon spanning region	Primer pairs		Expected Size (bp)	Tm (°C)	No.of cycles
	Forward Primer	Reverse Primer			
7-11	*5'-GTGTATCACCATGGAGGGCTGG-3'*	*5'-CTGAATTTGGATTTGGAGATCCGATGG-3'*	*437*	*55*	*35*
19-23	*5'-GAGCTGCACCTTAAGGAAAAGG-3'*	*5'-GGATGCCAAAGGAGATGAGG-3'*	*370*	*50*	*45*
30-34	*5'-CACTATGGCCAGAGCTGCCTC-3'*	*5'-GGACTTGATGAAGGTCCACAGC-3'*	*351*	*60*	*35*
8-11	**5'-GTCAATGATGCCGTAGGAAGG-3'**	**5'-CTGAATTTGGATTTGGAGATCCGATGG-3'**	**397**	**53**	**25**
8a-11	**5'-ATGCAAGACGCTATGGGCTAT-3'**	**5'-CTGAATTTGGATTTGGAGATCCGATGG-3'**	**397**	**53**	**25**
21-23	**5'-TACCACCATTTTCACCATTGAAATTGC-3'**	**5'-GGATGCCAAAGGAGATGAGG-3'**	**140**	**57**	**25**
22-23	**5'-AGGCAATGCAGACTATGTCTTCACTAGTATC-3'**	**5'-GGATGCCAAAGGAGATGAGG-3'**	**161**	**57**	**25**
31-34	**5'-AATTGATGTCATTCTCAGTGAGACTA-3'**	**5'-GGACTTGATGAAGGTCCACAGC-3'**	**187**	**53**	**25**
32-34	**5'-TGTTGATATAGCAATCACCGAGGTAC-3'**	**5'-GGACTTGATGAAGGTCCACAGC-3'**	**187**	**53**	**25**

For Polymerase Chain Reaction, primers (tab.1) were designed with DNAstar (Lasergene) and obtained from Sigma-Aldrich® (Singapore). GoTaq® flexi DNA polymerase (Promega) was used for amplification and diluted 120X in autoclaved H_2O together with 10 mM of dNTP, 5 mM specific Primers and 25 mM $MgCl_2$. Annealing temperature for primers was used according to the manufacturer's recommendation or determined by calculation as follows:

$$\mathbf{T_m = 4 \times (number\ of\ G\ or\ C) + 2 \times (number\ of\ A\ and\ T)}$$

The following PCR protocol was used for transcripts not exceeding 1kb in length, varying by the T_m, respectively (tab. 1):

The PCR protocol consisted of an initial denaturation step at 95°C for 2 min, followed by a further denaturation step of 95°C for 30 sec. The second denaturation step precedes the annealing phase of the specific primers at a temperature of 58 °C for 30 sec. touching down the temperature by 1 °C for each cycle to 53 °C. Between 56 °C and 53°C, 25 cycles were repeated. The extension time was chosen to be no longer than 30 sec for an amplicon length of ~1kb, and the final extension time was chosen to be 6½ min. PCR products of < 500 bp were identified on a 2% (w/v) agarose gel containing ethidium bromide. DNA was always directly compared against a positive control and a water control as negative control. The samples were stored at -20 °C.

2.3.3 Transcript scanning of mutually exclusive exons 8/8a, 21/22 and 31/32 and cloning into a pGEM®-T Easy vector

The transcript-scanning method (Soong et al., 2002) was used to screen for mutually exclusive exons,: 7-11 for 8/8a, 19-23 for 21/22 and 30-34 for 31/32 to determine their distribution in amygdala, hippocampus and the prefrontal cortex. Positive and non contaminated bands were identified under a UV-luminator and excised with a scalpel from the gel. The DNA was gel-extracted using manufacturer's method (Qiagen, Gel extraction kit). The PCR products were further sub-cloned into a pGEM®-T Easy vector and transformed into DH10B *E. coli.* A selection of colonies was performed according the blue/white screening system that allows the detection for a positive ligation. In brief: This system is based on the principle of a α-complementation of the enzyme β-galactosidase. The β-gal is encoded by *lacZa* which belongs to the *lac* operon of *E.coli.* If the *lac* coding region, which carries an internal multiple cloning site (MCS) is disrupted by the insert; no functional β-gal can be expressed. As the bacteria are grown in the presence of X-gal - a colorless derivative of lactose which is usually cleaved by an intact β-gal into a blue pigment (5, 5'-dibromo-4, 4'-dichloro-indigo) - the positive ligation can be observed in the white remaining colonies. Blue colonies indicate the existence of an intact *lacZa* system.

For transcript-scanning, at least 96 colonies per animal and brain region were picked and used for colony PCR. Positive colonies were picked then in 96-well plates containing LB medium (Amp.) and incubated at 37 °C for 16 hours. Two PCR reactions were carried out with exon specific primers for the detection of mutually exclusive exons (see tab.1).

Amplicon were detected on a 2% agarose gel and compared against a (+) control and water (-) control. At least 100 clones were sent for DNA sequencing and later compared against the genomic sequence (NC_000072; Gene ID: 12288) of the National Center for Biotechnology Information (NCBI) public databases using the Basic Local Alignment Search Tool (BLAST). For statistical analysis, a one way ANOVA was carried out between the anxiety models with additional Bonferroni correction. Data were considered as statistical significant at a 95% confidence interval.

2.4. Electrophysiology

2.4.1 The Patch-Clamp Technique

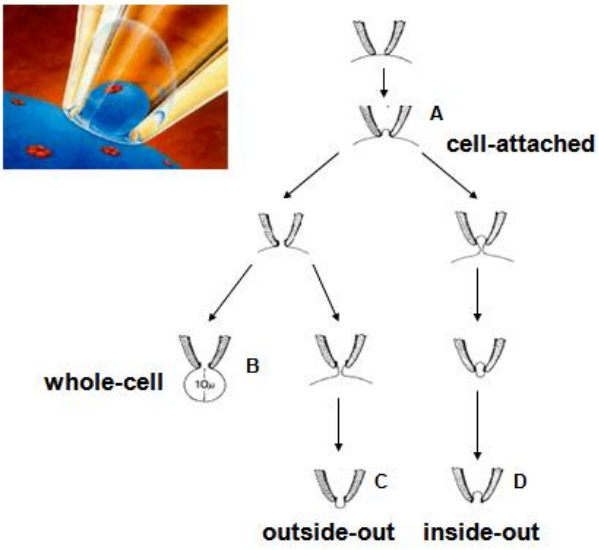

Figure 11: Overview of several patch clamp configurations. A: cell-attached (single-channel), B: Whole-cell, C. outside-out and D: Inside out.

Beyond doubt, Erwin Neher und Bert Sakmann can be nominated as the leading pioneers of the Patch-Clamp Technique which truly revolutionized the field in modern electrophysiology. For their seminal work to record single ion channel both were awarded the Nobel Prize in medicine and physiology in 1991 (Neher and Sakmann, 1976a; 1976b). Although, Hodgkin und Huxley already founded the basics of modern neuroscience with their work on *Loligo* in 1952, describing the flow of multivalent charge carriers over a "capacitor" like membrane leading to the Hodgkin Huxley model, Neher and Sakmann could successfully distinguish between ion currents and background

noise. This was possibly due to a highly isolated membrane part - the patch - which allowed, based on an achieved seal in the giga-ohm range, to detect micro-ampere currents with a conductance of several pico Siemens. For the very first time it was possible to study the nature of ion currents through the protein complexes (s. picture 1.a, *Cell-attached-Configuration*) and hence to understand the molecular processes and functional characteristic of these structures in more detail. With growing time and experience, more electrophysiological methods developed and are still important tools to understand the processes in modern cell biophysics and physiology.

2.4.1.1 Whole-cell configuration

Transiently transfected HEK 293 cells were treated by the calcium phosphate method (Tang et al., 2004). I_{Ba}^{2+} currents were detected at RT after 48-72 hours of transfection. External bath solution contained (in mM) 10 HEPES, 140 tetraethyl ammonium methanesulfonate, 5 $BaCl_2$, (pH was adjusted to 7.4 with CsOH and osmolarity to 290–310 with glucose). The internal pipette solution contained (in mM) 138 Cs-$MeSO_3$, 5 CsCl, 0.5 EGTA, 10 HEPES, 1 $MgCl_2$, 2 mg/ml Mg-ATP, pH 7.3 (adjusted with CsOH). Glucose was used to adjust the osmolarities of solutions to between290 and 330 mOsm. Junction potentials were not considered for any analysis. I_{Ba}^{2+} currents were detected with an Axopatch 200B amplifier (Axon Instruments). Raw data were filtered at 1 kHz and sampled at 10 kHz. The series resistance was usually <5 MΩ after 70% capacity compensation. Leak and capacity transients were subtracted with a *P/4* protocol. The IV relationship was determined from a holding potential of -100mV and a series of depolarizing test potentials (Δ10 mV increment) starting at -60mV to +50 mV, pulsed for

900ms. I_{Ba}^{2+} currents were normalized to the maximum peak current and the obtained IV curve was fitted with a Boltzmann and liner fit, respectively:

$$I_{Ba}^{2+} = G_{max}(V-E_{rev})/(1+exp((V-V_{1/2})/k))$$

Where G_{max} is the maximum conductance; E_{rev} the reverse potential; $V_{1/2}$is the half-activation potential and k is the slope. The steady-state activation (G-V curves) was determined by tail currents where cells were depolarized by a 20 ms test pulse of a serious of activating potentials starting from -60 mV to +120 mV. The tails were then measured after repolarisation to -50 mV for 10 ms. Normalized tails were fitted with a dual Boltzmann respectively,

$$G/G_{max} = F_{low}/ (1+exp ((V_{1/2,low}-V)/k_{low}))/(1-F_{low})/\{1-exp((V_{1/2,high}-V)/k_{high}))$$

With G as the tail current and G_{max} as the peak tail current, F_{low} is the fraction of low threshold component;$V_{1/2,low}$, $V_{1/2,high}$, k_{low}, and k_{high} are the half-activation potentials and slope factors for the low and high threshold components and $V_{1/2act}$ was determined when $G = 0.5G_{max}$.The steady-state inactivation was determined by stepping from a holding potential of -100mVto a 30-ms normalizing pulse to 10mVfollowedby a serious of 15-s prepulses starting from -120 to 10 mV. An additional 104 ms test pulse to 10 mV was recorded. After normalization data were fitted with a single Boltzmann fit:

$$I_{relative} = I_{min} + (I_{max} - I_{min})/(1 + exp((V_{1/2} - V)/k)$$

, where $I_{relative}$ is the normalized current; $V_{1/2}$ is the potential for half-inactivation, and k is the slope value.

2.4.1.2 The cell-attached configuration: detecting single ion channels

One aim of this PhD thesis is the characterization of $Ca_V1.2$ calcium channels in the cell-attached configuration, which allows detecting micro-ampere currents via a single ion channel. This configuration allows a closer insight into the biophysical and pharmacological nature of the channel and hence needs to be explained in more detail. The aim of this technique is to bring a borosilicate micropipette in close vicinity of the cell membrane in order to form a stable patch between the pipette and the membrane. A patch can be of several giga ohms (gigaseal) through a large resistance, whereas the current inversely decreases given through:

$$R_{seal} = U_{TP}/I_{Leak}$$

Of fundamental importance is the background electrical noise which needs to be considered in brief. Noise is of physical origin and can be described as charge fluctuations, appearing in several areas within the patch, the head stage and the pipette, resulting in an adverse signal/noise ratio (S/N). Large noise often results in errors during the analysis of the data and should be avoided strictly. A good S/N quality is

indispensable and eases any further raw data analysis. In this chapter, we will further focus on the basics of the patch clamp technique.

The setup is the heart of each patch-clamp system and is comprised of several modules (s.). The inverse microscope and fluorescence source should be usually placed within a faraday cage – being placed on a shock absorbing table - in order to keep away disturbing electromagnetic factors. The micromanipulator can be of electric or mechanic origin and its fine drive allows an easy interplay between the pipette and membrane and is essential. Detected signal will be transduced over a head stage which allows a first amplification (CV-4 Head stage, Gain x1/100, Axon Instruments) and then further inducted into a main amplifier (Axopatch 200B, Axon Instruments). Finally, the amplified, analogue signal is converted into a digital signal by a 16 bit AD/DA converter before it is saved by a CPU.

2.4.2 The Single-Channel Setup

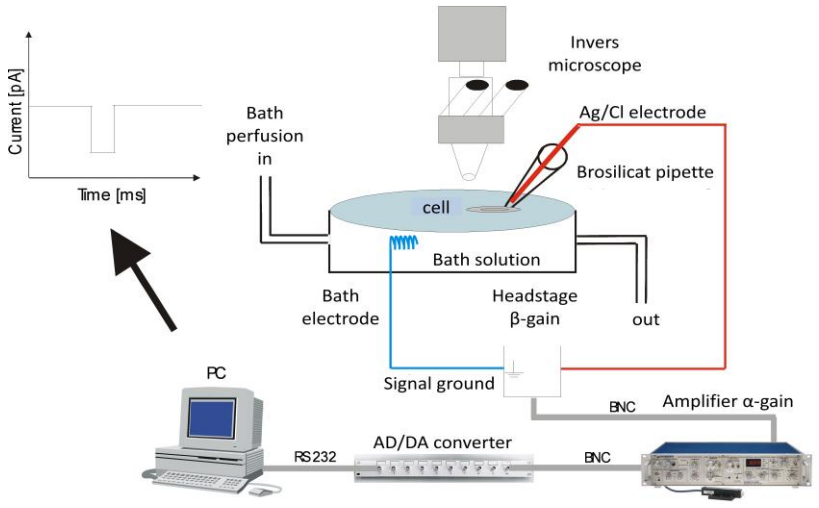

Figure 12: Oversimplified diagram of a patch-clamp setup. Cells can be selected according to their GFP distribution through an inverse microscope that is attached to a fluorescence source (not shown). Bath and stimulation electrode (β-Gain) are interconnected via a BNC (banana network cable) with the amplifier (α-Gain). The amplified signal (analogue) is converted via a 16 BIT AD/DA-converter into a digital signal and further supplied into a CPU.

2.4.3 Experimental design and theoretical background

As charge carrier, divalent Ba^{2+} ions (in mM)110 $BaCl_2$, 10 HEPES (pH 7.4 with TEA-OH) were used which show a higher permeability for Ba^{2+} then Ca^{2+} ions in HVA channels compared to LVA channels. This brings the advantage that Ba^{2+} ions also block native sodium channels, allowing us to detect for Ba^{2+} currents only. TEA added into the pipette solution additionally guaranteed that outward currents through potassium channels were eliminated.

The petri dishes containing depolarizing bath solution (in mM), 120 K-glutamate, 25 KCl, 2 $MgCl_2$, 10 HEPES, 2 EGTA, 1 $CaCl_2$,1 Na2-ATP, 10 dextrose (pH 7.4 with KOH)allows collapsing the membrane potential, bringing it close to ±0 mV. After immersing the pipette into the bath solution, the offset needs to be corrected due to appearing junction potentials between the ground- (U_{theo})/detecting- (U_{pip}) electrodes and the electrolyte solution in the bath chamber. The potential differences can be seen in forms of a baseline shift on the screen and need to be compensated through the offset, respectively:

$$U_{pip} + U_{theo} = 0\ mV$$

The positive pressure, that was acquired prior to the immersion of the pipette into the bath solution, will be released if the pipette tip is in close vicinity to the cell, whereas a giga seal forms through releasing the positive pressure**,** resulting in an under pressure. Additional suction through a catheter that is connected to the pipette holder can be performed to achieve a stable gigaseal and we achieve:

$$U_{patch} = U_{pip} - U_{RMP} = U_{pip},\ by\ U_{RMP} = 0\ mV$$

As we create capacity transients while charging the membrane we need to compensate those currents, respectively. Usually, the cells were hold at a holding potential (HP) of -100 mV, allowing the channels to fully close and pulsed over 160 ms to a testing

potential (TP) of +10 mV which allows the channels to open again. The gigaseal can be determined through the occurring leak current I_{leak} which leaked through the pipette tip. The total noise, recorded at a cut-off frequency of 5 kHz, was usually below an I_{RMS} of 300 fA whereas I_{RMS}> 350 were not considered for any recordings due to a bad S/N ratio and a likelihood to overestimate events. The activation of a channel (opening) can be explained by a Ba^{2+} influx and an efflux of positive charges out of the pipette solution. At the same time feedback compensation in form of a compensational current I_{comp} drives back the voltage to its theoretical value, respectively:

$$U_{(PIP)act} = U_{theo} ;$$

whereas the voltage difference is now being reconstituted. The electron flow can be further quantified through the redox-reaction (Ag/AgX), with Ag/AgCl | $BaCl_2$, respectively,

$$2\,Ag^0 + \boldsymbol{Ba}Cl_2 \leftrightarrow 2\,Ag^+Cl^- + 2e^- + \boldsymbol{Ba}^{2+}$$

The influx is based on a oxidation reaction, whereas Ba^{2+}-ions efflux out of the pipette. At the same time, the silver from the wire is being reduced; cations efflux out of the solution into the pipette (negative current).

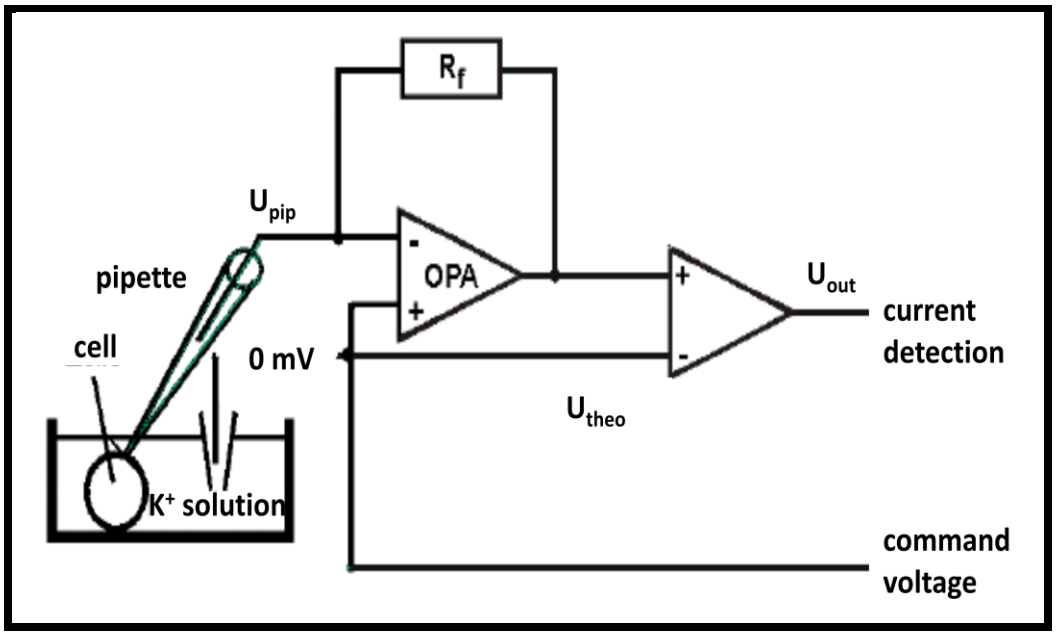

Figure 13: Indirect current registration of a patch clamp setup. The bath solution contains 140mM potassium, the pipette solution, 110 mM Ba2+. The aimed testing potential *UTP* of +5mV equal the holding-/test potential. The current circuitry is comprised of two operational amplifiers (*OPA*) in series (β-gain head stage and α-gain amplifier). Recharging of the membrane results in compensation currents, whereas the head stage indicates the difference between U_{theo} and U_{pip}. The compensational current I_{comp} flows through the circuitry R_f in order to correct the potential difference.

2.4.4 Data Analysis and Statistics

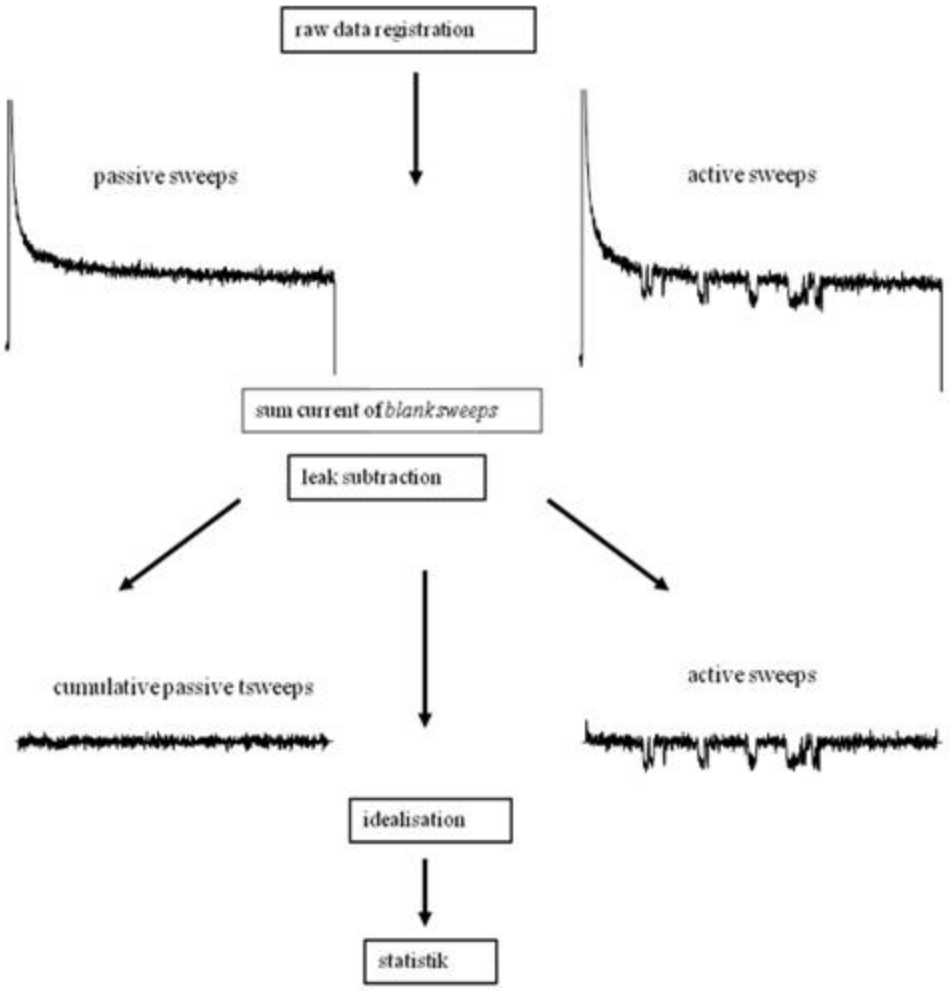

Figure 14: Overview how to analyze single-channel data from recording of raw data to idealizing traces. The summation of blank sweeps and the subsequent subtraction of active sweeps from the passive ones are called leak subtraction. This leads to a reduction in background noise as well as cutting out the capacity transients which built up the membrane charging process.

The depolarized current traces are of 160 ms length, whereas at least 180 consecutive traces were recorded for each experiment. Raw data acquisition was carried out with *P*clamp 10 (Molecular Device. The single-channel events were detected using the half-height criterion (Sachs et al., 1982) and raw data were digitally leak- and capacity-

corrected (Clampfit 10.2). The number of channels in the patch was estimated by the occurring number of staged openings recorded over several minutes at different test potentials. The mean ensemble average current was derived from 180 traces, whereas the local maximum *(I_{peak})* was estimated by using a simple smoothening algorithm (Fast Fourier transformation) to abolish high frequency noise (Origin 6.0). Fraction of active sweeps (availability) was calculated by the number of active traces *(M_{active})* divided by the total number of sweeps *(M_0)*. The binning of histograms was performed according to Sigworth and Sine and fitted with a mean simplex method (Sigworth and Sine 1987). The statistical analysis was either carried out with Origin 6.0 or GraphPad Prism 5. Pooled data are shown as mean values with standard error. Data were considered as statistical significant at a 95% confidence interval by using Student's t-test.

2.4.5 Writing event lists

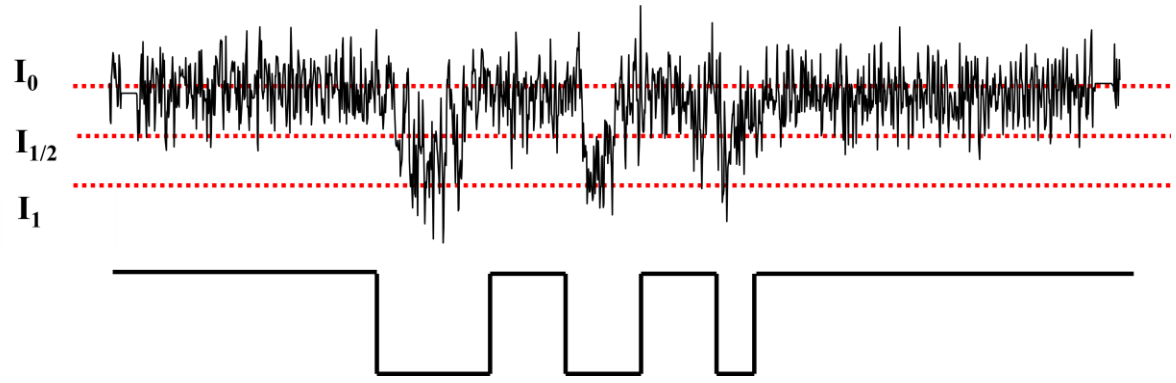

Figure 15: Illustration of a leak subtracted current trace with the activity of one calcium channel (T-type). Open levels *(I_1)* are defined by the half-height criterion *($I_{1/2}$)* and leak subtracted traces are transformed into rectangular current traces (Sachs et al., 1982).

The computational writing of event lists resulted from the leak subtraction and subsequent idealization of current traces. Leak subtraction aimed to cut off the capacity transient at the beginning and the end of the pulses minimized background noise. The objective is to add up and average all blank traces. What are left are the active traces. The average mean value of the passive traces depicts a timely superimposition of all artifact afflicted currents of passive traces. The idealizations first step is to define a baseline *(I_0)* of the leak subtracted current traces. It can be further understood as the standard noise *(σ)* of a mean value sometimes described as "Root Mean Scare" *(RMS)*. The unitary current amplitude sets apart from the standard noise and can be described as the first opening level *(I_1)*. Staggered openings can be described through several opening levels *(I_n)*, according to the channel number. Multi openings can be corrected later through the number of channels in the patch (Schröder et al., 1998). If an event is considered an opening or closure by the program, is based on the half height criterion (McManus et al., 1987; Sakmann und Neher, 1995). Current amplitudes – the detection is according to our sampling frequency (10 ms) - above the half height open level are registered as openings, whereas values below are considered as baseline (fig.15).

2.4.6 Determine the unitary current amplitude

Unitary current amplitude $I_{unitary}$ (pA) was determined from fully resolved openings after leak subtraction. Ten active traces were averaged which resulted in the size of $I_{unitary.}$ Furthermore, All Point Histograms were used to determine the amplitude size (data not shown). Thereby, the pA-value was depicted towards all collected data points by the

program, according to a 10 kHz sampling frequency, which results in a bi-exponential gauss distribution. The maximum of the standard distribution around a mean is considered the *RMS (σ)*, whereas the maximum amplitude is described as μ.

2.4.7 Correction of multiple channels (k ≥ 1)

The number of channels in the patch was estimated from staggered openings as described in Horn 1991. As the likelihood to record from a single ion channel ($k = 1$) is rather small (Horn 1991), the possibility is given to correct for the number of channels ($k \geq 1$), without losing any data information (Schröder et al., 1998, Schröder und Herzig, 1999; Hohaus et al., 2000; Meir et al., 2000; Barg et al., 2001; Michels et al., 2002). The minimum amount of channels in the patch can be estimated by the number of staggered openings. It can be described as the ratio of the highest detectable amplitude I_{max} and the unitary current amplitude $I_{unitary}$, whereas the number of channels is described as an integral multiple.

Ion channel can be described with the following parameters:

I. Fast gating

II. Slow gating

III. Sum and maximum current

IV. Kinetic time constant tau (τ)

I. Fast gating

Mean open time (*mot*)

This parameter describes the average mean open time of a channel. The MOT is the arithmetic mean of all open times and can be described by:

$$mot = \sum t_{openI...N} / N_{open} \text{ [ms]}$$

Mean open probability (P_{open}), or *mpo*

The ratio of total open time and total time of all active traces is described by:

$$mpo = \sum t_{openI...N} / M_{active} * t_0 [\%]$$

The Mean P_{open} considers the open time as a parameter of the fast kinetic as well as the availability, describing the slow gating, hence a parameter of fast and slow kinetics.

II. Slow gating

Availability (F_{active})

The availability describes a relative frequency (%) of active traces of an experiment.

It is the ratio of active traces to passive traces:

$$f = M_{active}/M_0 \quad [\%]$$

Correction of availability

Given that $k \geq 1$, we correct, respectively

$$\sqrt[2]{1} - f = 1 - f' \Leftrightarrow \quad f' = 1 - \sqrt[2]{1} - f$$

Correction of open probability

Given that k ≥ 1, we correct, respectively

$$P_{open} = mpo' = \sum t_{open\,I\ldots N} / n * f' * M_0 * t_0$$
$$P_{total} = \sum t_{open\,I\ldots N} / M_0 * t_0$$

$$\Leftrightarrow P_{open} = mpo/n * f/f'$$

3. Sum/ Peak current (peak ensemble average current I_{peak}) and I_{150}

The sum current describes a temporary delineation of all idealized traces of a single experiment, which are superimposed at the given instant t_i. The summation of all data points $I(t_i)$ at a given instant t_i over all traces *j is* divided by the amount of traces M_0 and given as:

$$I_{sum}(t_i) = \sum_j I^*(t_i)_j / M_0 \text{ [fA]}$$

Based on the sum current, the local maximum I_{peak} can be estimated (Schroder und Herzig, 1999) through:

$$I_{peak} \approx \sum p_i + I_{sum}(t_i) \text{ [fA]}$$

The maximum current arises out of the local extremum of the sum function $I_{sum}(t)$.The sum current was created with Origin 6.0 and smoothing done by a fast Fourier transformation FFT. Based on the smoothening the inactivation can be determined through:

$$I_{150} = 100 * (1 - I_{150/} I_{peak}) \text{ [\%]}$$

4. Kinetic Time constant *tau (τ) and MLE*

The biophysical parameter *tau* quantifies the open-state life/closed time (dwell-time) of a channel and is a parameter of the fast kinetic. As open times do not result of arithmetic nature they can be best described with a sum of exponential functions based on a Poisson distribution. *Tau* can be calculated by a "Maximum Likelihood Estimate *(MLE)* analysis. The local maximum of a mono-exponential *L* (τ)-function is estimated and specified by (τ_{max}). The first derivation of the *L* (τ)-function results in the maximum-likelihood value τ_{max}.

2.5 Statistics

Recorded raw data were analyzed for significance by Student's t-test. Comparison of parameter with more than 3 datasets was performed by using a one-way ANOVA with Bonferroni-corrected post-tests. Data were considered as significant at a confidence interval below 0.05. A p-value indicated with * is considered < 0.05, ** is < 0.01 and *** is < 0.001. P values > 0.05 were considered as not significant (n.s.). All data are given as mean values ± standard error of the mean, based on *n* as the number of independent experiments.

Chapter III

3. RESULTS

3.1 Exon 33 Deletion of murine $Ca_V1.2$ increases the current density by increasing single-channel open probability

Previous *in vitro* studies by our group showed altered functional and pharmacological properties for the exclusion of exon 33 ($33^{-/-}$) in a smooth muscle $Ca_V1.2$ splice variant when expressed in a recombinant HEK system (Liao et al., 2007). Whole-cell data revealed a hyperpolarizing shift in window current allowing us to speculate on a possible role this splice variant plays in generating or maintaining vasotone in arterial smooth muscle or in supporting cardiac contraction. We now investigated the physiological consequences in a knock-out model, where exon 33 ($33^{-/-}$) was ablated in the mouse genome, to further understand how altered $Ca_V1.2$ calcium channel property may relate to cardiac physiology. Consistent with the *in vitro* studies from Liao et al, data recorded from Dr Li Guang revealed a significant increase in current density (> 30 %) over a wide range of test potentials paired with an early onset in steady-state. Steady-state inactivation was shifted to more hyperpolarized potentials indicating an early inactivation The results were accompanied by investigating the ventricular action potentials and we found increased occurrence of early after depolarisation and delayed after depolarisation, and both parameters are associated with increased ability for the development of ventricular arrhythmia (unpublished data, Li et al., manuscript in preparation).To now further analyze if the increased current-density of Δ33 is the result of altered unitary channel

Figure 16: Representative isolated cardiomyocyte used for patch-clamp experiments. Cell morphology after Langendorf isolation. Kindly provided by Dr Li Guang.

gating or an increased number of functional channels, single-channel recordings were acquired.

The data, obtained from four (WT) and four ($33^{-/-}$) animals, clearly indicated a significant increase in open probability of individual channels (P_{open} (%); WT (n = 7), 5.6±1.0; $33^{-/-}$ (n = 6), 18.6±3.2, ***p < 0.001), fig. 21A.

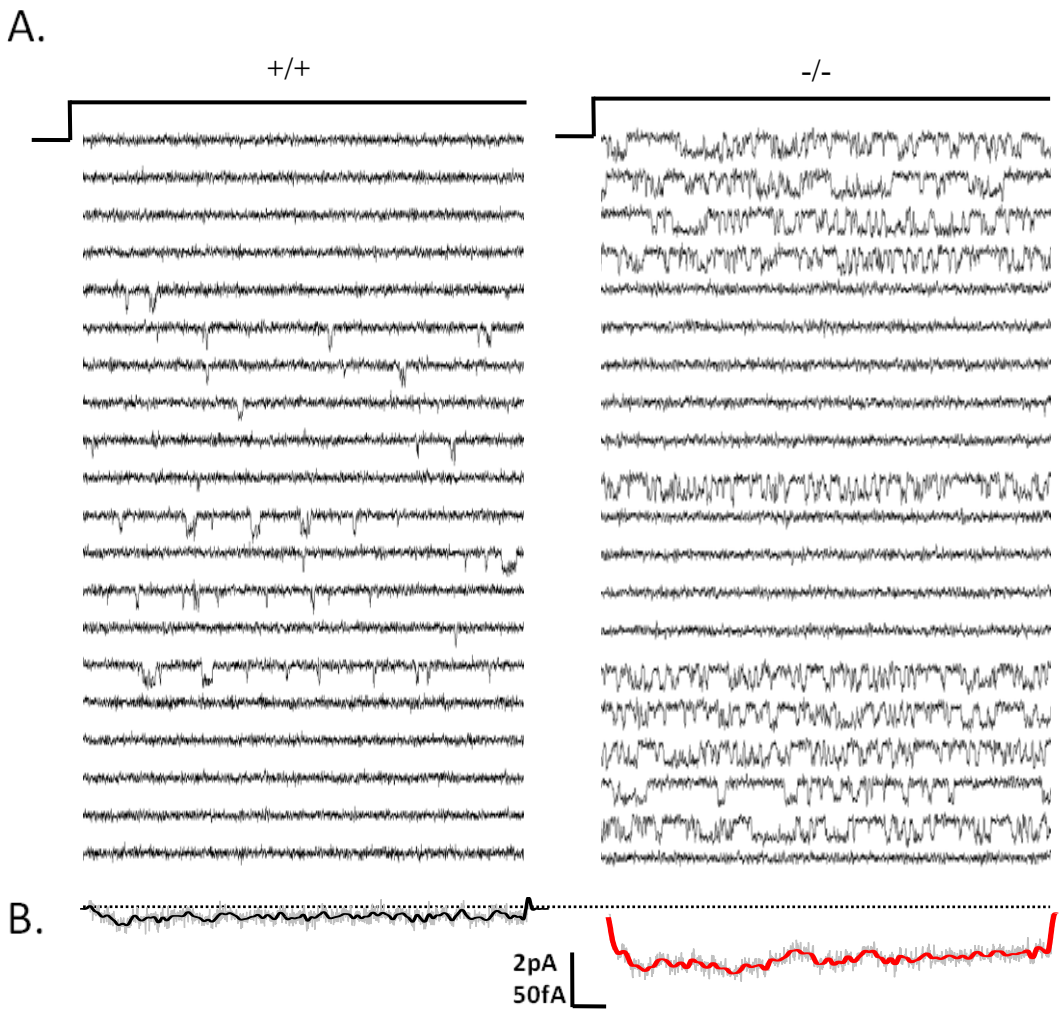

Figure 17: **20 consecutive exemplary** traces of murine ventricular $Ca_V1.2$ wild type (+/+) and $Ca_V1.233^{-/-}$ablated knock-out (-/-).**A**. Exemplary traces indicate increased basic gating properties of $33^{-/-}$. **B.** Mean ensemble average current obtained from 180 traces (n = 1) Cells were depolarized for 150ms from holding potential of -100mV to +10mV. Scale bar in pA refers to unitary events. Sum current is depicted in fA.

These data were accompanied by an increased mean ensemble average current (I_{peak} [fA] 180 traces, WT (n = 7), 48±8; $33^{-/-}$ (n = 6), 139±29, **p < 0.01), fig. 21B. Additionally**,** it could be shown how the open probability changes over higher depolarizing voltage steps (TP: -10, 0, 10, 20 mV) and it could be verified that channel open probability (NP_{open}) was significantly increased over all conditioned test potentials ($V50_{act.}$ (mV) WT (n = 5), 4.9±1.5; slope: 3.6, $33^{-/-}$ (n = 5); 13.4±7.8, slope: 3.9; p < 0,001 < 0.001 < 0.001 < 0.01), fig. 18A.

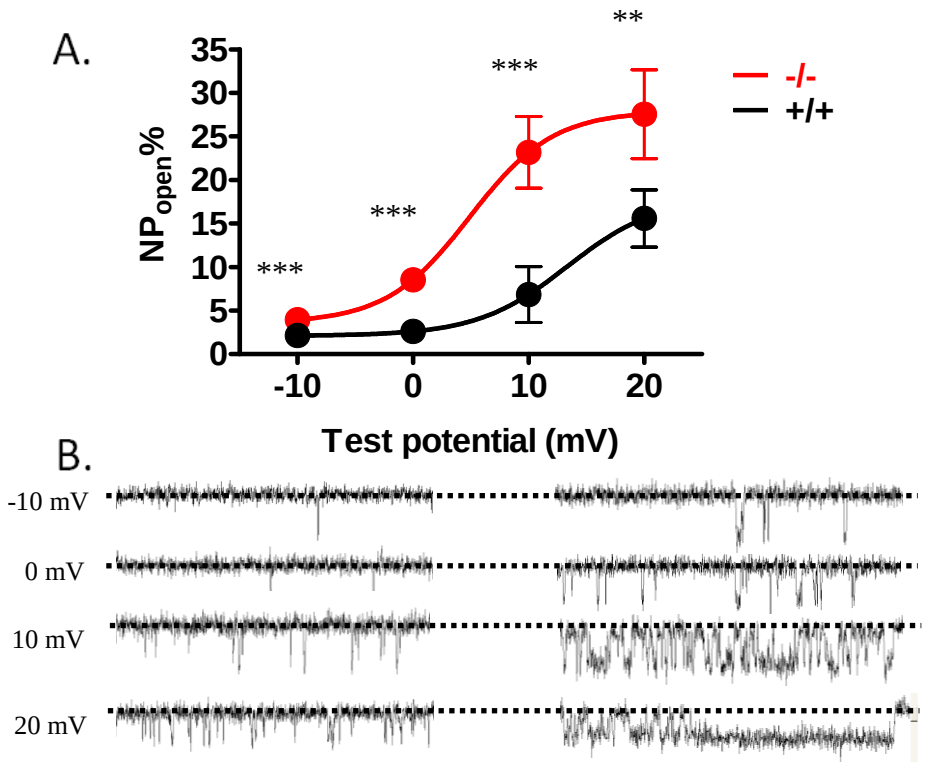

Figure 18: **A. Altered channel open probability NP_{open}** (k<2) of cardiomyocytes upon depolarization over several TP. Pooled datafrom 5 experiments. A significant difference in open probability could be observed for -/- over a wide range of tested potentials ($V50_{act.}$ (mV) WT, **4.9±1.5**; k: 3.6; $33^{-/-}$: **13.4±7.8**, k: 3.9; Students-t test was applied for each potential;*** p <0,001 < 0.001 < 0.001 ** < 0.01). Data were fitted with a single Boltzmann function. **B**: Exemplary traces at different test potentials.

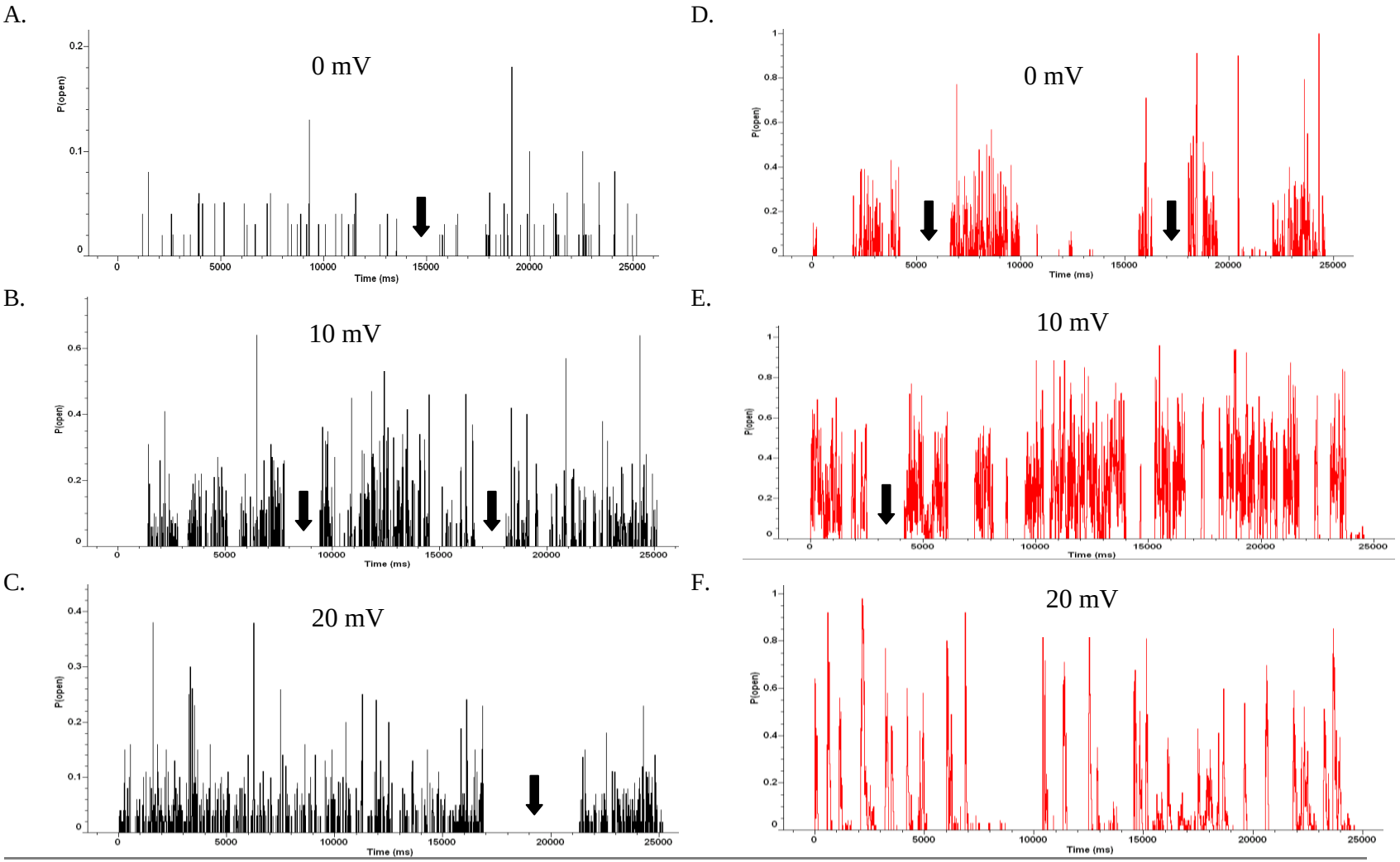

Figure 19: **Exemplary time course representing the open probability** of $Ca_V1.2$ wild type (+/+) (black) and the $Ca_V1.2$ 33-/- (red) at consecutive testing potential. A-C, D-F 0-20 mV, Arrows marking periods of mode 0 gating at which the channel is not available.

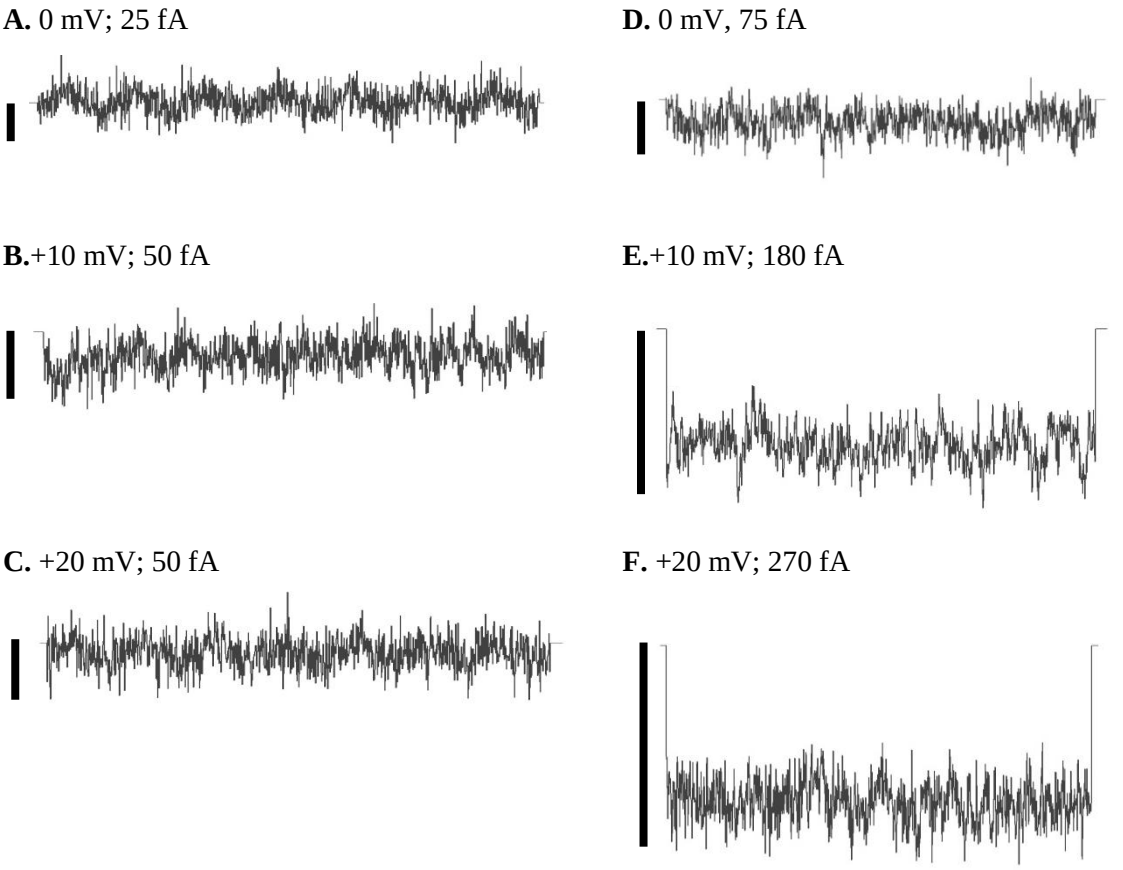

Figure: 20 A-C. Exemplary mean ensemble average currents from $Ca_V1.2$ wild type (+/+) and $Ca_V1.233^{-/-}$at different test potentials. **D-F** represents exemplary $Ca_V1.2$ $33^{-/-}$ mean currents at the same test potentials. Scale bars are represented in fA

This clearly indicates that globally the likelihood to detect the $33^{-/-}$ $Ca_V1.2$ channel in the open-state is increased by 3 times within a pulse length of 150 ms. The parameter describing slow gating of the channel was not altered in the experiments (availability (%)); WT (n = 7); 57±7; $33^{-/-}$(n = 6); 48±10, n.s.), fig. 21C.

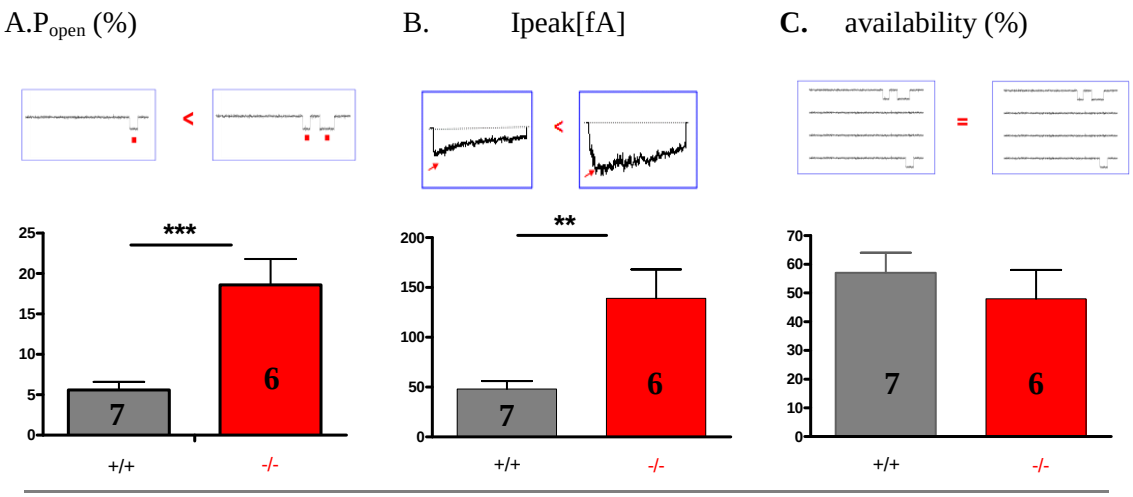

Figure 21: **Statistics for Single-channel experiments. A.** Parameter describing the likelihood to detect a channel in a given pulse length (P_{open})**B.** Local maximum derived from the mean ensemble average current of 180 consecutive traces (I_{peak}). **C.** Fraction of active traces (availability). Data were analyzed by Student's t-test, ***p < 0.001 and **p < 0.01.

3.1.1 Single-channel fast kinetic parameters of $Ca_V1.2$ $33^{-/-}$ are significantly altered compared to $Ca_V1.2^{(+/+)}$

To further determine the molecular determinants of this higher open probability, the fast kinetics of individual channels was analysed. Mean open time (MOT) of Δ33 already predicted to be increased, (WT (n = 7), 0.53±0.08; $33^{-/-}$ (n = 6), 0.83±0.07, ** p < 0.01) whereas the closed time was reduced by nearly 4 times (MCT (ms), WT, 12.1±1.4; $33^{-/-}$, 3.3±0.5, *** p < 0.001), fig. 22A and B.

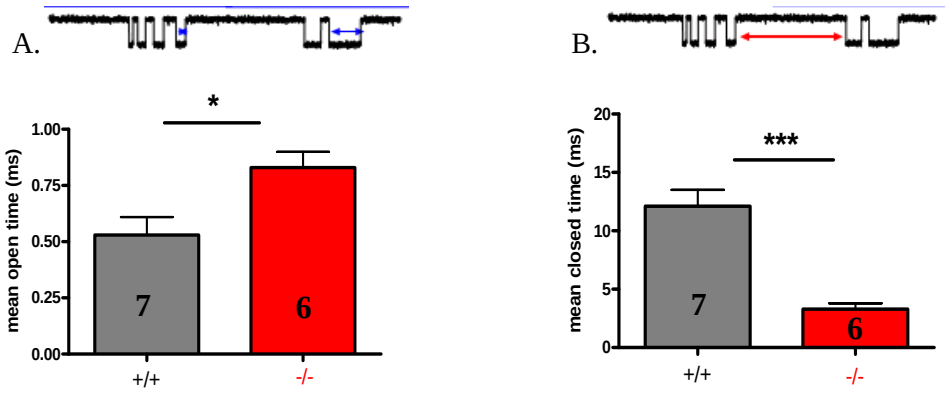

Figure 22: Open- and closed-time statistics describing arithmetic mean values. **A**. The mean open-(n =6) and **B**. the channel mean closed-time (n= 7) of real single-channel experiments. Data were analyzed by Student's t-test, $p < 0.05$ and $p < 0.001$.

However, since ion channels open and closed time cannot be represented in a Gaussian distributed manner, their probability density function PDF was assumed to be of a Poisson distributed origin.

Dwell-time histograms describing the more relevant biophysical time constant tau revealed the open-state live time of a single-channel being highly significant (τ_{fast} (ms); WT; 0.54±0.01; $33^{-/-}$; 0.36±0.04, τ_{slow} (ms); 1.5±0.12, n.s.), fig. 23C. Furthermore, a bi-exponential component could be fitted in all histograms for the $33^{-/-}$ with a probability portion of 0.34 (tab. 3)

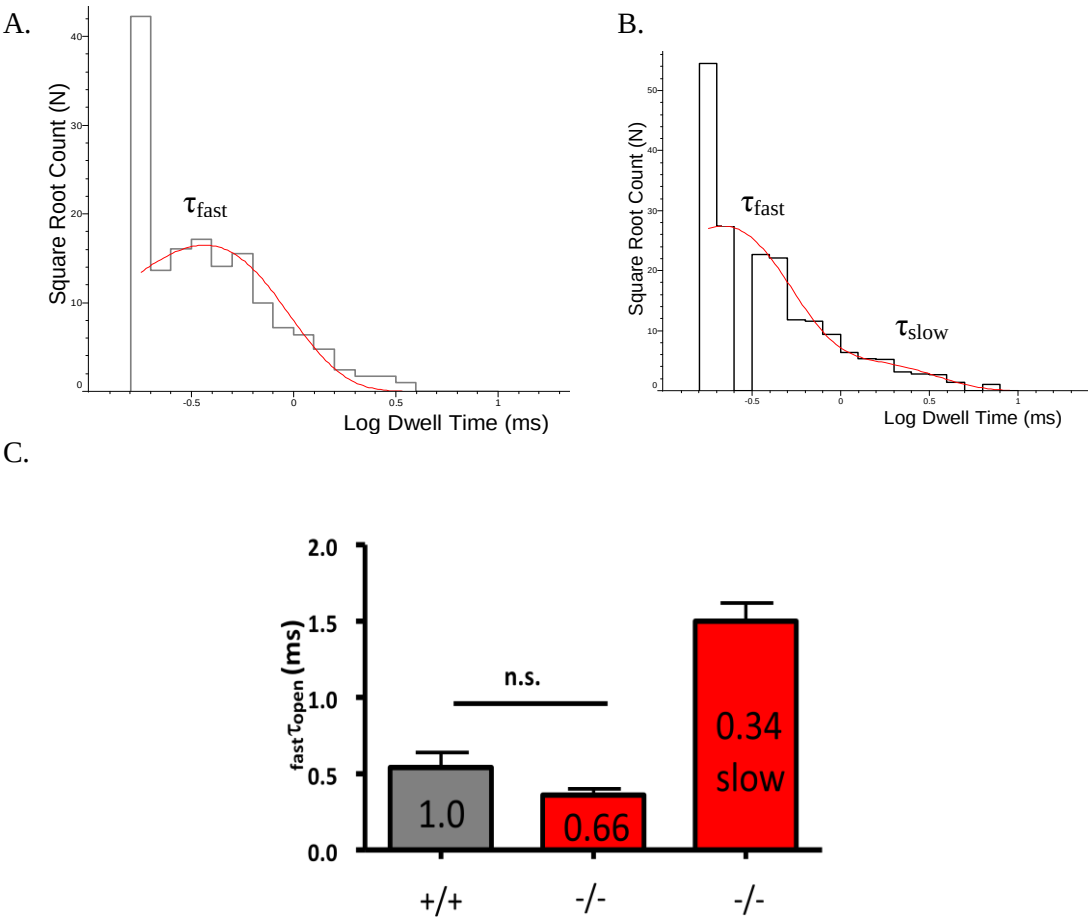

Figure 23: **Representative dwell-time open histograms** quantifying the open-state-life time. Tau values were obtained from mono-or bi-exponential fits with the mean-simplex method, 10bin/decade-width. **A**. WT with a single exponential component (τ_{fast} at 0.37ms) versus. **B**. The $33^{-/-}$ with a τ_{fast} exponential component at0.2ms, 0.84% and a second exponential component τ_{slow}at1.3ms, 0.16.**C**.Statistics describing the distribution of the fast and the slow component for the WT (grey) and $33^{-/-}$ (red).The second slow exponential component for the $33^{-/-}$ is represented with 0.34±0.04 %. Data were analyzed by Student's t-test, n.s.

Similar significant results were obtained for dwell-time histograms describing the tau values for the slow closed component of a single-channel ($\tau closed_{fast}$ (ms); WT; 0.47±0.09; $\tau closed_{slow}$ (ms); 12.1 ±1.1 and $33^{-/-}$; 0.56±0.07, $\tau closed_{slow}$ (ms); $\tau closed_{slow}$ (ms); 5.7±0.52, **p < 0.01), fig. 24C.

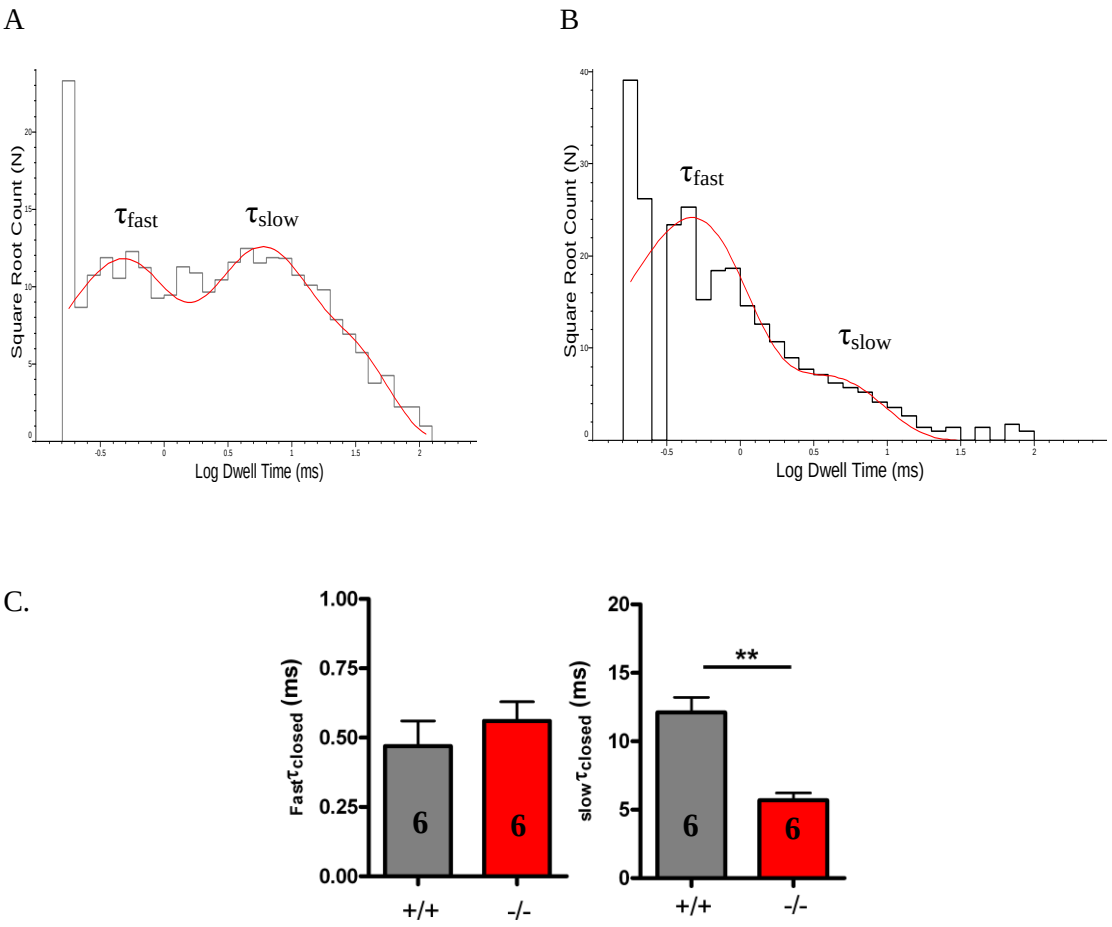

Figure 24: **Representative dwell-time close histograms** quantifying the channel closed-time**.** I-exponential fits were determined with the mean-simplex method based on a 10bin/decade-width. **B.** The $33^{-/-}$ shows a diminished second fit component τ_{slow} 3.7 ms; 0.24 towards the **A.**WT τ_{slow}9.8 ms; 0.54.**C**.Statistics describing the distribution of the fast and the slow component for the WT (grey) and $33^{-/-}$ (red). Data are based on WT (n=7) and $33^{-/-}$ (n=6) experiments. Data were analyzed by Student's t-test, **p < 0.01.

3.1.2 Single-channel activation of $Ca_V1.2$ $33^{-/-}$ is significantly reduced by 3 times compared to $Ca_V1.2^{+/+}$

Finally, the required time between first channel opening and applied test pulse, the mean first latency (MFL) was analyzed. $33^{-/-}$tends to open much faster when compared with the WT channel form (MFL (ms); WT; 17.2±1.9; $33^{-/-}$; 5.4±1.1, **p < 0.01), fig. 25B.

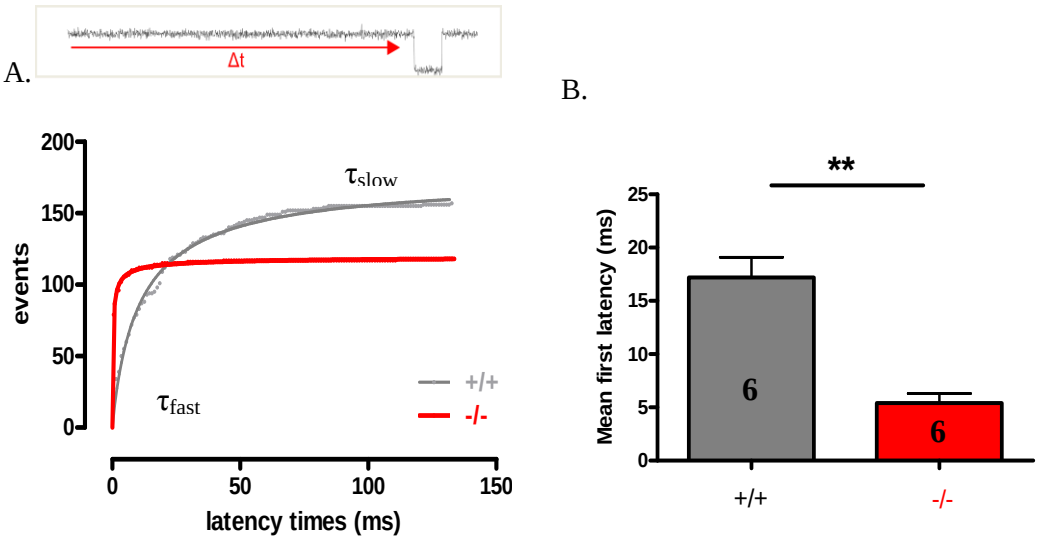

Figure 25:**A.Exemplary first latency distribution quantifying the channel activation time** of WT and $33^{-/-}$.WT activates with τ_{fast} 1.1 ms; τ_{slow} 10.5 ms. The $33^{-/-}$activates faster τ_{fast} 0.8 ms and τ_{slow} 4.0 ms compared to the WT.**B.** Mean first latency statistics based on n = 6 animals per group. Data were analyzed by Student's t-test, **p < 0.01.

Table 2: Synopsis of channel properties of murine $Ca_V1.2$ (+/+) and $Ca_V1.2$ Δ33 (-/-) based on real single-channel experiments (k =1). Both groups are based on 4 animals. Student's t-test was applied, *p< 0.05, **p<0.01, ***p<0.001.

Parameter	+/+	n	-/-	n	p
Availability (%)	57±7	7	48±10	6	n.s.
P_{open} (%)	5.6±1.0	7	18.6±3.2	6	0.001
I_{peak} [fA]	48±8	7	139±29	6	0.01
Mean first latency (ms)	17.2±1.9	6	5.4±1.1	6	0.01
Mean open time (ms)	0.53±0.08	7	0.83±0.07	6	0.01
$\tau_{open,fast}$ (ms)	0.54±0.01	7	0.36±0.04	6	n.s
$\tau_{open,slow}$ (ms)			1.5±0.12	6	
Fraction $\tau_{open,slow}$			0.34±0.04	6	
Mean closed time (ms)	12.1±1.4	6	3.3±0.5	6	0.001
$\tau_{closed,fast}$ (ms)	0.47±0.09	6	0.56±0.07	6	n.s.
$\tau_{closed,slow}$ (ms)	12.1±1.1	6	5.7±0.5	6	0.001
Fraction $\tau_{closed,slow}$	0.57±0.02	6	0.43±0.03	6	

3.2 Functional role of the N-terminus of hum $Ca_V1.2$ in a recombinant system (HEK 293) under whole-cell conditions.

3.2.1 Exon 1a/1b of hum$Ca_V1.2$ regulates channel inactivation in a voltage-dependent manner.

In order to study the functional role of the N-terminus of human $Ca_V1.2$ the SM isoform composed of exon 1b/8 and the CM isoform composed of 1a/8a were compared to their constructed counterparts 1b/8a and 1a/8 in a HEK 293 expression system. To analyze the steady-state kinetics of activation a tail protocol was run where the remaining tail at a steady resting potential of +60 mV and different activation potentials was analyzed (fig. 26, A and B). An ANOVA with post-test did not reveal any significant difference among groups (tab 3). However, a steady-state inactivation protocol revealed a significant alteration in an enhancing additive manner with the strongest inactivation when exon 1b is combined to exon 8a (fig. 27) ($V_{1/2inact.}$ -43.1±0.7 (9) vs.$V_{1/2inact.}$ -36.4±1.1 (9), ***$p < 0.001$). Interestingly, similar findings have been reported by our group in the past by the same $Ca_V1.2$ splicing variants obtained from a cDNA full length library from Wistar Kyoto (WKY) rats (Tang et al., 2004). The same holds true when comparing the activation profile of the IV relationship between 1b8a and 1a8a ($V_{1/2}$-16.7±1.2 (7) vs. -14.1±1.5 (11), n.s.). In fact, in Tang's publication from 2004 the 1b8a full length version was found to be present in the heart with 23% over the predominant 1a8a isoform which is expressed at 50%.

The steady-state activation of humCa$_V$1.2 isoforms

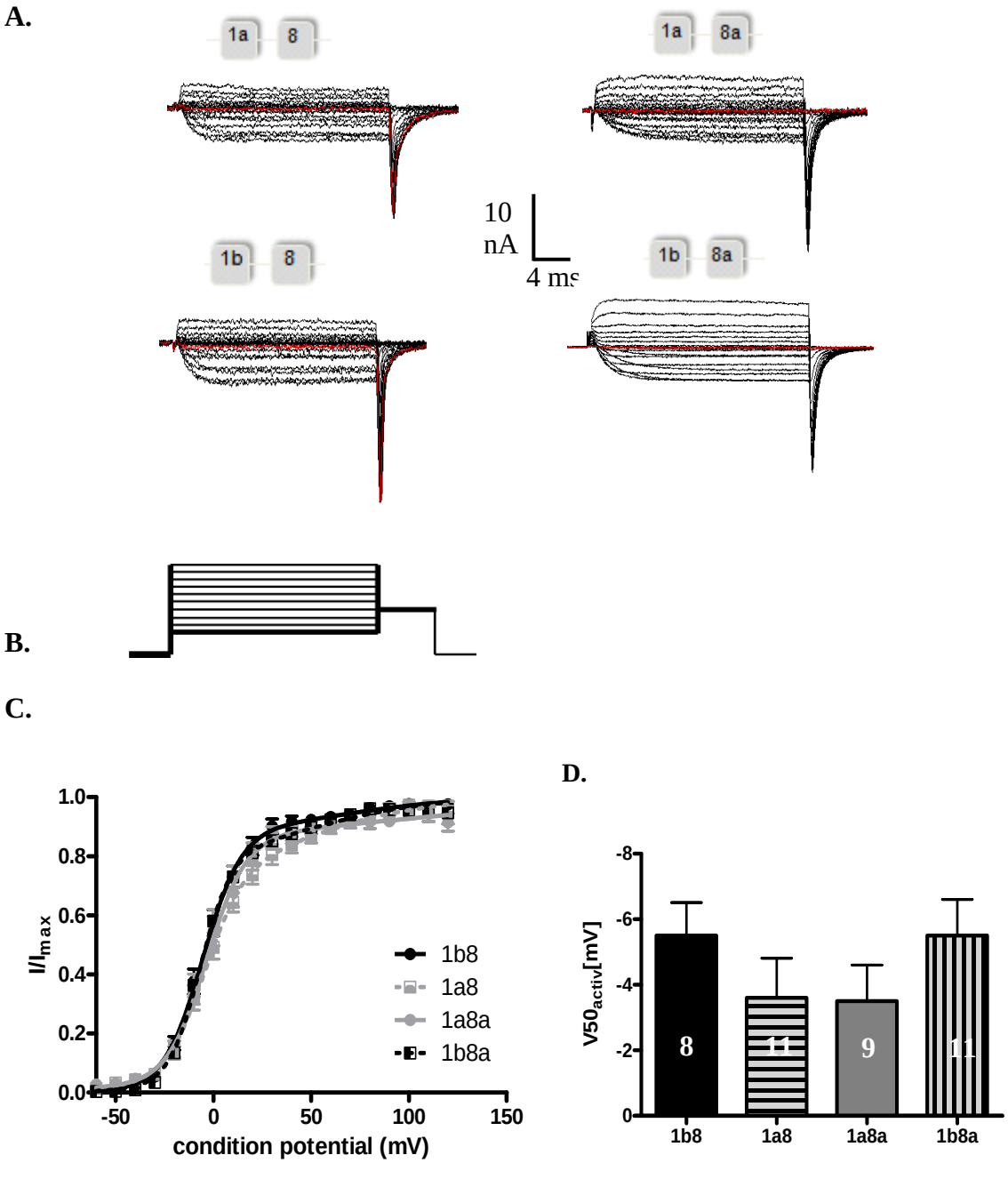

.

Figure 26: **Steady-state activation** obtained from tail currents. **A**. Exemplary traces. **B**. Pulse protocol, cells were pulsed from a HP of -100mV to various TP, Δ10 mV, for 20ms under 5mM Ba^{2+}. **C.** Activation curve fitted with a dual Boltzmann equation**.** Statistics was analyzed with a one-way ANOVA, Bonferroni corrected.

In this work we also showed that the predominant SM $Ca_V1.2$ 1b8 isoform significantly differs in inactivation from the 1b8a isoform ($V_{1/2inact.}$: -37.3±1.0 (10) vs. - 43.1±0.7 (9),* $p < 0.05$) fig. 27C,D, hence pointing out the importance of assessing the influence of alternative splicing on steady state inactivation in a combinatorial fashion and in this regards between exons 1a/1b and exons8/8a. The biggest difference in inactivation of more then -10mV was observed when comparing the 1a8 and 1b8a isoform ($V_{1/2,inact.}$: -31.2±0.7 (8) vs.- 43.1±0.7 (9), ***$p < 0.001$), fig. 27C,D. The predominantly expressed isoforms from CM 1a8a and SM 1b8 do not differ in their steady-state inactivation profiling ($V_{1/2inact.}$: -36.4±1.1 (9) vs. -37.3±1.0 (10), n.s.) fig. 27C,D. However, it is noteworthy to mention that the 1a8 isoform has not been reported to be functionally expressed until now.

3.2.2 Exon 1b/1a of hum$Ca_V1.2$ influences the current density [pA/pF]

The analysis of the IV relationship clearly indicated that the N-terminal portion encoding exon 1b significantly increased the current density by nearly 2 times. An increased Ba^{2+} current could be observed over a wide range of testing potentials (fig. 28D) with exon 1b8 and 1b8a overall showing a larger current-density compared to exon 1a8 and 1a8a ($V_{1/2,act}$: -35.2±0.8 and -39.7±1.6 towards -19.4±2.2 and -19.1±0.2, ***$p < 0.001$). Additionally, these experiments could be further replicated by using a GV curve obtained from a tail protocol to analyze the current density (fig. 29) Again, 1b8a and 1ba showed a current density significantly increased over 1a8 and 1a8a ($V_{1/2,act}$: 315.2±11.2 and 117.7±6.2 towards 96.3±6.4 and -80.1±7.1, ***$p < 0.001$) but this time much more pronounced as under simple IV conditions. To now further analyze the functional change

that resulting from the utilization of exon 1b, we looked into the individual channel gating.

The steady-state inactivation (SSI) of humCa$_V$1.2 isoforms

A.

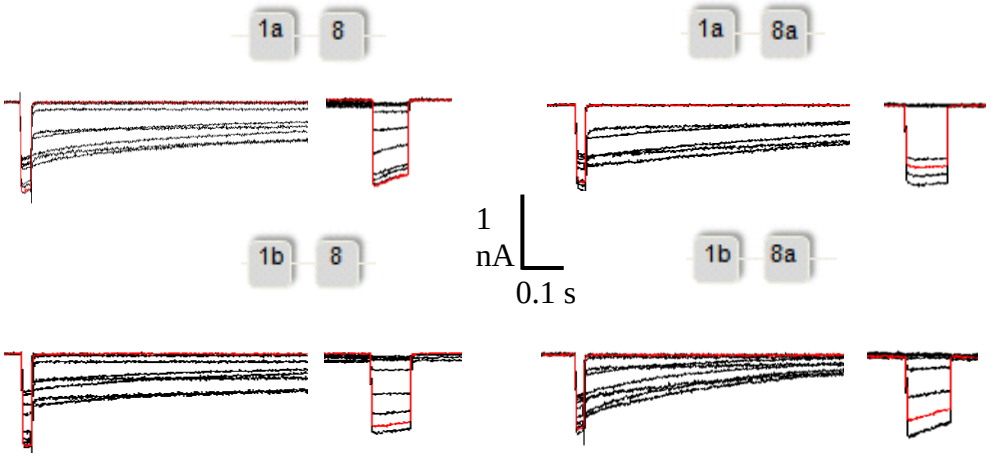

B.

C.

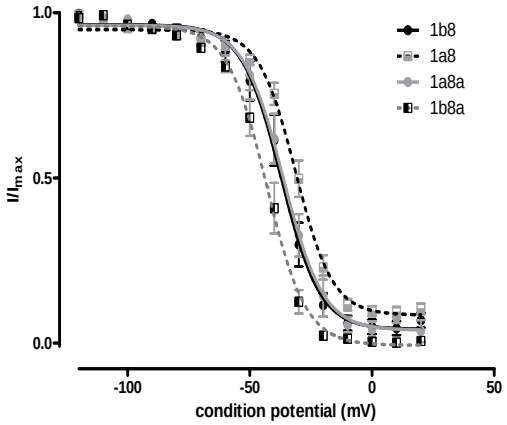

D.

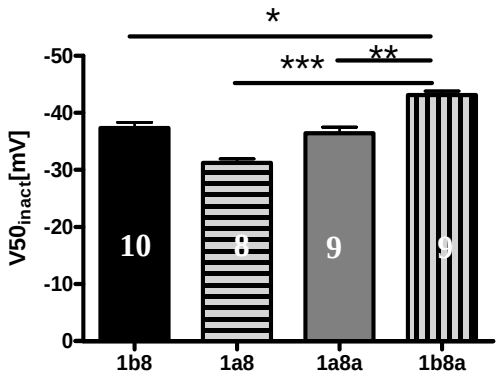

Figure 27: **Steady-state inactivation** SSI by stepping and prepulses **A**. Exemplary traces. **B**. Pulse protocol, cells were pulsed from a HP of -100mV to various TP, Δ10 mV, for 30ms followed by a 15s prepulse from-120 to +10 mV. A test pulse of 104 ms to +10mV was recorded finally. **C.** Inactivation curve fitted with a single Boltzmann equation..**D**. Statistics was analyzed with a one-way ANOVA, Bonferroni corrected, *p<0.05, **p<0.01, ***p<0.001).

3.2.2.1 The N-terminal exon 1b increases the current-density of humCa$_V$1.2 (IV)

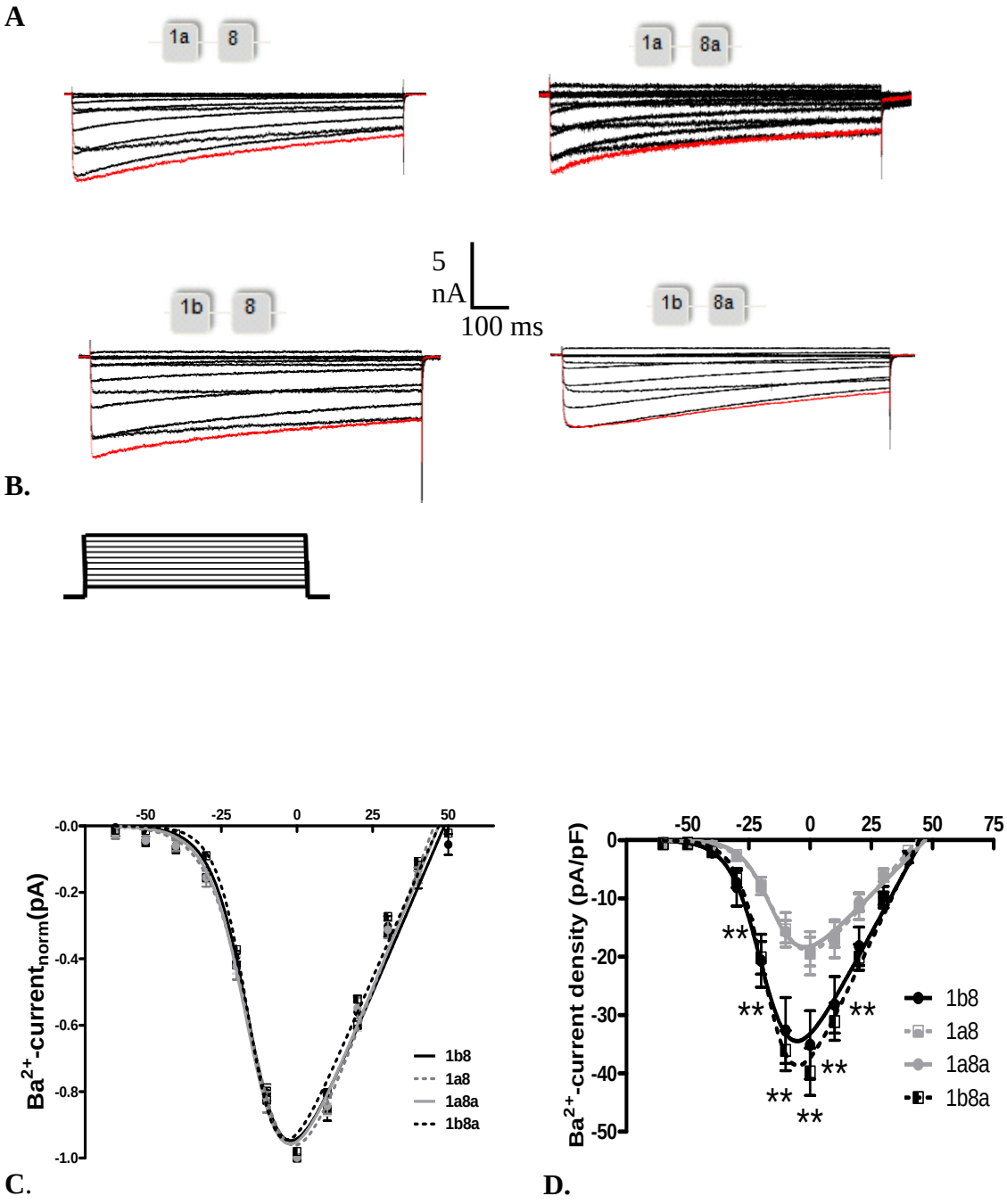

Figure 28: IV relationship of Ca$_V$1.2 SM and CM isoforms. **A.** Exemplary traces were pulsed to their maximum currents. **B.** Pulse protocol: Cells were held at -100mV and pulsed from -50 to +50 mV for 900 ms. **C.** Normalized current. **D.** Current density pA/pF, Data were tested for significance by a one-way ANOVA and a Bonferroni post-test, **p < 0.01.

3.2.2.2 The N-terminal exon 1b increases the current-density of humCa$_V$1.2 (GV)

A.

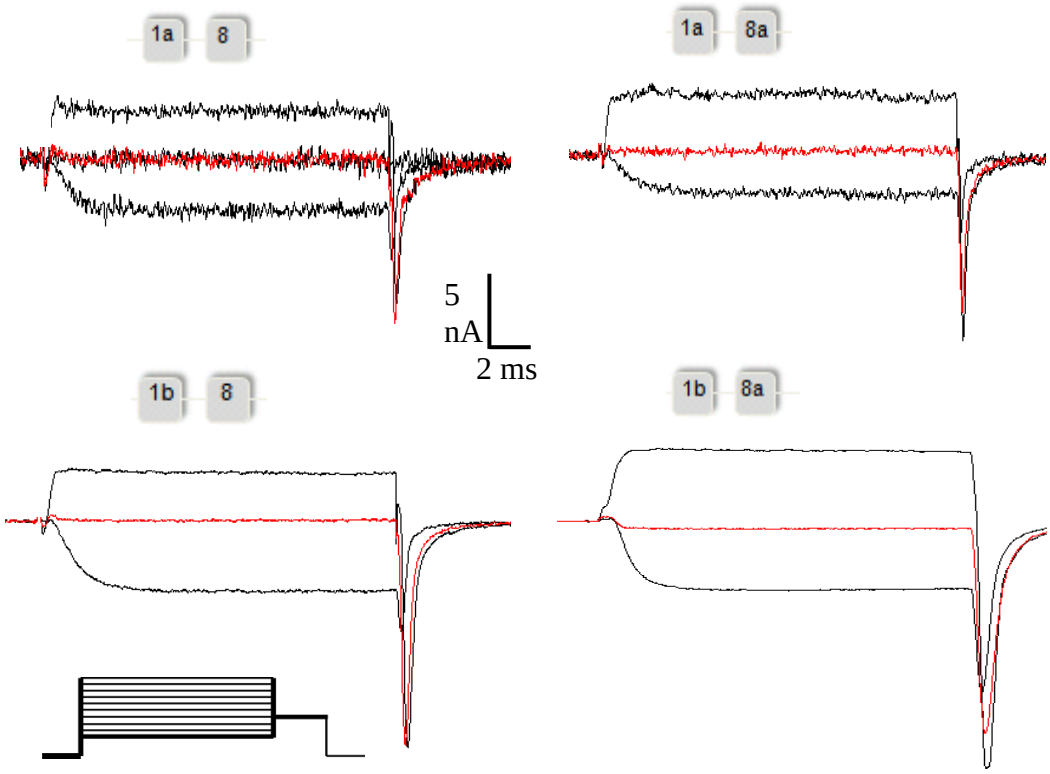

B.

.

C.

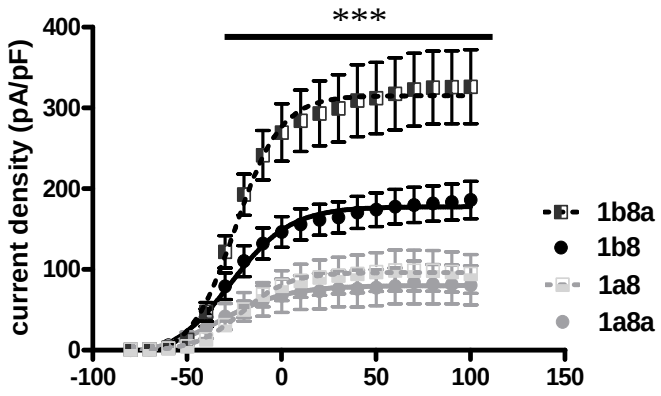

Figure 29: **Current density obtained from tail currents**. **A.** Exemplary tails. **B.** Current density plot. Data were analyzed for significance by a one-way ANOVA, Bonferroni corrected, *** p<0.001

3.3 Structure and functional analysis of the N-terminus of hum $Ca_V1.2$ under single-channel conditions

3.3.1 The N-terminus of hum $Ca_V1.2$isoforms does not alter single-channel gating properties

In order to reveal the significance behind altered channel inactivation and the increased current density obviously modulated by exon 1b, we analyzed single-channel events to reveal if a possible modulating character of exon 1b is manifested in the basic gating properties of $Ca_V1.2$. A higher channel current density can be either explained by a higher channel open probability or an increased channel surface expression. The former did not hold true as basic gating parameters under single-channel conditions remained unaltered among analyzed groups (one-way ANOVA, $p > 0.05$; s. table 4). Figure 30 depicts twenty consecutive exemplary traces representing the gating properties of all used $Ca_V1.2$ isoforms recorded under 110 mM Ba^{2+}. The open probability (P_{open} (%):5.0±0.9 (6), 4.3±0.5 (6), 3.8±0.6 (5), 6±0.6 (8), n.s.), tab.4 as well as the channel availability (availability (%):53±5 (6); 72±9 (6); 64±8 (5), 54±10 (8), n.s.), tab.4, are consistent with the overall analyzed isoforms. Figure 32 (A-D) demonstrates an exemplary time-course distribution of the open probability. Channel open probability was consistent over 19000 ms and below 10% in all groups. Appearance of mode gating was rare, although occasionally this was observed. Open- and closed-time histograms were fitted according a maximum-likelihood estimated (*MLE*) function. Exemplary Dwell-time histograms

quantifying the open-state life time were best described using a single-exponential fitting function (fig. 31, A-D), whereas closed-time histograms were bi-exponentially fitted (fig. 31, E-H). Exemplary latency histograms were fitted with a bi-exponential function best describing the activation of the channel going through two closed-states before entering the open-state (Herzig et al., 2007). Overall, the basic gating parameters should not profoundly be significantly different among the $Ca_V1.2$ isoforms.

3.3.2 Exon 1b of hum$Ca_V1.2$ decelerates and exon 1a accelerates time-dependent inactivation in single-channel experiments (I_{150ms})

We further wanted to verify if the effect of the N-terminus (exon 1a/1b) on inactivation could be detected at the single-channel level. For that, the inactivation of the mean-ensemble average current was detected by determine the percental amount (%) of remaining current after 150ms (Herzig et al., 2007, Jangsangthong et al., 2009). Fig. 33 A-E, clearly indicates that exon 1b8 decelerates the channel inactivation at a given TP of +10mV whereas exon 1a8a accelerates channel inactivation (I_{150ms} (%): 24±5 (5) vs.52±21 (5), ***$p < 0.001$), fig. 33E. A similar trend was found among the isoforms 1b8a and 1a8 (I_{150ms} (%):32.6±7.6 (5) vs.39.3±11.6 (5), n.s.), fig. 33E, although not significantly different.

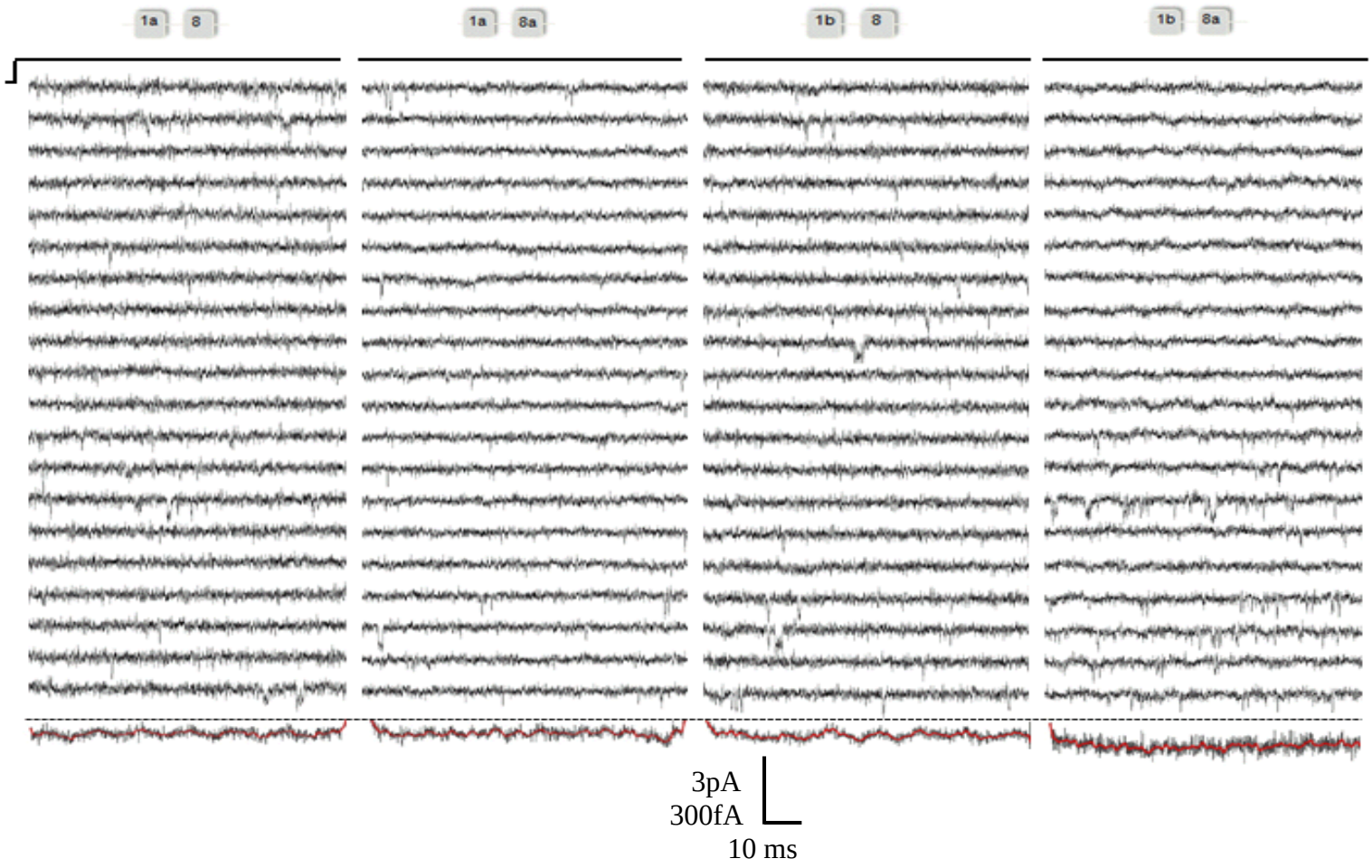

Figure 30**: Consecutive exemplary single-channel traces**, respectively 1a8, 1a8a, 1b8 and 1b8a.**Above**.20 consecutive exemplary traces showing the basic gating properties. **Below.** Mean ensemble average current obtained from 180 traces Cells were depolarized for 160ms from holding potential of -100mV to +10mV. Scale bar in pA refers to unitary events. Average currents are depicted in fA.

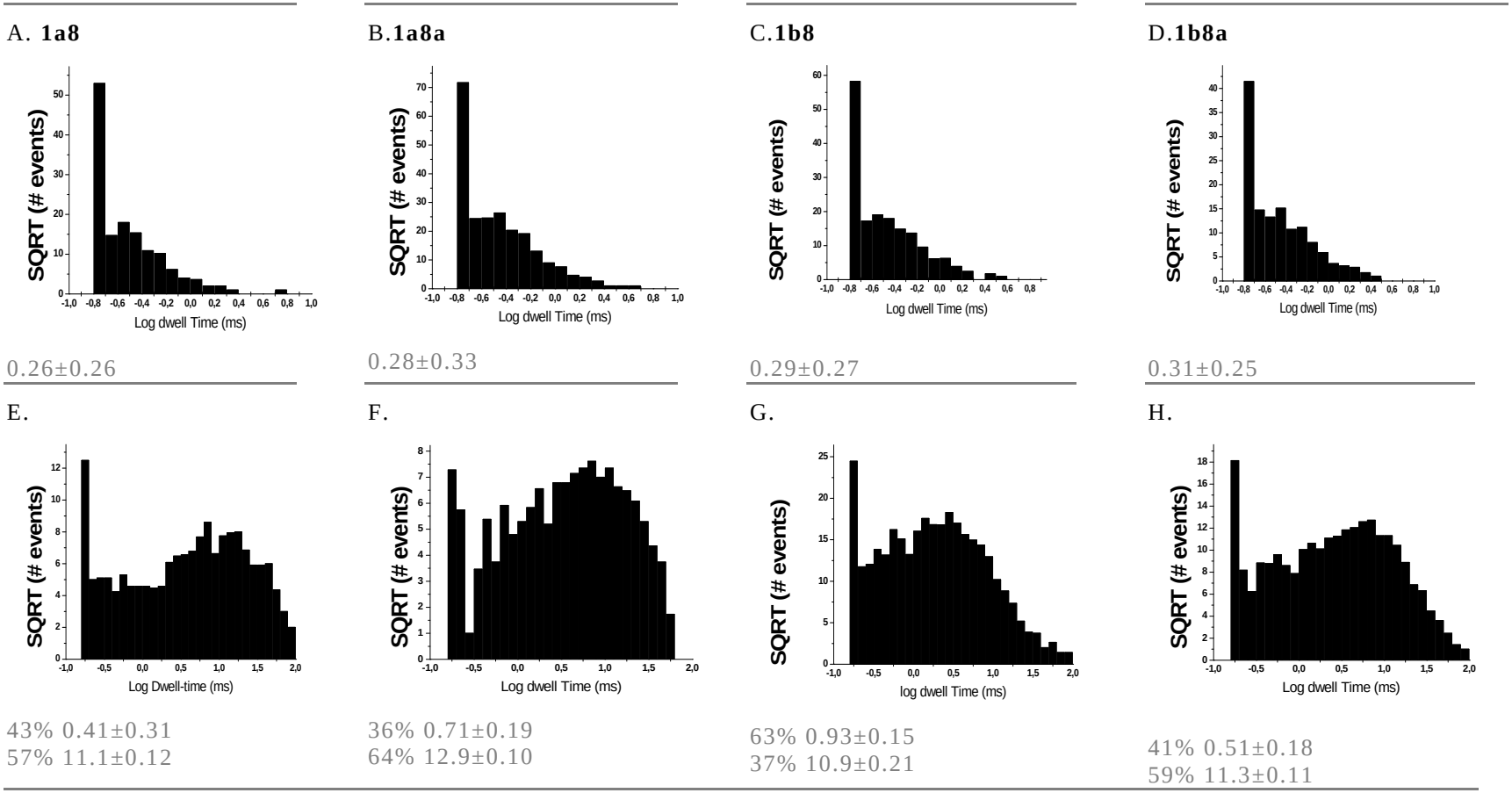

Figure 31: **Representative exemplary dwell time histograms** describing the open-and shut-times of four real single-channel experiments at a TP of +10 mV, respectively 1a8, 1a8a, 1b8 and 1b8a. **A-D** Open-time histograms were described by a mono-exponential probability-density function (PDF) with a single tau component**. E-H** Closed-time histograms were described by a bi-exponential PDF. Histograms were fitted based on a 10bin/decade-width by *MLE*, square-root method. Exemplary data are given as mean values with standard deviation (SD) and their percentage amount on PDF.

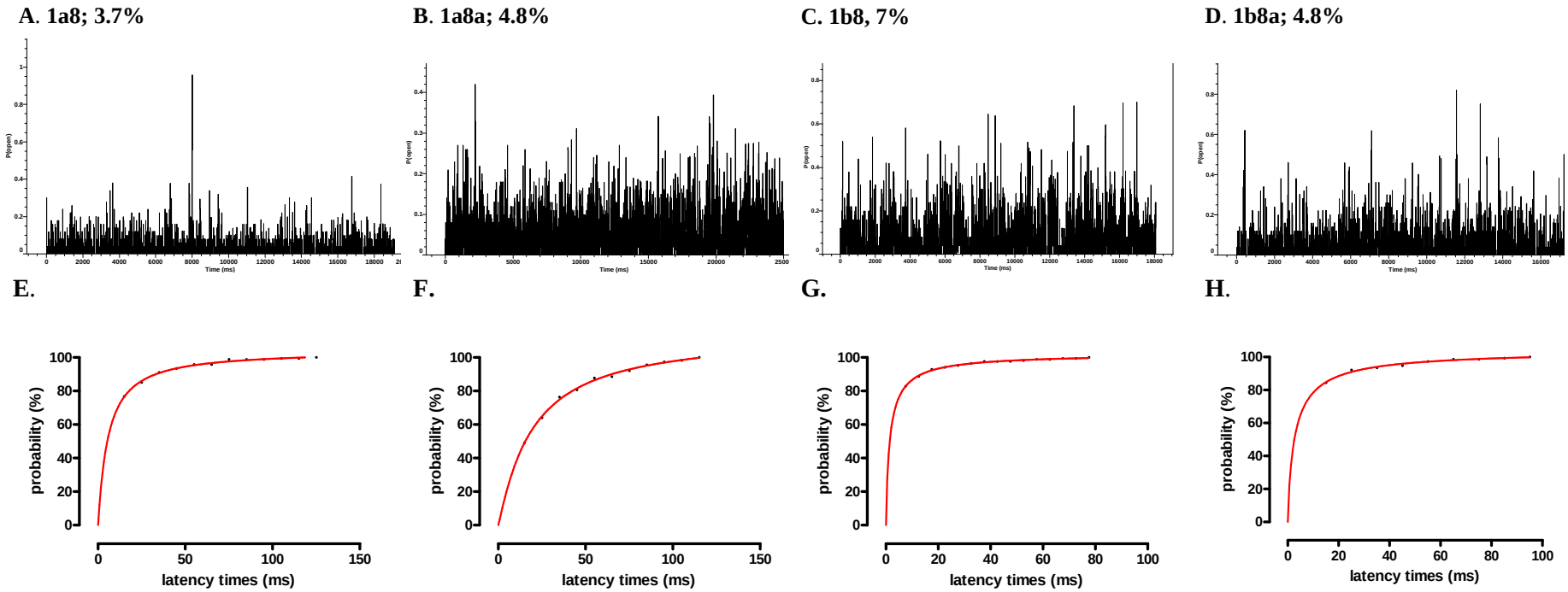

Figure 32: **A-D. Exemplary time-course distribution of $Ca_V1.2$ isoforms** representing the open probability at +10 mV, respectively 1a8, 1a8a, 1b8 and 1b8a. Channel time-course was recorded over 180 traces and gave no hint upon channel non availability mode (MODE 0) **E H.** Cumulative first latency function showing a bi-phasic distribution upon activation.

Exon 1a/1b of $Ca_V1.2$ influences the time-dependent inactivation (I_{150}ms)

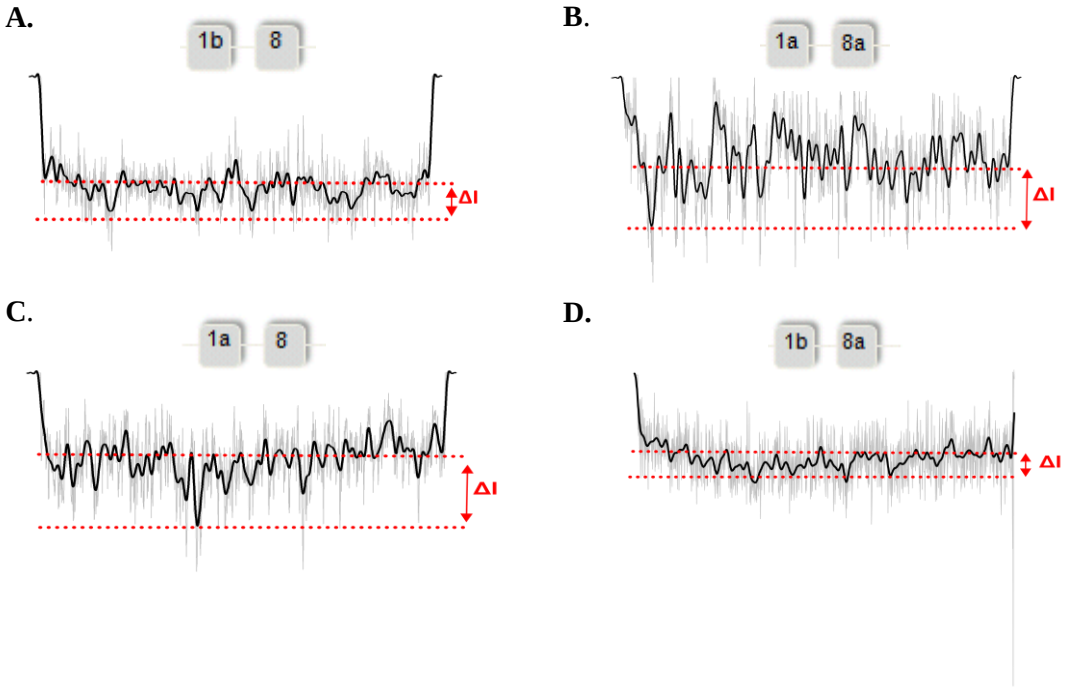

E.

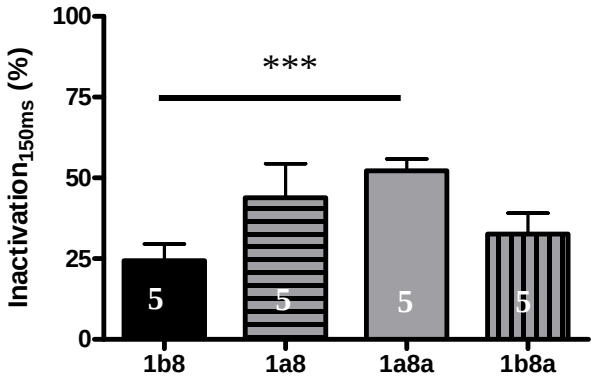

Figure 33: Channel inactivation estimated from mean-ensemble average currents. A-D Exemplary traces. ΔI was calculated from the local maximum I_{peak} and the remaining current after 150 ms at +10mV. E. Statistical significance was determined by an ANOVA with Newman-Keuls multiple comparison, ***p < 0.001.

3.3.3 Exon 1b of humCa_V1.2 increases channel surface expression in HEK 293 cells (A gating current analysis)

Since the findings at the single-channel level turned out to be not significantly different in regards to channel open probability, we wanted to determine the mechanism by which exon 1b increases the current density of Ca_V1.2. For that, the ON-gating currents *(Q_{ON}),* describing the capacitive voltage-sensor movement across the cell membrane upon channel activation, was analyzed. Cells were pulsed to depolarizing potentials at which the remaining net current was nearly zero (ionic inward current and outward currents compensate) when holding at the reversal potential, E_{rev}.(Baig et al., 2011, Wang et al., 2011) We found that exon 1b8a and exon 1b8 clearly increase Q_{ON} compared to exon 1a8a and exon 1a8 to a significant level by > 50% (Q_{ON}*:* 11.0±1.6 (9)and 8.7±2.0 (9) vs. 3.5±1.0 (11) and 3.7±1.3 (9),* $p < 0.05$,** $p < 0.01$), s. tab. 3 and fig. 34C.This clearly indicates for a higher number of functional Ca_V1.2 1b8a and 1b8 in the cell membrane of HEK 293 cells. Figure 34 describes the gating current analysis in more detail. Figure 34 A shows representive currents close or at $E_{rev.}$ Fig. 34B shows the magnification of the capacity transients upon repolarisation.

Taken together, these data in combination with our whole-cell and single-channel experiments strongly support our findings that exon1b of Ca_V1.2 increased the channel surface expression.

Exon 1b of humCa$_V$1.2 increases channel surface expression in HEK 293 cells

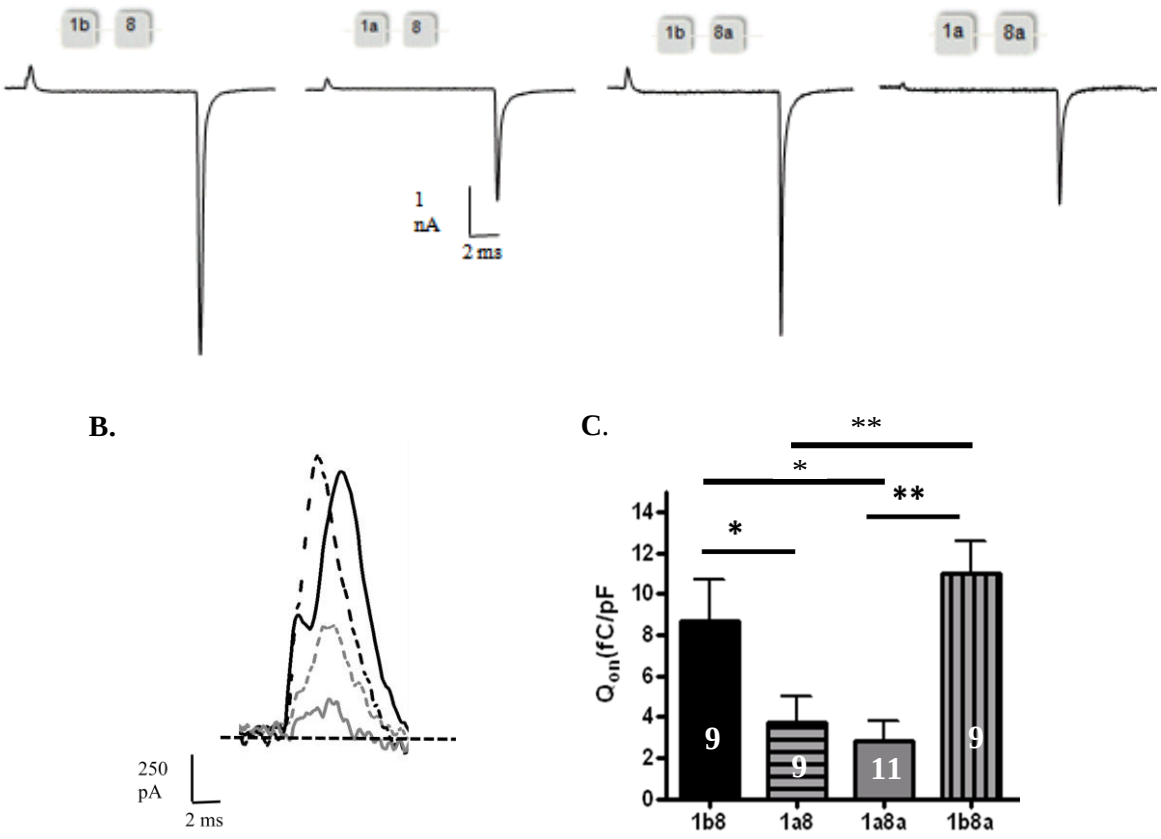

Figure 34**Gating current analysis**. **A**. Representative current traces show Q_{ON} determined by tail currents when holding to the E_{rev}.**B**. Magnification representing the capacitive transient evoked when holding to E_{rev}.**B**. Data were analyzed with a one-way ANOVA, Bonferroni corrected, *p < 0.05, **p < 0.01.

Table 3: Electrophysiological properties of $Ca_V1.2$ isoforms recorded in 5mM Ba2+ at a glance. Electrophysiological effect of the N-terminus of exon 1a/1b on $Ca_V1.2$ channel isoforms. A one-way ANOVA was carried out among the groups. The significance tests were then performed between the WT and their mutant counterparts. Data in bold show a significant difference with †/†p < 0.05*, #/#p < 0.001** and Δp < 0.001***. The n number of experiments is given in parenthesis.

Isoform	IV			G-V			SSI		GC
$Ca_V1.2$	$V_{1/2act}$	k	E_{rev}	$V_{1/2act}$	k_{low}	k_{high}	$V_{1/2inact}$	k	Q_{on}(pA/pF)
1b8 (SM)	-17.8±2.1 (5)	-6.4±1.5	45.7±2.8	-5.5±1.0 (8)	10.3±1.2	28.9±26.1	-37.3±1.0 (10)†	-8.0±0.9	8.7±2.0 (9)†/†
1b8a (778a)	-16.7±1.2 (7)	-5.8±0.8	44.7±1.6	-5.5±1.1 (9)	8.4±1.5	33.3±14.0	-43.1±0.7 (9)†/#/Δ	-8.0±0.7	11.0±1.6 (9)#/#
1a8a (CM)	-14.1±1.5 (11)	-6.1±1.0	47.1±1.5	-3.5±1.1 (11)	10.1±1.2	63.1±22.7	-36.4±1.1 (9)#	-8.1±0.9	3.5±1.0 (11)†/#
1a8 (1a77)	-12.3±2.3 (9)	-6.8±1.5	41.1±2.3	-3.6±1.2 (11)	10.5±1.5	37.6±6.5	-31.2±0.7 (8)Δ	-7.6±0.6	3.7±1.3 (9)†/#

Table 4: Single-channel properties of $Ca_V1.2$ isoforms recorded with 110 mM Ba^{2+} at a glance. Effect of the N-terminus of exon 1a/1b on $Ca_V1.2$ channel isoforms. All data were recorded and analyzed at a HP of -100mV and a TP of +10mV. Pulse length was 160 ms with inter pulse duration of 1 Hz. Sampling rate was 10 kHz. A one-way ANOVA was carried out among the groups. The significance tests were performed between the WT and their mutant counterparts. The *n* number of recorded cells is given in parenthesis.

Parameter	**1a8a**	**1a8**	**1b8a**	**1b8**	**p**
Availability	53±5 (6)	72±9 (6)	64±8 (5)	54±10 (8)	n.s.
P_{open}(%)	5±0.9 (6)	4.3±0.5 (6)	3.8±0.6 (5)	6±0.6 (8)	n.s.
I_{peak}[fA]	40±9 (6)	54±8 (6)	53± 18(4)	54±11 (8)	n.s.
I_{150} ms[%]	52±21 (5)*	39.3±11.6 (5)	32.6±7.6 (5)	24±5 (5)*	0.001
Mean first latency (ms)	26.9±7.6 (3)	19±3.7 (4)	17 (1)	18.8±4.1 (4)	n.s.
MOT (ms)	0.44±0.4 (6)	0.44±0.4 (6)	0.44±0.4 (5)	0.49±0.9 (8)	n.s
τ_{open} (ms)	0.28±0.3 (6)	0.34±0.04 (6)	0.35±0.05 (5)	0.34±0.05 (8)	n.s.
τ_{closed} fast (ms)	0.54±0.03 (3)	0.61±0.07 (4)	0.51 (1)	0.95±0.16 (4)	
τ_{closed} slow(ms)	12.8±3.8 (3)	19.1±4.7 (4)	11.3 (1)	19.6±4.4 (4)	n.s.

3.4. Splicing profile and distribution of murine $Ca_V1.2$mutually exclusive exons of HAB/LAB and NAB mice did not reveal any differences in brain areas associated with fear/anxiety

3.4.1 Generation of exon specific transcripts of mutually exclusive hot spot regions of the murine alpha1C subunit (Cav1.2).

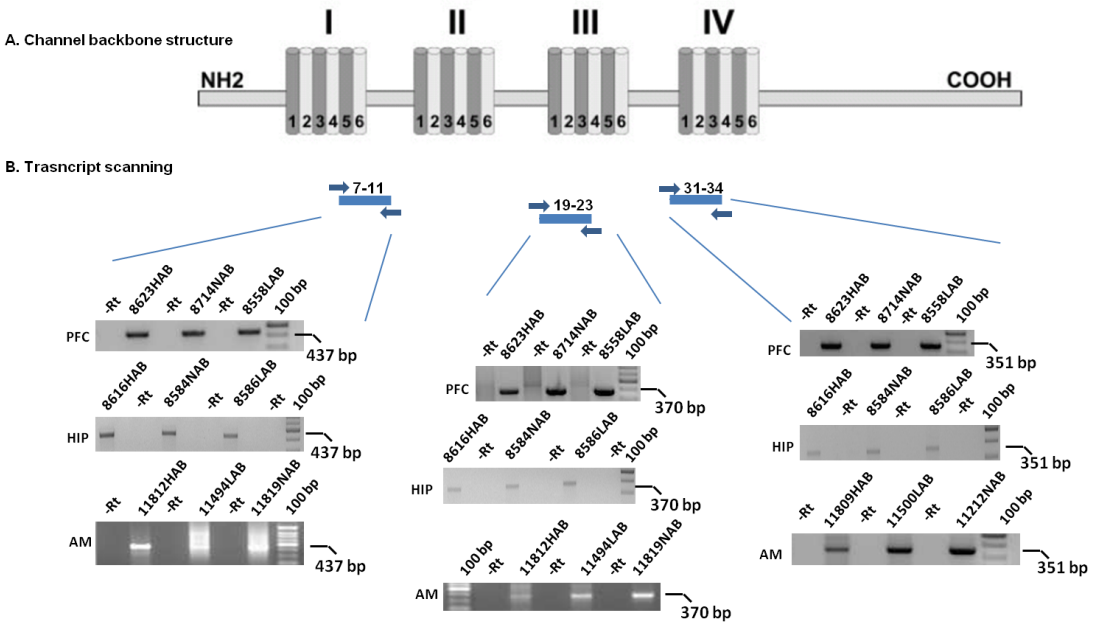

Figure 35 Transcript scanning of alpha1C from prefrontal cortex (PFC), hippocampus (HIP) and amygdala (AM). A. Backbone structure of the alpha1C subunit shows the hexa-helical structures of the domains I to IV. B. Relative exon assembly of targeted amplicons within the channel structure. Representative gels (1%) showing the expected amplicon size together with the negative control (-RT.) The flanking primers are highlighted with blue arrows.

We wanted to test our hypothesis that the $Ca_V1.2$ subunit of mice manifesting different traits of anxiety, respectively high-, low and normal-anxiety (HAB/LAB/NAB) shows altered splicing patterns in brain areas associated with anxiety/fear. For that, we looked into the mutually exclusive splice loci of the $Ca_V1.2$ subunit – we named them hot spot regions – which have already been associated with pathological conditions in neurological and cardiovascular disorders (Splawski et al., 2004, Tiwari et al., 2006). At first, we generated amplicons with RT-PCR and flanking primers for amplicon 7-11 to analyze exons 8/8a, amplicon 19-23 for exons 21/22 and amplicon 30-34 for exons 31/32 (fig. 35) A negative control (-RT) was always used to make sure that a prior RNA contamination could be excluded from other sources. Three animals of each trait (HAB/LAB/NAB) where analyzed regarding their hippocampus and amygdala expression patterns. For the prefrontal cortex only one animal triplicate was analyzed. The dissected amplicon regions were ligated in a pGEM-T Easy system and transformed in E-*coli* for final detection with the blue/white selection method. For each amplified region 96 bacteria colonies from HIP, 46 from AM and 96 from the PFC were screened.

3.4.2 Exon patterns of mutually exclusive regions in $Ca_V1.2$ of HAB/LAB/NAB mice do not reveal any significant difference among animals with trait anxiety

In the next step we wanted to reveal mutually exclusive exon expression by PCR with region specific primers (tab. 1) by colony screening. Figure 36 shows representative gels describing the exon distribution from different brain areas of HAB/LAB/NAB animals.

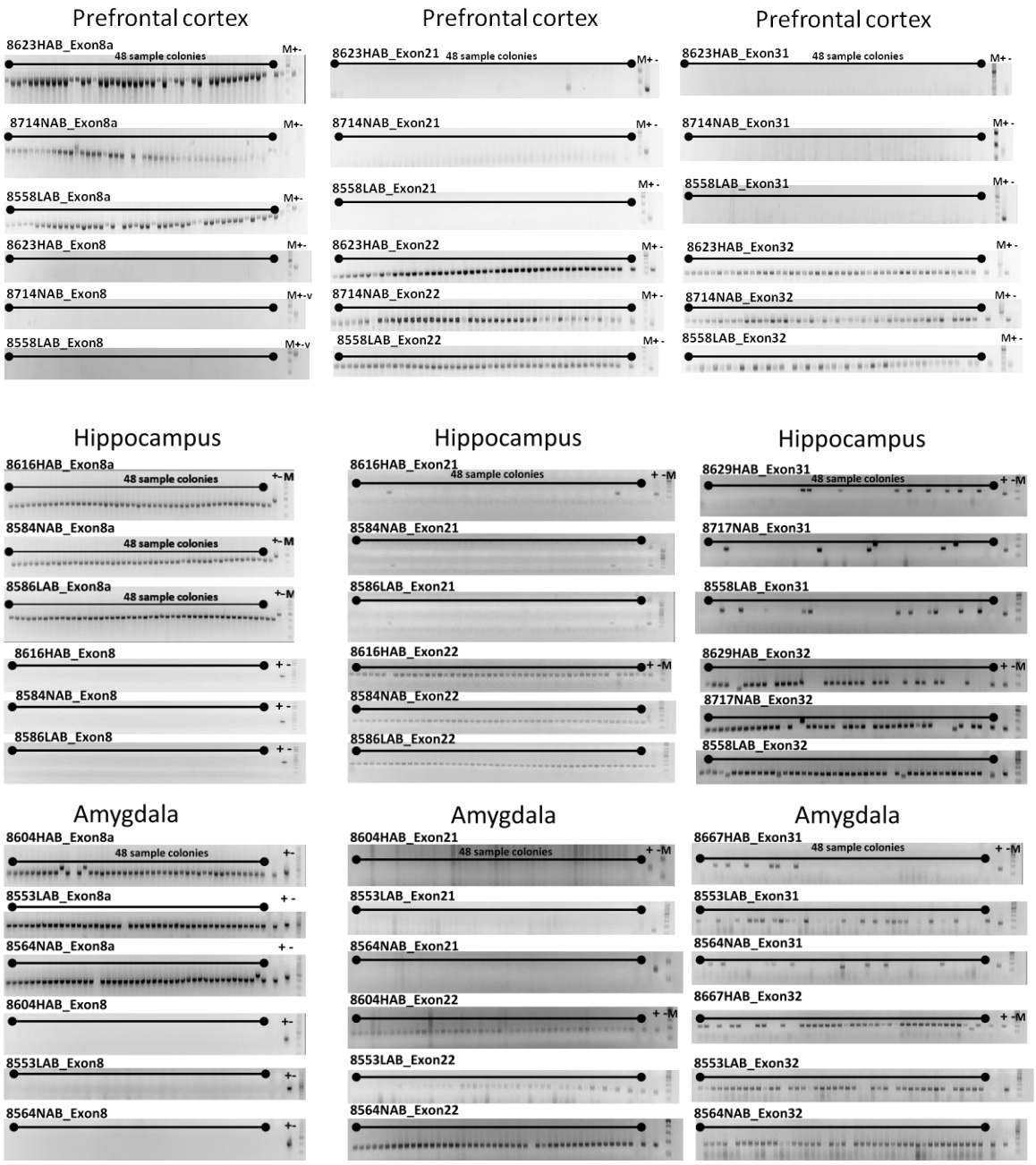

Figure 36.Exemplary gel photos showing specific exon profiles of mutually exclusive hot spot regions in alpha1C from different brain areas of HAB/LAB/NAB mice. A negative water control is indicated as – whereas the + positive control was used from already established amplicons carrying tissue specific exons. A 100bp marker was used to discriminate among exons.

A water negative control was used to assess any DNA contamination from other sources and a positive control from a clone containing the respective amplicon was used (left ventricle and cerebellum for 8/8a, aorta and left ventricle for 21/22 and left ventricle and aorta for 31/31). Bands detected from hippocampus and amygdalae were excised and send for sequencing. Bands from prefrontal cortex were estimated according to their relative size to the positive controls. More than 95% of the screened clones from HIP, AM and PFC express exon 8a. Similar findings were also observed for exon 22 in all areas in which expression level was more than 95%. The expression patterns regarding exon 32 are also consistent among the analyzed groups at 80-90% and 20-10% for exon 31. An ANOVA analysis did not reveal any significant difference among groups.

Taken together, these results implicated that mutually exclusive exons encoding for $Ca_V1.2$ do not differ among mice with different manifestations of trait anxiety and that exon combination 8a/22/32 are the predominantly expressed splice pattern in hippocampus, amygdala and prefrontal cortex.

3.4.3 Combinatorial splicing of HAB/NAB and LAB animals

Figure 37 gives an overview of a total of 16 identified $Ca_V1.2$ isoforms of HAB/LAB and NAB animals obtained by sequencing. Most of these isoforms have been described already by our group in the past to be expressed in the human brain. M5, M8, M9, M14, M15 and M16 are predicted to be non functional (Tang et al., 2004)

Sequencing Nr.	Exon profile	expected bp size	Exon profile distribution in % Hippocampus HAB n > 150	Hippocampus NAB n > 150	Hippocampus LAB n > 150	Amygdala HAB n >150	Amygdala NAB n > 150	Amygdala LAB n > 150	Prefrontal cortex HAB n > 100	Prefrontal cortex NAB n > 50	Prefrontal cortex LAB n < 100
M1	7 8a 9 10 11	**437**	**95.1**	**96.2**	**93.1**	**94.9**	**95.7**	**96.4**	**99.1**	**90.8**	**100.0**
M2	7 8a 9 9* 10 11	512	0.0	0.0	0.7	2.2	0.7	0.0	0.0	0.0	0.0
M3	7 8 9 10 11	**437**	**0.7**	**2.0**	**0.0**	**0.7**	**0.7**	**0.0**	**0.9**	**0.0**	**0.0**
M4	7 8 9 9* 10 11	512	0.0	0.4	0.0	0.7	0.0	0.0	0.0	9.2	0.0
M5	7 9 10 11	333	4.2	1.4	6.2	1.5	2.9	3.6	0.0	0.0	0.0
M6	19 20 22 23	**370**	**97.6**	**97.6**	**97.9**	**98.6**	**98.6**	**96.4**	**77.3**	**100.0**	**100.0**
M7	19 20 21 23	**370**	**1.0**	**2.0**	**0.7**	**0.0**	**0.7**	**2.9**	**22.7**	**0.0**	**0.0**
M8	19 20 21 22 23	430	0.0	0.4	0.0	0.0	0.0	0.0	0.0	0.0	0.0
M9	19 20 23	310	1.4	0.0	1.4	1.4	0.7	0.7	0.0	0.0	0.0
M10	30 32 33 34	**295**	**85.1**	**79.5**	**82.3**	**78.3**	**76.8**	**73.2**	**100.0**	**100.0**	**100.0**
M11	30 31 33 34	**295**	**9.0**	**10.4**	**9.4**	**16.7**	**21.8**	**25.4**	**0.0**	**0.0**	**0.0**
M12	30 31 34	262	0.0	0.7	0.0	0.0	0.7	0.0	0.0	0.0	0.0
M13	30 32 34	262	0.7	0.7	1.4	2.2	0.0	0.0	0.0	0.0	0.0
M14	30 31 32 33 34	323	1.4	0.7	1.0	0.7	0.7	0.7	0.0	0.0	0.0
M15	30 31 32 34	290	0.0	0.4	0.0	0.0	0.0	0.0	0.0	0.0	0.0
M16	30 33 34	267	3.8	7.6	5.9	2.2	0.0	0.7	0.0	0.0	0.0

Figure 37:**A total of 16 different splice combinations** were identified with the transcript scanning method. Data from hippocampus and amygdala are pooled data from 3 animals of each group. Prefrontal cortex data are based on one animal triplet only. The absolute abundance of the transcripts of HAB, NAB and LAB mice is based on at least 100 picked clones

Chapter IV

4. DISCUSSION

4.1 Final discussion

This thesis provides evidence and highlights the usefulness of single-channel recordings compared to commonly used whole-cell techniques to elaborate posttranscriptional modification of alternatively spliced $Ca_V1.2$ calcium channels*in vitro* and *ex vivo*. As far as we are aware we here describe for the very first time how complex pathophysiological conditions that are associated with alternative splicing alter the channel biophysical properties and hence electrophysiological properties of a single $Ca_V1.2$ calcium channel. Furthermore, this thesis exemplifies how the cell-attached configuration represents a suitable tool to augment whole-cell recording in order to better understand functional changes evaluated in *in vitro* and *ex vivo* systems.

4.2 Exon 33 of mouse $Ca_V1.2$plays an important role in channel function with severe pathophysiological consequences.

We demonstrated in a previous work about the significant role of the inclusion/exclusion of the cassette exon 33 of $Ca_V1.2$in a recombinant system altering the general gating properties of the channel. (Liao et al., 2007). However, since an *in vitro* system can never predict the actual physiological responses that coincide with altered electrophysiological properties, a KO model was established where the cassette exon 33 of *CACNA1C*was ablated from the mouse genome. We hypothesized that this ablation of exon 33 which encodes for an extra cytosolic motif in the IS3 segment of domain IV changes the electrophysiological properties of $Ca_V1.2_{\Delta 33}$ changing the overall current density. This

increased current density was already detected in a previous work in $Ca_V1.2_{\Delta 33}$cardiomyocytes by whole-cell recordings performed by Dr Li Guang. At the same time an increased $Ca_V1.2_{\Delta 33}$ surface expression which can also explain a higher current density could be excluded. However the whole-cell current *(I)* depicts a function of both the number of functional channels and their individual properties and can be best described by (Schröder et al., 1998):

$$\boldsymbol{I = N * i * P_{open} * F_{active}}$$

Whereas ***N*** represents the number of functional channels, ***i*** is the unitary current amplitude, ***P*** the open probability and ***F***, the availability of the channel. Hence, we speculated that the higher current density we see in our whole-cell experiments can be either due to a higher $Ca_V1.2_{\Delta 33}$ channel open probability, channel availability or alterations in the biophysical parameter ***i*** which describes an overall conductance of the channel by the unitary current amplitude. The latter one could be excluded due to visual estimation (data not shown). The first two parameters are known to be mediated physiologically by cAMP-dependent phosphorylation (Reuter et al., 1983, Yue et al., 1990, Herzig et al., 1993, Hirano et al., 1994).

Our hypothesis was confirmed showing a 4-fold increase in single-channel open probability (P_{open}) when comparing the currents of cardiomyocytes of KO $Ca_V1.2_{\Delta 33}$and WT$Ca_V1.2$ of 4 individuals (6-8month) of each group leading to a severe form of arrhythmia in 50% of our animals. These results suggest that exon 33 plays a crucial role in mice developing cardiac arrhythmia and possibly serves as a protecting factor in the

development of arrhythmia. We came to this conclusion when analysing the distribution of exon 33 in human samples with a cardiovascular history. In these samples, exon 33 was significantly up regulated (data not shown) letting us speculate about the potentially protective or adaptive role of exon 33.

In fact our single-channel data are reminiscent of already published data from Stefan Herzig's group (Schröder et al., 1998) in human cardiomyocytes with a heart failure background. The same trend can be seen when comparing the single-channel data of both groups with an increased channel open probability and an altered fast gating kinetics. Although the molecular background in Schroeder's publication was not the subject of their work, it is tempting to speculate about the possible role of exon 33 in failing human hearts. An additional aspect of our increased channel open probability arising from exon 33 deletion with no change in channel surface expression is corroborated by the publication of Gröner et al., 2004. In this work a transgenic mouse model with a significant over expression of$Ca_V1.2$ channel was described to be of lower or unaltered single-channel open probability when compared with the wild type.

The Additional data analysis for describing the fast kinetic parameters mean open/closed time (MOT, MCT) and mean first latency (MFL) of $Ca_V1.2_{\Delta 33}$ allowed us a deeper insight into aberrant channel kinetics. For the data analysis we assumed a simple sequential three-state model underlying our channel kinetics with two closed- and one open-state (Brown et al., 1982, Fenwick et al., 1982). Although not precise (ion channels are known to have several open and closed states) (Bezanilla et al., 2000, Chanda et al., 2004), it turned out to be sufficient in describing our short < 1ms and long open states >1ms with nearly no long open states in our WT. This finding supports the idea that exon

33 deletion enhances the longer open periods of $Ca_V1.2_{\Delta 33}$in a voltage-dependent manner. The opposite effect seems to occur when the channel dwells in the closed-state. The second closed-state is reduced ("depressed") allowing the channel finally to become faster activated again.

All our additionally obtained biophysical data matched the program predicted data of MOT and MCT and are in good agreement with already published data describing the kinetics of $Ca_V1.2$ in cardiomyocytes of mice (Gröner et al., 2004). This is particularly relevant in the context that single-channel recording was established in our group for the first time and that data usually recorded under old *DOS* based programs may not match with newer windows based version of Clampfit10.

Taken together the data perfectly matched a higher channel $Ca_V1.2_{\Delta 33}$open probability in the context that the channel relatively seen closed faster and was easier to activate. Moreover, the data are in accordance with the already obtained whole-cell data by Dr. Li Guang from our group. Although, a head to head comparison of whole cell and single-channel recordings is difficult to balance, a higher whole-cell current density can certainly be explained by a larger single-channel open probability that is accompanied by a longer open time. The larger mean ensemble average current describing the local current maximum I_{peak} of $Ca_V1.2_{\Delta 33}$ (tab. 2) is an additional bonus allowing us to speculate on an analogy of two independently derived kinetics.

What is finally the biophysical explanation behind the higher gating frequency of $Ca_V1.2_{\Delta 33}$? Cassette exon 33 encodes a peptide sequence which is in close vicinity to the voltage sensor of domain IV. Hence it is tempting to speculate that steric effects may

alter channel gating of $Ca_V1.2_{\Delta 33}$to an extent where open and closed-dwell times are simply differentially affected to enhance the overall open probability of the channel. In the same manner, this could explain a smaller channel mean first latency allowing the channel to open faster. However, this approach of steric prediction is highly speculative and difficult to prove.

In summary, these data give a good insight into $Ca_V1.2$channel gating under aberrant alternative splicing conditions. This work demonstrated how to pinpoint the severe effects of exon 33 deletion in *CACNA1C* in a complex pathophysiological context, all the way downstream to a molecular single-channel level. The higher channel open probability of $Ca_V1.2_{\Delta 33}$clearlyexplains the previously described results in action potentials prolongation in the QT interval, displaying more after-depolarization and autonomous action potentials. These typical features of human arrhythmia in cardiac ventricles of the mouse may represent a suitable model to study the pathological origin of arrhythmia in human patients. Supporting human data from failing heart patients indicate for a significant aberrant transcript regulation of cassette exon 33 in *CACNA1C.* Samples from heart failure patients indeed showed clearly the inclusion of exon 33 is significantly up regulated letting us to suggest a potential compensatory effect of exon 33 to ameliorate the symptoms of arrhythmia (Manuscript in preparation). Hence, the established arrhythmia model of our group may also represent an important target to study new pharmacological tools on a DHP basis under single-channel recordings.

4.2.1 Limitations of this study

Although the trend of single-channel parameters of $Ca_V1.2_{\Delta 33}$is in agreement with previous studies from failing heart, this work does not consider a possible physiological role of phosphatase (PP2A/PP2B) in the context of cAMP stimulation (Schröder et al., 1998, Yue et al., 1990). Schroeder *et al* (1998) showed using an, elegant approach in Markov modelling to indicate a possible role of blunted phosphatase activity. This could be demonstrated by the significant increased parameter of channel availability under the administration of 8-Br-cAMP. However, due to time and scholarship limitations these questions could not be addressed in this context and remained speculative.

4.3 The N-terminus of $Ca_V1.2$ regulates channel inactivation and surface expression

Ion channel inactivation is a fundamental mechanism in biological systems which aim to prevent ionic gradients to collapse and to determine action potentials of nerve cells in their duration. Voltage-dependent inactivation (VDI) of$Ca_V1.2$ calcium channels and calcium-dependent inactivation (CDI) are precisely tuned mechanisms that obviate cell toxicity due to calcium overload. Whereas CDI is regulated and controlled by the C-terminus and calmodulin CAM (Peterson et al., 1999) the mechanism behind VDI is not fully understood in detail.

Our data on the structure and functional relationship of the N-terminus of $Ca_V1.2$ isoforms clearly indicate for a significant functional role of exon 1a and 1bin both whole-cell and single-channel electrophysiology. Voltage-dependent inactivation of isoform

1b8a is significantly shifted to more hyperpolarised potentials when compared with their SM and CM counterparts 1b8 and 1b8a. Although, 1a8 shows a massive right shift in SSI the data are not significant different when compared to 1b8 and 1b8a, revealed by an ANOVA ($p > 0.05$). Based on these findings we can confirm a functional role of the N-terminus where exon 1b modulates $Ca_V1.2$ to close at more hyperpolarised potentials. This effect is completely compensated and abolished among the predominant SM and CM isoforms 1b8 and 1a8a. Additionally and only to some extent, single-channel results on the time-dependent inactivation support our findings that exon 1b/1a influences $Ca_V1.2$ channel inactivation with a faster inactivation rate for exon 1a and a slower inactivation rate for exon 1b. This finding was supported at least to some extent by an ANOVA ($p < 0.05$). The SM isoform 1b8 inactivates 50 % slower compared to the CM isoform 1a8a and a trend can be seen for 1b8a and 1a8, respectively. Another supporting source regarding the role of N-terminal macroscopic inactivation comes from our own group. Tang et al., could show in 2007 that the 1b8a isoform is indeed functionally expressed with 23% in Wistar-Kyoto rats (WKY) analysing full-length transcripts of *CACNAIC* from the heart. His finding is overlapping with our findings in terms of the steady-state inactivation kinetics with the 1b8a isoform to inactivate at more hyperpolarised states ($V_{1/2inact.}$ of -40.11±1.51 and our data $V_{1/2inact.}$-43.1±0.7). However, any mechanism behind an alteration of hum$Ca_V1.2$ inactivation by the N-terminal exons 1b/1a is not clear and remains speculative. The shorter version of the N-terminal 16 aa encoding heart isoform of exon 1a and the longer smooth muscle encoding 46 aa long 1bisoform have been described not to be of functional character by Nathan Dascal's group (Blumenstein et al., 2002). However, their findings were more focused on a

modulating role of PKC than a functional role of the N-terminus. In publications from recent years, the VDI has been described to arise at least in part by theα1-subunit itself and to be modulated also by auxilliary β-subunits (Lacerda et al., 1991, Varadi et al., 1991). Consistent with our findings regarding a possible role of exon8/8a in VDI the data fit well with the assumption of Richard Tsien's group describing the involvement of the IS6 segment in inactivation which is encoded by exon 8/8a (Zhang et al., 1994). Tsien's group suggested a sort of concerted interaction of all IS6 segments to induce inactivation. A further functional role of the N-terminus in inactivation has been described by Annette Dolphin's group in the $Ca_V2.2$ α1-subunit. Truncation of the amino-terminus of $Ca_V2.2$clearly accelerated the channel inactivation and suggested an additional role for theβ-subunit in inactivation (Stephens et al., 2000).Additional reminiscent findings to our data comes from Jonathan Jagger's group. In their work they could combine their findings on the N-terminus of the$Ca_V1.2$ and differentβ-subunits to influence channel inactivation(Cheng et al., 2007).Cheng reports that theβ-subunit (β_{1b},β_{2a} and β_3) expressed either with the 1b or 1c isoform from cerebral arteries caused shifts in both steady-state activation and inactivation

Comparing the findings from recent years to our findings on our macroscopic inactivation kinetics we conclude that the shift in SSI is at least partially induced by the β_{2a} we used in our experiments. In agreement with Zamponi's interpretation about the VDI in their publication from 2001 we suggest that the N-terminus (1a/1b) of different length possibly interacts with the β-subunit with a different affinity, initiating channel inactivation with different characteristics.

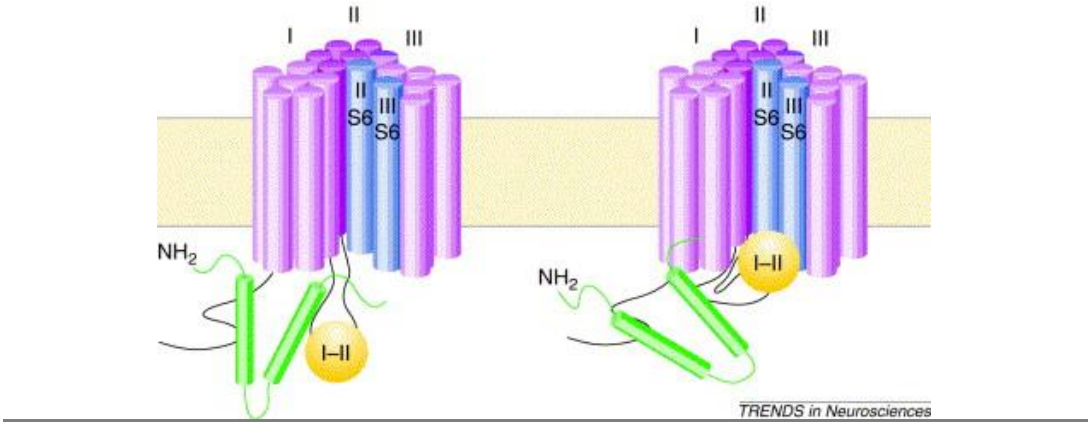

Figure 38. Hypothetical model of calcium channel inactivation. Multiple elements of the alpha1C subunit could contribute to channel inactivation including the cytoplasmic transmembrane motifs S6 (blue) in a concerted manor. The cytoplasmatic I-II linker of the pore (purple) interacts with the beta subunit (green) and the N-terminal long (46 aa) or short (16aa) form of the N-terminus of alpha1C. Adopted from Stotz and Zamponi, 2001)

The data regarding channel inactivation on the single-channel level (only tested at one TP) only support our findings to some extend and need be further evaluated in more detail. Additional single-channel experiments analysing the I_{150} rate at different holding potentials with a constant testing potential should light up the role of exon 1a/1b in $Ca_V1.2$ channel inactivation.

We here further demonstrate in our work by running a simple IV protocol that the current density is significantly increased when comparing the SM isoform 1b8 with the CM isoform 1a8a. The same finding holds true when analysing the 1b8a and 1a8a isoforms suggesting that the N-terminus of $Ca_V1.2$ determines the current density. We further verified in a second approach channel current densities by a tail current analysis (Takahashi et al., 2003, Wang et al., 2011). $Ca_V1.2$ channel current densities of SM isoform 1b8 and 1b8a were significantly increased by more than 40% over the cardiac

isoform 1a/8a and 1a/8 isoform. Similar significant findings hold true for the tail currents being larger by more than 50%.

Ion channel surface expression can be determined by either western blotting analysis in combination with channel tagging or by immune-staining (Li et al., manuscript in preparation). Analysing gating currents which predicts the movement of ion charges in the membrane due to depolarising test potentials is a well accepted semi-quantitive measurement which allows making predictions on channel surface expression (Armstrong and Bezanilla, 1973; Hodgkin and Huxley, 1952). This could be already demonstrated by others and our group in the past (Wang et al., 2011).

In a representative number of experiments here the demonstrated data support the hypothesis that SM $Ca_V1.2$channel surface expression is enhanced by the increased maximum gating currents (Fang and Colecraft, 2011). This is in strong agreement with already obtained whole-cell data of the various used $Ca_V1.2$isoforms used in this study indicating a similar gating profile. Analyses of whole-cell steady-state kinetics and single-channel experiments demonstrated that an increased current density induced by the SM isoform was theoretically underpinned by a higher $Ca_V1.2$channel surface expression. Wang *et al*., could show in 2011 that channel surface expression of $Ca_V1.2$ indeed correlated with the maximum gating currents. The cytosolic N-terminal portion is known to interact with various signalling molecules and enzymes. Moreover auxiliary $Ca_V1.2$ subunits like the beta or alpha2delta is known to support channel trafficking via a retention signal from the ER. Bannister could show in his work from 2011 that arterial smooth muscle cells that both expressed exon 1b and1c showed different surface expression patterns in arterial smooth muscle cells. This was further evaluated by a

mechanism with different preferential trafficking of the alpha1C subunit by the alpha2delta subunit. Such a potential mechanism should indeed be analysed by expressing different alpha2delta subunits with the $Ca_V1.2$ channel pore.

4.4 Physiological/Pathophysiological relevance and limitations

Alternative splicing was reported over the last decades to be linked to diseases, development, sex determination and physiology in general. (Hammes et al., 2001, Gerzanich et a., 2003, Ule et al., 2003). A widely accepted idea today is that the number of occuring splice variants in a system is linked to a certain condition, rather than being expressed in a random manner (Neves et al., 2004).With this thesis we show for the first time on the single-channel level that the N-terminus by all means determines the structure and functional relationship of hum $Ca_V1.2$ calcium channelsin a HEK 293 system. To our knowledge, we are the first group comparing the predominantly expressed $Ca_V1.2$ SM isoform 1b/8/9/22/32 with the predominantly expressed cardiac isoform 1a/8a/9/22/32 in a broad electrophysiological approach. In previous publications by others and our group the hum $Ca_V1.2$ 1b splice variant has been reported to be predominantly expressed together with exon 8ain the brain> 50%and to a lesser extend in the heart (Blumenstein et al., 2002, Soldatov et al., 1992, Tang et al., 2004).On the other hand, the human cardiac 1a isoforms occurs in combination with exon 8a in the heart with more than 50 % expression level (Tang et al., 2004). We now show in our experiments that exon 1b8a significantly shifts the inactivation of hum $Ca_V1.2$ to more hyperpolarised potentials and

at the same time increases the current due to a larger channel surface expression. Differences in SSI could not be observed for the SM specific 1b8 isoform when compared to the cardiac expressed 1a8a CM isoform. The 1b8a isoform could be indeed described to be functionally expressed in the heart (Tang et al., 2007) and we do have reasonable arguments, *a posteriori*, that it could be the predominantly expressed isoform in the brain and also in smooth muscle tissue. A shifting window current to more hyperpolarized potentials is linked to a faster inactivation of $Ca_V1.2$ channel population which on the other hand allows the channels to get activated earlier. Hence the diminished window current for 1b8a would reduce the time period of channel activation-inactivation cycle allowing a faster channel response upon membrane depolarization. Furthermore, a predominant expression of exon 8 over 8a in smooth muscle cells would benefit any calcium channel blocker induced pharmacological application due to a higher DHP sensitivity described to exon 8 over exon 8a (Welling et al., 1997). Such a selective distribution of alternatively spliced exons would certainly be beneficial knowledge when deciding on any potential treatment with DHPs in mood disorders in a dose-dependent manner.

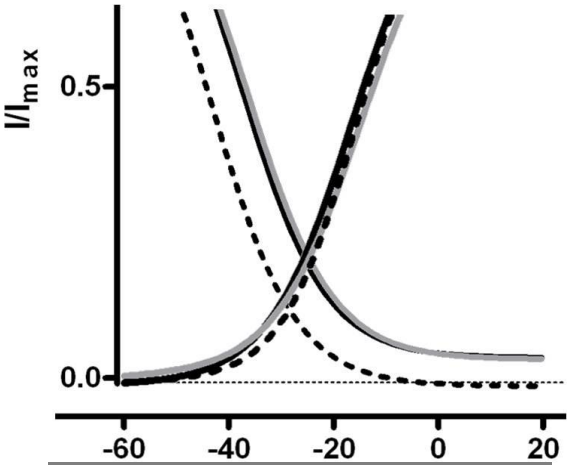

Figure 39: Idealized steady-state activation/inactivation kinetics for the SM (black) and cardiac (grey) isoform. The 1b8a isoform is depict in a dashed line (black)

However, any predictions of physiological significance for the utilization of the predominant 1b8a isoform remains unsolved; and the mystery why a cell requires a

plethora of different splice isoforms for optimal biological function still remains speculative. That's why it is important to establish specific alternative exon KO models to better study the functional and physiological/pathophysiological consequences which may be associated with a particular alternative splicing profile.

4.5 The N-terminus of $Ca_V1.2$ does not alter basic single-channel gating properties.

To further evaluate the origin of altered current densities mediated by exon 1a/1b we looked into single-channel events recorded under 110 mM Ba^{2+}. As already described in the first part of this thesis a larger current density can be either a result from a higher channel surface expression or due to higher channel open probability. However, the results did not indicate any changes in basic gating properties among the analysed groups. Although there are limitations in real single-channel events, the data are consistent and *a posteriori* unlikely to differ in basic gating, even at higher amounts of real single-channel experiments. In recent years, $Ca_V1.2$ has been extensively studied under single-channel conditions by various groups *in vitro* and *ex vivo*. Here the underlying *in vitro* results recorded under similar conditions in regards with charge carrier and used $Ca_V1.2$species strongly matched with already published cell-attached data from smooth muscle cells and heart (Benham et al., 1987; Herzig et al., 2007, Jangsangthong et al., 2009). For our kinetic analysis we again assumed a sequential 3-state model although mode gating could be observed to some extent. Exemplary dwell-time histograms were described with a

mono- (open-time) or biexponential fit (shut times). Mean first latency was further analysed by a bi-exponential fitting function according to Herzig et al., 2007.

Hence, a change in channel surface expression of SM $Ca_V1.2$ is the most likely scenario which could explain a higher channel current density underlying exon 1b.

4.6 Alternative splicing of $Ca_V1.2$ in animals with trait anxiety does not reveal any potential pathophysiological splicing fingerprints.

Here we demonstrated with preliminary data that alternative splicing of $Ca_V1.2$ might be subject to anxiety related behaviour in rodents (HAB/LAB/NAB mice). Previous publications about the role of $Ca_V1.2$ in mood and mental disorders have already uncovered the physiological implications and the potential pharmacological benefit of $Ca_V1.2$ as a drug target (Busquet et al., 2008, Sinnegger-Brauns et al., 2004, Casamassima et al., 2010). For the first time, we looked into specific brain regions associated with anxiety and fear related behaviour of mouse strains manifesting different traits of anxiety, respectively high-, low- and no- anxiety related behaviour. Our data revealed no characteristic changes in splicing patterns as we hypothesized. Mutually exclusive exons 8/8a, 21/22 and 32/33 were detected in a broad attempt with specific primers by colony PCR over all samples from amygdala, hippocampus and prefrontal cortex with no flamboyant expression profile in HAB/LAB and NAB animals. Our data indicate that exon 8a is the predominant expressed isoform in the brain of mice. This finding is overlapping to already published data from Nicolas Soldatov and our group

although in human brain samples (Tang et al.,2004, Soldatov et al., 1992). These results need further clarifications as the brain contains neurons, glia and is highly vascularised suggestion presence of smooth muscles. Franz Hofmann's group described in 1997 about the tissue specific dihydropyridine sensitivity of the IS6 segment of $Ca_V1.2$ in cardiac and smooth muscle cells with the 8 isoform being exclusively expressed in the aorta and the 8a isoform being reduced to smooth muscle cells (Welling et al., 1997). The smooth muscle variant 8 is known to be more sensitive to DHP compared to the cardiac 8a variant(Welling et al., 1997, Liao et al., 2007) which provides useful information to our findings since an anti-depressant-like effect in rodents has been reported by several groups in the past (Cohen et al., 1997, Galeotti et al., 2006). Several case studies also reported about the potential beneficial characteristic of calcium channel blockers in patients with depressions (Biriell et al., 1989, Hullet et al., 1988). However, the evidence is rather controversial at this point and needs to be further evaluated.

Colony PCR further revealed that exon 22 isoform being the predominantly expressed isoform in the brain with more than 90 %. This finding has been also described in the past in rat (Soldatov et al., 1995, Tang et al., 2004). Furthermore, exon 22 is also involved in DHP binding with a higher sensitivity over exon 21 (Soldatov et al., 1995).Exon 32 is expressed to the highest extent in all three brain regions at a level of more then 80 %.

The data we present here are the first approach describing mutually exclusive exon distribution in the brain of rodents. We did not find any convincing argument which supports the hypothesis that anxiety may correlate to some extent with exon profiling. Our data based on 16 discovered exon combinations indicate that exon 8a, 22 and 32 built the fundamental backbone structure of $Ca_V1.2$ in the mouse brain. Since the brain and

brain activity is sustained by an intense blood flow though blood vessels it is difficult to speculate about the exact origin of our detected exons. However, it is likely that the combinations found in our samples originate from the larger amount of brain tissue analysed in our study. Supporting data about the predominant expression of exon 22 and 32 in human brain comes from the Soldatov and our group. An exact clarification could be obtained by an approach to screen for full length $Ca_V1.2$ transcripts in the rodent brain. Moreover, the expression levels of exon 1a and 1b in our anxiety samples could not be addressed in this project due to limited time of this PhD. Real time PCR should clarify about the expression levels in the brain. Furthermore, the already described exon 1c isoform described in the brain and human and rodent samples from Jonathan Jaggar's group would be of additional interest.

However, we have indeed good reason to believe that $Ca_V1.2$ plays a significant pathological role in mental disorders. Whether $Ca_V1.2$ is the primary trigger in a potential pathological history still remains elusive at this time. We could see in a first approach by real-time PCR (data not shown) that $Ca_V1.2$ is significantly increased in the hippocampus of our HAB animals when comparing it to LAB and NAB animals. A similar trend for an up regulation of $Ca_V1.3$ transcripts could be seen in HABs towards LAB animals. In this context it would be certainly of interest to assess whether the expression levels exons 1a/1b and 1c isoforms may alter in the various brain areas associated with trait anxiety. Especially if exon 1b could play a role in the up regulation of $Ca_V1.2$ in the hippocampus of our trait anxiety animals should be evaluated in further experiments.

4.7 General conclusion and future prospects

This PhD thesis delivers useful information on how to combine single-channel patch clamp recordings in addition to whole-cell patch clamp recordings. It furthermore provides a good guideline on how to analyse and evaluate single-channel raw data. It is demonstrate that the exclusion of a single cassette exon (exon 33) of *CACNA1C* encoding for $Ca_V1.2$is tethered to severe pathophysiological consequences in a mouse model with *Torsade de pointes* arrhythmia. Various groups have shown in previous publications that aberrant alternative splicing of $Ca_V1.2$ can result in severe cardiovascular and neurological dysfunction (Tiwari et al., 2006; Gidh-Jain et al., 1995). In this thesis it is demonstrated that alternative splicing is not only subject to developmental and tissue dependent function and regulation, but also to pathological states. The single-channel data underpin these data and exemplify the pathophysiological background in terms of altered biophysical channel function to a large extend. In subsequent studies, it needs to be further clarified to which extend other modulating proteins such as PP2B are involved in the pathophysiology of arrhythmia (Schröder et al., 1998). Single-channel recordings of our Δ33 cardiomyocytes under application of okadaic acid, 8-cAMP with or without a stimulating prepulse should make channel availability more profound. An additional gating analysis will show on how a possible pathophysiological role of PP2B may correlate to arrhythmia in our KO animals.

The role of the N-terminus of $Ca_V1.2$ could only be addressed in this thesis to some extend due to the limited time of the project. Although here evidence was provided that exon 1a/1b of $Ca_V1.2$ indeed regulates channel kinetics, the regulatory mechanisms behind it could not be revealed. The increased current density that is linked to an elevated

surface expression under exon1b should be analyzed to a broader extend. The human exon 1c isoform which could not be detected so far should be implicated in this project. Further electrophysiological analysis of exon 1a/1b/1c in a recombinant system expressed with different auxiliary subunits (alpha2delta$_{1-4}$ and beta$_{1-4}$) should clarify the structure and functional role of the N-terminus of $Ca_V1.2$. Moreover, knock down experiments of alpha2delta in a native system would be reasonable in terms of$Ca_V1.2$ channel integration into the cell membrane (Bannister et al., 2011). A possible implication of RGK proteins like Rem or Rad which interact with exon1 of $Ca_V1.2$ and alter the surface expression should be considered as shown by Henry Colecraft's group.

The hypothesis about a pathophysiological role of $Ca_V1.2$ in trait anxiety due to aberrant splicing could not be verified. Bona fide, we analyzed HAB/LAB/NAB animals in terms of altered splicing profiles in *CACNA1C* of brain areas associated with fear. Indicators of isoform specific splicing correlating with trait anxiety in our animals could not be found. However, the transcript scanning experiments and the colony PCR provide useful insight into the expression pattern of mutually exclusive exons of *CACNA1C* in the brain of rodents and match with already published data. It would be further interesting to evaluate the transcript levels of mutually exclusive exon 1a/1b in the brain of the trait anxiety model. Preliminary data obtained by real time PCR clearly indicate for significant altered transcript levels of alpha1C and alpha1D in HABs towards NABs and LABs (data not shown). Based on these findings it would be interesting to verify how full length transcript of alpha1c and alpha1D correlate in terms of alternative splicing.

Chapter V

5. REFERENCES

Abernethy, D.R., and Soldatov, N.M. (2002). Structure-functional diversity of human L-type Ca^{2+} channel: perspectives for new pharmacological targets. J Pharmacol Exp Ther *300*, 724-728.

An, R.H., Davies, M.P., Doevendans, P.A., Kubalak, S.W., Bangalore, R., Chien, K.R., and Kass, R.S. (1996). Developmental changes in beta-adrenergic modulation of L-type Ca^{2+} channels in embryonic mouse heart. Circulation research *78*, 371-378.

Anon, G. (2000). Cross-national comparisons of the prevalences and correlates of mental disorders. WHO International Consortium in Psychiatric Epidemiology. Bulletin of the World Health Organization *78*:413-26

Arikkath, J., and Campbell, K.P. (2003). Auxiliary subunits: essential components of the voltage-gated calcium channel complex. Curr Opin Neurobiol *13*, 298-307.

Armstrong, C.M., and Bezanilla, F. (1973). Currents related to movement of the gating particles of the sodium channels. Nature *242*, 459-461.

Bannister, J.P., Thomas-Gatewood, C.M., Neeb, Z.P., Adebiyi, A., Cheng, X., and Jaggar, J.H. (2011). $Ca_V1.2$ channel N-terminal splice variants modulate functional surface expression in resistance size artery smooth muscle cells. The Journal of biological chemistry *286*, 15058-15066.

Barg, S., Ma, X., Eliasson, L., Galvanovskis, J., Gopel, S.O., Obermuller, S., Platzer, J., Renstrom, E., Trus, M., Atlas, D., *et al.* (2001). Fast exocytosis with few Ca^{2+} channels in insulin-secreting mouse pancreatic B cells. Biophys J *81*, 3308-3323.

Bartels, P., Behnke, K., Michels, G., Gröner, F., Schneider, T., Henry, M., Barrett, P.Q., Kang, H.-W., Lee, J.-H., Wiesen, M.H.J., *et al.*(2009). Structural and biophysical determinants of single $Ca_V3.1$ and $Ca_V3.2$ T-type calcium channel inhibition by N_2O. Cell Calcium *46*, 293-302.

Bauer, E.P., Schafe, G.E., and LeDoux, J.E. (2002). NMDA receptors and L-type voltage-gated calcium channels contribute to long-term potentiation and different components of fear memory formation in the lateral amygdala. The Journal of neuroscience: the official journal of the Society for Neuroscience *22*, 5239-5249.

Bean, B.P. (1985). Two kinds of calcium channels in canine atrial cells. Differences in kinetics, selectivity, and pharmacology. J Gen Physiol *86*, 1-30.

Benham, C.D., Hess, P., and Tsien, R.W. (1987). Two types of calcium channels in single smooth muscle cells from rabbit ear artery studied with whole-cell and single-channel recordings. Circulation research *61*, I10-16.

Bers, D.M. (2000). Calcium fluxes involved in control of cardiac myocyte contraction. Circulation research *87*, 275-281.

Bers, D.M. (2002). Cardiac excitation-contraction coupling. Nature *415*, 198-205.

Bers, D.M., and Guo, T. (2005). Calcium signaling in cardiac ventricular myocytes. Ann N Y Acad Sci *1047*, 86-98.

Bezanilla, F. (2000). The voltage sensor in voltage-dependent ion channels. Physiol Rev *80*, 555-592.

Biel, M., Ruth, P., Bosse, E., Hullin, R., Stuhmer, W., Flockerzi, V., and Hofmann, F. (1990). Primary structure and functional expression of a high voltage activated calcium channel from rabbit lung. FEBS Lett *269*, 409-412.

Biriell, C., McEwen, J., and Sanz, E. (1989). Depression associated with diltiazem. Bmj *299*, 796.

Black, D.L. (1998). Splicing in the inner ear: a familiar tune, but what are the instruments? Neuron *20*, 165-168.

Bosch, O.J., and Neumann, I.D. (2008). Brain vasopressin is an important regulator of maternal behavior independent of dams' trait anxiety. Proceedings of the National Academy of Sciences of the United States of America *105*, 17139-17144.

Brown, A.M., Camerer, H., Kunze, D.L., and Lux, H.D. (1982). Similarity of unitary Ca^{2+} currents in three different species. Nature *299*, 156-158.

Burge, C.B., Tuschl, T., and Sharp, P.A. (1999). 20 Splicing of Precursors to mRNAs by the Spliceosomes. Cold Spring Harbor .

Busquet, P., Hetzenauer, A., Sinnegger-Brauns, M.J., Striessnig, J., and Singewald, N. (2008). Role of L-type Ca^{2+} channel isoforms in the extinction of conditioned fear. Learn Mem *15*, 378-386.

Busquet, P., Nguyen, N.K., Schmid, E., Tanimoto, N., Seeliger, M.W., Ben-Yosef, T., Mizuno, F., Akopian, A., Striessnig, J., and Singewald, N. (2010). $Ca_V1.3$ L-type Ca^{2+} channels modulate depression-like behaviour in mice independent of deaf phenotype. Int J Neuropsychopharmacol *13*, 499-513.

Canteras NS, Resstel LB, Bertoglio LJ, Carobrez Ade P, Guimaraes FS (2010). Neuroanatomy of anxiety. Curr. Top. Behav. Neurosci. 2:77-96.

Carbone, E., and Lux, H.D. (1984). A low voltage-activated, fully inactivating Ca channel in vertebrate sensory neurones. Nature *310*, 501-502.

Casamassima, F., Hay, A.C., Benedetti, A., Lattanzi, L., Cassano, G.B., and Perlis, R.H. (2010). L-type calcium channels and psychiatric disorders: A brief review. American journal of medical genetics Part B, Neuropsychiatric genetics : the official publication of the International Society of Psychiatric Genetics *153B*, 1373-1390.

Catterall, W.A., and Few, A.P. (2008). Calcium channel regulation and presynaptic plasticity. Neuron *59*, 882-901.

Catterall, W.A., Striessnig, J., Snutch, T.P., and Perez-Reyes, E. (2003). International Union of Pharmacology. XL. Compendium of voltage-gated ion channels: calcium channels. Pharmacol Rev *55*, 579-581.

Chan, C.S., Gertler, T.S., and Surmeier, D.J. (2010). A molecular basis for the increased vulnerability of substantia nigra dopamine neurons in aging and Parkinson's disease. Movement disorders : official journal of the Movement Disorder Society *25 Suppl 1*, S63-70.

Chanda, B., Asamoah, O.K., and Bezanilla, F. (2004). Coupling interactions between voltage sensors of the sodium channel as revealed by site-specific measurements. J Gen Physiol *123*, 217-230.

Cheng, X., Liu, J., Asuncion-Chin, M., Blaskova, E., Bannister, J.P., Dopico, A.M., and Jaggar, J.H. (2007). A novel Ca(V)1.2 N terminus expressed in smooth muscle cells of resistance size arteries modifies channel regulation by auxiliary subunits. J Biol Chem *282*, 29211-29221.

Cohen, C., Perrault, G., and Sanger, D.J. (1997). Assessment of the antidepressant-like effects of L-type voltage-dependent channel modulators. Behavioural pharmacology *8*, 629-638.

Cribbs, L. (2010). T-type calcium channel expression and function in the diseased heart. Channels (Austin, Tex) *4*, 447-452.

Dolmetsch, R.E., Pajvani, U., Fife, K., Spotts, J.M., and Greenberg, M.E. (2001). Signaling to the nucleus by an L-type calcium channel-calmodulin complex through the MAP kinase pathway. Science *294*, 333-339.

Fang, K., and Colecraft, H.M. (2011). Mechanism of auxiliary Î²-subunit-mediated membrane targeting of L-type $Ca_V1.2$ channels. The Journal of physiology *589*, 4437-4455.

Fenwick, E.M., Marty, A., and Neher, E. (1982). A patch-clamp study of bovine chromaffin cells and of their sensitivity to acetylcholine. J Physiol *331*, 577-597.

Fossat, P., Dobremez, E., Bouali-Benazzouz, R., Favereaux, A., Bertrand, S.S., Kilk, K., Leger, C., Cazalets, J.R., Langel, U., Landry, M., *et al.* (2010). Knockdown of L calcium channel subtypes: differential effects in neuropathic pain. J Neurosci *30*, 1073-1085.

Galeotti, N., Bartolini, A., and Ghelardini, C. (2006). Blockade of intracellular calcium release induces an antidepressant-like effect in the mouse forced swimming test. Neuropharmacology *50*, 309-316.

Gerzanich, V., Ivanov, A., Ivanova, S., Yang, J.B., Zhou, H., Dong, Y., and Simard, J.M. (2003). Alternative splicing of cGMP-dependent protein kinase I in angiotensin-hypertension: novel mechanism for nitrate tolerance in vascular smooth muscle. Circulation research *93*, 805-812.

Gidh-Jain, M., Huang, B., Jain, P., Battula, V., and el-Sherif, N. (1995). Reemergence of the fetal pattern of L-type calcium channel gene expression in non infarcted myocardium during left ventricular remodeling. Biochemical and Biophysical Research Communications *216*, 892-897.

Grabowski, P.J., and Black, D.L. (2001). Alternative RNA splicing in the nervous system. Prog Neurobiol *65*, 289-308.

Green, E.K., Grozeva, D., Jones, I., Jones, L., Kirov, G., Caesar, S., Gordon-Smith, K., Fraser, C., Forty, L., Russell, E., *et al.* (2010). The bipolar disorder risk allele at CACNA1C also confers risk of recurrent major depression and of schizophrenia. Mol Psychiatry *15*, 1016-1022.

Greenberg, D.L., Payne, M.E., MacFall, J.R., Steffens, D.C., and Krishnan, R.R. (2008). Hippocampal volumes and depression subtypes. Psychiatry research *163*, 126-132.

Gröner, F., Rubio, M., Schulte-Euler, P., Matthes, J., Khan, I.F.Y., Bodi, I., Koch, S.E., Schwartz, A., and Herzig, S. (2004). Single-channel gating and regulation of human L-type calcium channels in cardiomyocytes of transgenic mice. Biochemical and Biophysical Research Communications *314*, 878-884.

Hammes, A., Guo, J.K., Lutsch, G., Leheste, J.R., Landrock, D., Ziegler, U., Gubler, M.C., and Schedl, A. (2001). Two splice variants of the Wilms' tumor 1 gene have distinct functions during sex determination and nephron formation. Cell *106*, 319-329.

Herzig, S., Khan, I.F.Y., Gründemann, D., Matthes, J., Ludwig, A., Michels, G., Hoppe, U.C., Chaudhuri, D., Schwartz, A., Yue, D.T., *et al.* (2007). Mechanism of $Ca_V1.2$ channel modulation by the amino terminus of cardiac beta2-subunits. The FASEB Journal *21*, 1527-1538.

Herzig, S., Patil, P., Neumann, J., Staschen, C.M., and Yue, D.T. (1993). Mechanisms of beta-adrenergic stimulation of cardiac Ca^{2+} channels revealed by discrete-time Markov analysis of slow gating. Biophys J *65*, 1599-1612.

Hirano, Y., and Hiraoka, M. (1994). Dual modulation of unitary L-type Ca^{2+} channel currents by $[Ca^{2+}]i$ in fura-2-loaded guinea-pig ventricular myocytes. The Journal of physiology *480 (Pt 3)*, 449-463.

Hodgkin, A.L., and Huxley, A.F. (1952). A quantitative description of membrane current and its application to conduction and excitation in nerve. The Journal of physiology *117*, 500-544.

Hohaus, A., Poteser, M., Romanin, C., Klugbauer, N., Hofmann, F., Morano, I., Haase, H., and Groschner, K. (2000). Modulation of the smooth-muscle L-type Ca^{2+} channel alpha1 subunit (alpha1C-b) by the beta2a subunit: a peptide which inhibits binding of beta to the I-II linker of alpha1 induces functional uncoupling. Biochem J *348 Pt 3*, 657-665.

Horn, R. (1991). Estimating the number of channels in patch recordings. Biophys J *60*, 433-439.

Hullett, F.J., Potkin, S.G., Levy, A.B., and Ciasca, R. (1988). Depression associated with nifedipine-induced calcium channel blockade. The American journal of psychiatry *145*, 1277-1279.

Hullin, R., Khan, I.F.Y., Wirtz, S., Mohacsi, P., Varadi, G., Schwartz, A., and Herzig, S. (2003). Cardiac L-type calcium channel beta-subunits expressed in human heart have differential effects on single-channel characteristics. The Journal of biological chemistry *278*, 21623-21630.

Jangsangthong, W., Kuzmenkina, E., Khan, I.F., Matthes, J., Hullin, R., and Herzig, S. (2009). Inactivation of L-type calcium channels is determined by the length of the N-terminus of mutant beta1 subunits. Pflugers Arch *459*, 399-411.

Kanevsky, N., and Dascal, N. (2006). Regulation of maximal open probability is a separable function of Ca(v)beta subunit in L-type Ca^{2+} channel, dependent on NH2 terminus of alpha1C (Ca(v)1.2alpha). The Journal of general physiology *128*, 15-36.

Kessler, R.C., Berglund, P., Demler, O., Jin, R., Koretz, D., Merikangas, K.R., Rush, A.J., Walters, E.E., and Wang, P.S. (2003). The epidemiology of major depressive disorder: results from the National Comorbidity Survey Replication (NCS-R). JAMA *289*, 3095-3105.

Lacerda, A.E., Kim, H.S., Ruth, P., Perez-Reyes, E., Flockerzi, V., Hofmann, F., Birnbaumer, L., and Brown, A.M. (1991). Normalization of current kinetics by interaction between the alpha 1 and beta subunits of the skeletal muscle dihydropyridine-sensitive Ca^{2+} channel. Nature *352*, 527-530.

Lareau, L.F., Green, R.E., Bhatnagar, R.S., and Brenner, S.E. (2004). The evolving roles of alternative splicing. Current Opinion in Structural Biology *14*, 273-282.

Levy, N.A., and Janicak, P.G. (2000). Calcium channel antagonists for the treatment of bipolar disorder. Bipolar Disord *2*, 108-119.

Li, C., Chan, J., Haeseleer, F., Mikoshiba, K., Palczewski, K., Ikura, M., and Ames, J.B. (2009). Structural insights into Ca^{2+}-dependent regulation of inositol 1,4,5-trisphosphate receptors by CaBP1. J Biol Chem *284*, 2472-2481.

Liao, P., Yong, T.F., Liang, M.C., Yue, D.T., and Soong, T.W. (2005). Splicing for alternative structures of $Ca_V1.2$ Ca^{2+} channels in cardiac and smooth muscles. Cardiovascular Research *68*, 197-203.

Liao, P., Yu, D., Li, G., Yong, T.F., Soon, J.L., Chua, Y.L., and Soong, T.W. (2007). A smooth muscle $Ca_V1.2$ calcium channel splice variant underlies hyperpolarized window current and enhanced state-dependent inhibition by nifedipine. The Journal of biological chemistry *282*, 35133-35142.

Liao, P., Yu, D., Lu, S., Tang, Z., Liang, M.C., Zeng, S., Lin, W., and Soong, T.W. (2004). Smooth muscle-selective alternatively spliced exon generates functional variation in $Ca_V1.2$ calcium channels. J Biol Chem *279*, 50329-50335.

Lister, R.G. (1987). The use of a plus-maze to measure anxiety in the mouse. Psychopharmacology (Berl) *92*, 180-185.

Livak, K.J., and Schmittgen, T.D. (2001). Analysis of relative gene expression data using real-time quantitative PCR and the 2(-Delta Delta C(T)) Method. Methods *25*, 402-408.

Llinas, R., Sugimori, M., Lin, J.W., and Cherksey, B. (1989). Blocking and isolation of a calcium channel from neurons in mammals and cephalopods utilizing a toxin fraction (FTX) from funnel-web spider poison. Proceedings of the National Academy of Sciences of the United States of America *86*, 1689-1693.

Llinas, R., and Yarom, Y. (1981). Electrophysiology of mammalian inferior olivary neurons in vitro. Different types of voltage-dependent ionic conductances. J Physiol *315*, 549-567.

Mallinger, A.G., Thase, M.E., Haskett, R., Buttenfield, J., Luckenbaugh, D.A., Frank, E., Kupfer, D.J., and Manji, H.K. (2008). Verapamil augmentation of lithium treatment improves outcome in mania unresponsive to lithium alone: preliminary findings and a discussion of therapeutic mechanisms. Bipolar disorders *10*, 856-866.

Mangoni, M.E., Couette, B., Bourinet, E., Platzer, J., Reimer, D., Striessnig, J.r., and Nargeot, J.l. (2003). Functional role of L-type $Ca_V1.3$ Ca^{2+} channels in cardiac pacemaker activity. Proceedings of the National Academy of Sciences of the United States of America *100*, 5543-5548.

Marsh, J.D. (1989). Co regulation of calcium channels and beta-adrenergic receptors in cultured chick embryo ventricular cells. The Journal of clinical investigation *84*, 817-823.

Matlin, A.J., Clark, F., and Smith, C.W. (2005). Understanding alternative splicing: towards a cellular code. Nat Rev Mol Cell Biol *6*, 386-398.

McKinney, B.C., and Murphy, G.G. (2006). The L-Type voltage-gated calcium channel $Ca_V1.3$ mediates consolidation, but not extinction, of contextually conditioned fear in mice. Learn Mem *13*, 584-589.

McManus, O.B., Blatz, A.L., and Magleby, K.L. (1987). Sampling, log binning, fitting, and plotting durations of open and shut intervals from single-channels and the effects of noise. Pflugers ArchIV : European journal of physiology *410*, 530-553.

Meir, A., Bell, D.C., Stephens, G.J., Page, K.M., and Dolphin, A.C. (2000). Calcium channel beta subunit promotes voltage-dependent modulation of alpha1B by G beta gamma. Biophys J *79*, 731-746.

Michels, G., Er, F., Khan, I., Südkamp, M., Herzig, S., and Hoppe, U.C. (2005). Single-channel properties support a potential contribution of hyperpolarization-activated cyclic nucleotide-gated channels and If to cardiac arrhythmias. Circulation *111*, 399-404.

Michels, G., Matthes, J., Handrock, R., Kuchinke, U., Gröner, F., Cribbs, L.L., Pereverzev, A., Schneider, T., Perez-Reyes, E., and Herzig, S. (2002). Single-channel pharmacology of mibefradil in human native T-type and recombinant $Ca_V3.2$ calcium channels. Mol Pharmacol *61*, 682-694.

Modrek, B., and Lee, C. (2002). A genomic view of alternative splicing. Nature Genetics.

Moosmang, S., Haider, N., Klugbauer, N., Adelsberger, H., Langwieser, N., Muller, J., Stiess, M., Marais, E., Schulla, V., Lacinova, L., *et al.*(2005). Role of hippocampal $Ca_V1.2$ Ca^{2+} channels in NMDA receptor-independent synaptic plasticity and spatial memory. J Neurosci *25*, 9883-9892.

Murgatroyd, C.A. (2005). Impaired repression at a vasopressin promoter polymorphism in a rat model of trait anxiety and depression.

Neher, E., and Sakmann, B. (1976a). Noise analysis of drug induced voltage clamp currents in denervated frog muscle fibres. The Journal of physiology *258*, 705-729.

Neher, E., and Sakmann, B. (1976b). Single-channel currents recorded from membrane of denervated frog muscle fibres. Nature *260*, 799-802.

Neves, G., Zucker, J., Daly, M., and Chess, A. (2004). Stochastic yet biased expression of multiple Dscam splice variants by individual cells. Nature genetics *36*, 240-246.

Niwa, K., Nakazawa, M., Tateno, S., Yoshinaga, M., and Terai, M. (2005). Infective endocarditis in congenital heart disease: Japanese national collaboration study. Heart (British Cardiac Society) *91*, 795-800.

Nowycky, M.C., Fox, A.P., and Tsien, R.W. (1985). Three types of neuronal calcium channel with different calcium agonist sensitivity. Nature *316*, 440-443.

Olivera, B.M., Miljanich, G.P., Ramachandran, J., and Adams, M.E. (1994). Calcium channel diversity and neurotransmitter release: the omega-conotoxins and omega-agatoxins. Annual review of biochemistry *63*, 823-867.

Ospina, J.K., Gonsalvez, G.B., Bednenko, J., Darzynkiewicz, E., Gerace, L., and Matera, A.G. (2005). Cross-talk between snurportin1 subdomains. Molecular biology of the cell *16*, 4660-4671.

Pazzaglia, P.J., Post, R.M., Ketter, T.A., Callahan, A.M., Marangell, L.B., Frye, M.A., George, M.S., Kimbrell, T.A., Leverich, G.S., Cora-Locatelli, G., *et al.* (1998). Nimodipine monotherapy and carbamazepine augmentation in patients with refractory recurrent affectIVe illness. J Clin Psychopharmacol *18*, 404-413.

Pellow, S., Chopin, P., File, S.E., and Briley, M. (1985). Validation of open:closed arm entries in an elevated plus-maze as a measure of anxiety in the rat. Journal of Neuroscience Methods *14*, 149-167.

Peterson, B.Z., DeMaria, C.D., Adelman, J.P., and Yue, D.T. (1999). Calmodulin is the Ca^{2+} sensor for Ca^{2+} -dependent inactivation of L-type calcium channels. Neuron *22*, 549-558.

Pine DS (2009). Integrating research on development and fear learning: A vision for clinical neuroscience? Depress. Anxiety, 26(9): 775-779.

Ravindran, L.N., and Stein, M.B. (2010). Pharmacotherapy of post-traumatic stress disorder. Curr Top Behav Neurosci *2*, 505-525.

Reuter, H. (1979). Properties of two inward membrane currents in the heart. Annual review of physiology.

Reuter, H., Cachelin, A.B., De Peyer, J.E., and Kokubun, S. (1983). Modulation of calcium channels in cultured cardiac cells by isoproterenol and 8-bromo-cAMP. Cold Spring Harb Symp Quant Biol *48 Pt 1*, 193-200.

Sachs, F., Neil, J., and Barkakati, N. (1982). The automated analysis of data from single ionic channels. Pflugers Archiv : European journal of physiology *395*, 331-340.

Sakmann, B. (1995). Single-Channel Recording.

Schröder, E., Magyar, J., Burgess, D., Andres, D., and Satin, J. (2007). Chronic verapamil treatment remodels $I_{Ca,L}$ in mouse ventricle. American journal of physiology Heart and circulatory physiology *292*, H1906-1916.

Schröder, F., Handrock, R., Beuckelmann, D.J., Hirt, S., Hullin, R., Priebe, L., Schwinger, R.H., Weil, J., and Herzig, S. (1998). Increased availability and open probability of single L-type calcium channels from failing compared with non failing human ventricle. Circulation *98*, 969-976.

Schröder, F., and Herzig, S. (1998). [Cyclosporine]. Dtsch Med Wochenschr *123*, 121-122.

Schröder, F., and Herzig, S. (1999). Effects of beta2-adrenergic stimulation on single-channel gating of rat cardiac L-type Ca^{2+} channels. Am J Physiol *276*, H834-843.

Shistik, E., IVanina, T., Blumenstein, Y., and Dascal, N. (1998). Crucial role of N terminus in function of cardiac L-type Ca^{2+} channel and its modulation by protein kinase C. The Journal of biological chemistry *273*, 17901-17909.

Shistik, E., Keren-Raifman, T., Idelson, G.H., Blumenstein, Y., Dascal, N., and IVanina, T. (1999). The N terminus of the cardiac L-type Ca^{2+} channel alpha(1C) subunit. The initial segment is ubiquitous and crucial for protein kinase C modulation, but is not directly phosphorylated. The Journal of biological chemistry *274*, 31145-31149.

Sigworth, F.J., and Sine, S.M. (1987). Data transformations for improved display and fitting of single-channel dwell time histograms. Biophysical journal *52*, 1047-1054.

Sinnegger-Brauns, M.J., Hetzenauer, A., Huber, I.G., Renstrom, E., Wietzorrek, G., Berjukov, S., Cavalli, M., Walter, D., Koschak, A., Waldschutz, R., *et al.*(2004). Isoform-specific regulation of mood behavior and pancreatic beta cell and cardiovascular function by L-type Ca^{2+} channels. J Clin Invest *113*, 1430-1439.

Sklar, P., Ripke, S., Scott, L.J., Andreassen, O.A., Cichon, S., Craddock, N., Edenberg, H.J., Nurnberger, J.I., Jr., Rietschel, M., Blackwood, D., *et al.* (2011). Large-scale genome-wide association analysis of bipolar disorder identifies a new susceptibility locus near ODZ4. Nat Genet *43*, 977-983.

Sobocki, P.A., and Wittchen, H.U. (2005). Cost of affective disorders in Europe. European Journal of \ldots.

Soldatov, N.M. (1992). Molecular diversity of L-type Ca^{2+} channel transcripts in human fibroblasts. Proceedings of the National Academy of Sciences of the United States of America *89*, 4628-4632.

Soldatov, N.M., Bouron, A., and Reuter, H. (1995). Different voltage-dependent inhibition by dihydropyridines of human Ca^{2+} channel splice variants. The Journal of biological chemistry *270*, 10540-10543.

Soldatov, N.M., Zuhlke, R.D., Bouron, A., and Reuter, H. (1997). Molecular structures involved in L-type calcium channel inactivation. Role of the carboxyl-terminal region encoded by exons 40-42 in alpha1C subunit in the kinetics and Ca^{2+}dependence of inactivation. J Biol Chem *272*, 3560-3566.

Soong, T.W., DeMaria, C.D., Alvania, R.S., Zweifel, L.S., Liang, M.C., Mittman, S., Agnew, W.S., and Yue, D.T. (2002). Systematic identification of splice variants in human P/Q-type channel alpha1(2.1) subunits: implications for current density and Ca^{2+}-dependent inactivation. Audio, Transactions of the IRE Professional Group on *22*, 10142-10152.

Splawski, I., and Keating, M.T. (2004). Alterations in the long QT syndrome genes KVLQT1 and SCN5A and methods for detecting same. United States Patent; Patent No: US 6,342,357 B1

Splawski, I., Timothy, K.W., Sharpe, L.M., Decher, N., Kumar, P., Bloise, R., Napolitano, C., Schwartz, P.J., Joseph, R.M., Condouris, K., *et al.* (2004). $Ca_V1.2$ calcium channel dysfunction causes a multisystem disorder including arrhythmia and autism. Cell *119*, 19-31.

Splawski, I., Timothy, K.W., Decher, N., Kumar, P., Sachse, F.B., Beggs, A.H., Sanguinetti, M.C., and Keating, M.T. (2005). Severe arrhythmia disorder caused by cardiac L-type calcium channel mutations. Proc Natl Acad Sci U S A *102*, 8089-8096; discussion 8086-8088.

Stephens, G.J., Page, K.M., Bogdanov, Y., and Dolphin, A.C. (2000). The alpha1B Ca^{2+} channel amino terminus contributes determinants for beta subunit-mediated voltage-dependent inactivation properties. J Physiol *525* Pt 2, 377-390.

Stotz, S.C., and Zamponi, G.W. (2001). Identification of inactivation determinants in the domain IIS6 region of high voltage-activated calcium channels. The Journal of biological chemistry *276*, 33001-33010.

Sylvers P, Lilienfeld SO, Laprairie JL (2011). Differences between trait fear and trait anxiety: Implications for psychopathology Clin. Psychol Rev. (31)1: 122-137, 20817327.

Takahashi, S.X., Mittman, S., and Colecraft, H.M. (2003). Distinctive modulatory effects of five human auxiliary beta2 subunit splice variants on L-type calcium channel gating. Biophysical journal *84*, 3007-3021.

Tang, Z.Z., Hong, X., Wang, J., and Soong, T.W. (2007). Signature combinatorial splicing profiles of rat cardiac- and smooth-muscle $Ca_V1.2$ channels with distinct biophysical properties. Cell Calcium *41*, 417-428.

Tang, Z.Z., Liang, M.C., Lu, S., Yu, D., Yu, C.Y., Yue, D.T., and Soong, T.W. (2004). Transcript scanning reveals novel and extensive splice variations in human l-type voltage-gated calcium channel, $Ca_V1.2$ alpha1 subunit. The Journal of biological chemistry *279*, 44335-44343.

Tang, Z.Z., Liao, P., Li, G., Jiang, F.L., Yu, D., Hong, X., Yong, T.F., Tan, G., Lu, S., Wang, J., *et al.* (2008). Differential splicing patterns of L-type calcium channel $Ca_V1.2$ subunit in hearts of Spontaneously Hypertensive Rats and Wistar-Kyoto rats. Biochimica et biophysica acta *1783*, 118-130.

Thom, T., Haase, N., Rosamond, W., Howard, V.J., Rumsfeld, J., Manolio, T., Zheng, Z.J., Flegal, K., O'Donnell, C., Kittner, S., *et al.* (2006). Heart disease and stroke

statistics--2006 update: a report from the American Heart Association Statistics Committee and Stroke Statistics Subcommittee. Circulation *113*, e85-151.

Tiwari, S., Zhang, Y., Heller, J., Abernethy, D.R., and Soldatov, N.M. (2006). Atherosclerosis-related molecular alteration of the human $Ca_V1.2$ calcium channel alpha1C subunit. Proceedings of the National Academy of Sciences of the United States of America *103*, 17024-17029.

Tsien, R.W., Lipscombe, D., Madison, D.V., Bley, K.R., and Fox, A.P. (1988). Multiple types of neuronal calcium channels and their selective modulation. Trends in neurosciences *11*, 431-438.

Ule, J., Jensen, K.B., Ruggiu, M., Mele, A., Ule, A., and Darnell, R.B. (2003). CLIP identifies Nova-regulated RNA networks in the brain. Science *302*, 1212-1215.

Varadi, G., Lory, P., Schultz, D., Varadi, M., and Schwartz, A. (1991). Acceleration of activation and inactivation by the beta subunit of the skeletal muscle calcium channel. Nature *352*, 159-162.

Wang, J., Thio, S.S.C., Yang, S.S.H., Yu, D., Yu, C.Y., Wong, Y.P., Liao, P., Li, S., and Soong, T.W. (2011). Splice variant specific modulation of $Ca_V1.2$ calcium channel by galectin-1 regulates arterial constriction. Circulation research *109*, 1250-1258.

Watase, K., Barrett, C.F., Miyazaki, T., Ishiguro, T., Ishikawa, K., Hu, Y., Unno, T., Sun, Y., Kasai, S., Watanabe, M., *et al.* (2008). Spinocerebellar ataxia type 6 knockin mice develop a progressive neuronal dysfunction with age-dependent accumulation of mutant $Ca_V2.1$ channels. Proceedings of the National Academy of Sciences *105*, 11987-11992.

Welling, A., Ludwig, A., Zimmer, S., Klugbauer, N., Flockerzi, V., and Hofmann, F. (1997). Alternatively spliced IS6 segments of the alpha 1C gene determine the tissue-specific dihydropyridine sensitivity of cardiac and vascular smooth muscle L-type Ca^{2+} channels. Circulation research *81*, 526-532.

Yang, Y., Chen, X., Margulies, K., Jeevanandam, V., Pollack, P., Bailey, B.A., and Houser, S.R. (2000). L-type Ca^{2+} channel alpha 1c subunit isoform switching in failing human ventricular myocardium. Journal of molecular and cellular cardiology *32*, 973-984.

Yue, D.T., Herzig, S., and Marban, E. (1990). Beta-adrenergic stimulation of calcium channels occurs by potentiation of high-activity gating modes. Proceedings of the National Academy of Sciences of the United States of America *87*, 753-757.

Zhang, J.F., Ellinor, P.T., Aldrich, R.W., and Tsien, R.W. (1994). Molecular determinants of voltage-dependent inactivation in calcium channels. Nature *372*, 97-100.

Zhang, Z., He, Y., Tuteja, D., Xu, D., Timofeyev, V., Zhang, Q., Glatter, K.A., Xu, Y., Shin, H.S., Low, R., *et al.* (2005). Functional roles of $Ca_V1.3$ (alpha1D) calcium channels in atria: insights gained from gene-targeted null mutant mice. Circulation *112*, 1936-1944.